5-2019

Identification of Molecules by Spectral Imaging

Qamar Alshammari
Chapman University, qalshammari@chapman.edu

Identification of Molecules by Spectral Imaging

A Thesis by

Qamar A. Alshammari

Chapman University

Irvine, CA

School of Pharmacy

Submitted in partial fulfillment of the requirements for the degree of

Master of Science in Pharmaceutical Sciences

May 2019

Committee in charge:

Dr. Surya Nauli, Ph.D., Chair

Dr. Aftab Ahmed, Ph.D.

Dr. Innokentiy Maslennikov, Ph.D.

The Thesis of Qamar A. Alshammari is Approved

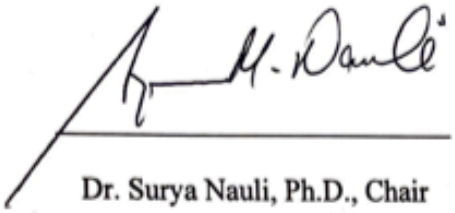

Dr. Surya Nauli, Ph.D., Chair

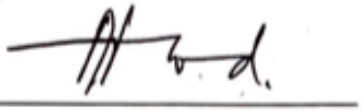

Dr. Aftab Ahmed, Ph.D.

Dr. Innokentiy Maslennikov, Ph.D.

May 2019

Identification of Molecules by Spectral Imaging

by Qamar A. Alshammari

ACKNOWLEDGEMENTS

First of all, I'm thankful to God Almighty for the strength, wisdom and good health he bestowed upon me in order to finish this research. My appreciation and profound gratitude for the help and guidance are prolonged to the following persons who in a single way or some other have contributed in making this research possible.

I would like to express my deepest appreciation and gratitude to my respected mentor, Dr. Surya Nauli, Professor, Chapman University School of Pharmacy, for his advices, support, guidance, valuable suggestions and comments that benefited in the success and completion of this study; who gave his care, timely advices, scientific approach, in doing this research. His prompt inspiration, enthusiasm and constant supervision have enabled me to complete my thesis. I'm very thankful for having such a good and distinguished mentor like him.

I would also like to extend my sincere gratitude to my thesis committee members, Dr. Aftab Ahmed, Research Associate Professor and Dr. Innokentiy Maslennikov, Assistant Professor, Chapman University School of Pharmacy for their valuable suggestions and constructive comments which were needed for the study.

I would like to thank Basir Syed, Chapman University School of Pharmacy, for his expertise and help with laboratory instruments.

I submit my heartiest thanks and gratitude to my husband Saud Alshammari, for his patience, advice and help during my research. In addition, my very profound thanks to my parents and family for their unfailing supports and prayers throughout my years of study and throughout the process of my research and this thesis preparation.

I also would like to thank all my colleagues and friends at Chapman University for their valuable suggestions.

Finally, I express my best appreciations to my institute Northern Border University, Saudi Arabia for providing financial support during my studies at Chapman University as well as Saudi Arabian Cultural Mission.

Qamar A. Alshammari

Dedicated this thesis to

My husband

for his help, advice, patience and gratitude

My parents and family

for their love, prayers, ultimate care and support

My son

for his tolerance

ABSTRACT

Identification of Molecules by Spectral Imaging

by Qamar A. Alshammari

Spectral imaging is a powerful technique which uses the wavelength to identify/quantify the exact location and amount of the molecules. It facilitates the identification of materials and studying their properties through analyzing the way they interact with light. The study of light interaction with elements is called spectroscopy; spectroscopy examines how light behaves in the target and recognizes materials based on their spectral signatures. Spectral signatures can be compared to fingerprints which can be used to identify a person; spectral signatures can be used to identify materials. Therefore, we hypothesize that identifying the exact location and quantity of molecules present in the given cells samples can be done by using a spectral imaging system. In this study, we identify the exact UV-Vis and fluorescence spectra of organic substances including Rhodamine 6G, Doxorubicin and UV-Vis spectra inorganic compounds including silver (Ag), gold (Au) nanoparticles (NPs). After that, we used the Q-TOF LC/MS system to quantify the maximum and minimum detectable concentrations of Rhodamine 6G and Doxorubicin by checking the chemicals spectrum based on the molecular weight. In addition, we used HPLC system to quantify the chemicals basing on their UV spectrum. Forwards, we used spectral imaging system to determine the exact amount and location of the molecules within cells samples. For Rhodamine 6G and doxorubicin, we started with the minimum detectable concentration by Q- TOF and consider it as a maximum limit with spectral imaging. And for NPs we used the maximum concentration for the analysis. Using the spectral imaging we were able to

detect the exact location of Rhodamine 6G which was in the cytoplasm, Doxorubicin in the nucleoplasm, and NPs in both. Furthermore, spectral imaging was able to detect much lower concentrations of Rhodamine 6G and Doxorubicin by the spectrum in comparison to Q-TOF LC/MS.

TABLE OF CONTENTS

LIST OF TABLES

LIST OF FIGURES

ABBREVIATIONS

3D	Three-dimensional
HSI	Hyperspectral Imaging
UV	Ultraviolet
VIS	Visible
Ag	Silver
Au	Gold
NPs	Nanoparticles
Q-TOF	Quadruple Time of Flight
LC/MS	Liquid Chromatography / Mass Spectrometry
PFA	Paraformaldehyde
TFA	Trifluoroacetic Acid
DOX	Doxorubicin
RHOD	Rhodamine
HPLC	High Performance Liquid Chromatography
SKY	Spectral Karyotyping

Chapter 1

INTRODUCTION

1.1. General Introduction

Spectral imaging merges of two elements imaging and spectroscopy. The need to establish a three-dimensional (3D) information which consists of various images of the same item, makes this merging not meaningless. While other imaging systems can give the intensity at a broad wavelengths, spectral imaging gives a spectrum at every pixel. This is a 3D informational collection and can be seen as a cube shape of data (Fig 1). Combining the features of imaging and spectroscopy is a superior way to understand the aspect of spectral imaging. Imaging is an innovative science of getting spatial and temporal information from items for the reason of collecting data. Right now, computerized imaging is the most developed and appropriate strategy where data are recorded utilizing an advanced camera, for example, a charged coupled device (CCD). In biologic examinations, the images can be estimated either by basic optical strategies, for example, optical microscopy or by further developed techniques like time-lapse imaging. The quality of an image decides the measure of information that can be extracted from it. The most basic parameters that describe the gained images: spatial resolution 250 nm (in-plane) at λ 500 nm, most reduced signal relies upon the quantum productivity of the detector (the higher the better).

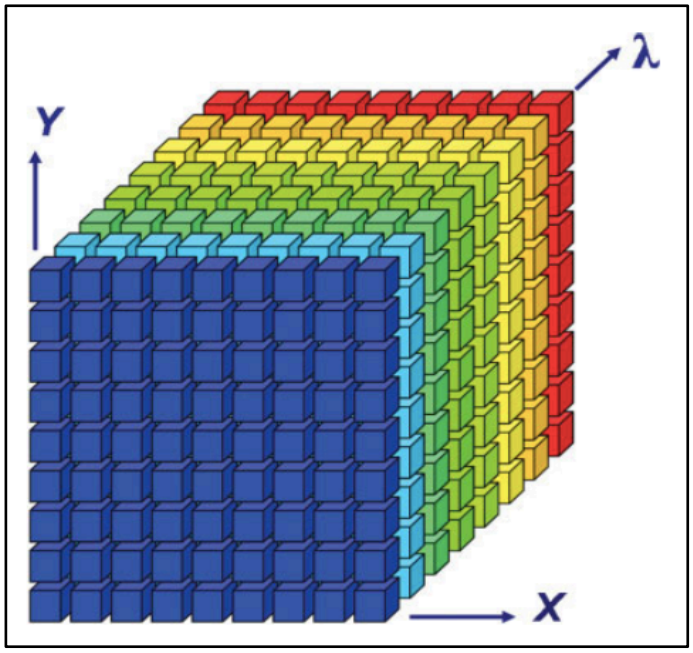

Figure 1 Demonstrating of a spectral image data, each point in the cube clarify a single number. Because spectral image is explained as $I(x,y,\lambda)$, it can be observed as spectrum $I(\lambda)$ at every pixel $I(x,y)$ or as an image $I(x,y)$ at each wavelength $I(\lambda)$

1.2. Spectroscopy

Spectroscopy, the study of securing and clarifying the spectral qualities of an object, is a science that has been generally studied for centuries. A spectrum is a collection of light intensities at various wavelengths. The structure of particles and atoms is specifically identified with spectroscopy. The spectrum is an immediate estimation of the energy levels of the defined structure. To quantify a spectrum, the light is scattered into its different wavelength (or color) elements, and the intensity at every wavelength is estimated. Most valuable features of a spectrum include spectral resolution 1–20 nm (may depend on λ) within spectral range of 400–900 nm. Spectral imaging approaches can be separated into the following techniques: (1) Wavelength-scan approaches that measure the pictures at one wavelength at any given moment. (2) Spatial-scan techniques that measure the entire spectrum of a part of the image at a time and scan the picture (e.g., line by line). (3) Time-scan methods that measure a set of images where every single one of

them is a superposition of spectral or spatial picture data. Toward the finish of the capturing, the information is converted to the real spectral image (e.g., by Fourier strategies) image (e.g., by Fourier strategies). (4) Approaches that measures the entire spectral picture at the same time, but accord on the number of points in the spectrum, the spatial resolution (Garini et al., 2006).

1.3. Spectral Imaging Types

Spectral imaging can be separated into multispectral imaging, hyperspectral imaging (HSI), and ultra-spectral imaging. Multispectral imaging system gathers information in few and generally noncontiguous wide spectral bands, estimated in micrometers or tens of micrometers, whereas HSI can collect hundreds of spectral bands. Ultra-spectral imaging system gathers considerably more data. One of the significant benefits of spectral imaging technique is that it can obtain reflectance, retention, or fluorescence spectrum for every pixel in the image, which can be utilized to distinguish the biochemical alteration of items that cannot be analyzed by conventional gray or color imaging techniques. As indicated by the electromagnetic hypothesis, diverse biochemical constituents regularly have distinctive spectral signatures or marks. These marks generally created by the associations amongst materials and electromagnetic waves, for example molecule vibration. (Li et al., 2013).

1.4. Spectral Imaging Applications

The biological and pathological differences in tissues and organs have a close connection with the spectra. Spectral aspects in various wavelength areas yield a detectable spectral signature, making pathological alteration observable. Along these lines, the spectral imaging method additionally can be reached out to the biomedical engineering field to evaluate the physiological status of living

tissues, since it can exploit the spatial connections among the diverse spectra in a neighborhood. This innovation opens new prospects for science by which researchers can recognize and evaluate the connections among biologically active molecules, analyze living life forms noninvasively, carry out histopathological and fluorescent analyses, and improve natural explaining of illnesses. This character makes it conceivable not exclusively to distinguish some physiological changes of organic tissues by their spectral marks, yet additionally for early conclusion of a few ailments since the states of the spectra yield data about natural samples (Li et al., 2013). To date, tissue fluorescence was an outstanding amongst other techniques for improving the customary endoscopic determination of gastrointestinal (GI) sores. Tissues are lighted with ultraviolet (UV) or short wavelength visible (VIS) light from a laser or separated light source. This kind of tissue fluorescence that can be seen in the tissues is called "autofluorescence." The chemical groups in charge of the autofluorescence are called "fluorophores". Each group of fluorophores is identified by unmistakable excitation and emission wavelength ranges. It is normal for a single excitation wavelength to energize numerous fluorophores. Tissues additionally contain chemical groups called "chromophores" that retain light without re-discharge of fluorescence. The retention is firmly wavelength dependent and may fundamentally adjust the in vivo fluorescence range visible at the tissue surface. The fundamental chromophore in the live tissues in the obvious wavelength (400–700 nm) is hemoglobin. While each fluorophore has a particular fluorescence spectrum, tissues have a blend of many fluorophores that appear at in various concentration and at various depth. Changes in the characteristic fluorescence of the tissue layers with illness are because of modifications in their biochemical organization (metabolic state, microenvironment). Furthermore, alterations in the layer thicknesses or the blood components lead to the fluorescence contrasts seen amongst normal and unhealthy tissues. These fluorescence contrasts might be

adequate to recognize ordinary and infected tissues. In this manner, one of the application example is the utilization of autofluorescence for identification of early malignancies or premalignant colonic sores is subject to a changes in at least one of the accompanying components: (a) the tissue construction (mucosal thickening); (b) the light retention and scattering aspect at every layer, (c) the dispersion and concentration of fluorophores in the distinctive layers; (d) the biochemical microenvironment of the tissue, that may modify the fluorescence output or spectral form (DaCosta et al., 2007).

Chapter 2

METHODOLOGY

2.1. Materials

The chemicals in this project include: anhydrous methanol HPLC grade (99.8%) and acetonitrile HPLC grade (≥ 99.9%) were purchased from SIGMA-ALDRICH, Rhodamine 6G (MW: 479.01 g/mol) from SIGMA. Doxorubicin (MW: 579.98 g/mol) was obtained from TCI AMERICA. Trifluoroacetic Acid (TFA) from EMD Millipore Corporation, Formic Acid, and sucrose from Fisher Scientific (Fair Lawn, NJ). LL-CPK1 (ATCC® CL101.1TM) porcine renal epithelial cells from proximal tubule were obtained from American Type Culture Collection (ATCC; Manassas, VA). Trypsin, penicillin-streptomycin solution, Phosphate Buffered Saline (PBS) and Dulbecco's Modified Eagle Medium (DMEM) were purchased from Corning (Manassas, VA). Fetal bovine serum (FBS) was obtained from Seradigm (Logan, UT). Paraformaldehyde (PFA) from Electron Microscopy Services (Hatfield, PA) and Mounting Media HistoChoice® from AMRESCO.

2.2. Cell culture

LL-CPK1 cells were cultured to a confluent monolayer in Dulbecco's Modified Eagle Medium (DMEM) supplemented with 10% fetal bovine serum (FBS) and 1% penicillin/streptomycin at 37°C in 5% CO2 and 95% humidity. Cells were trypsinized (using a 0.05% solution of trypsin) regularly for passage when reached 70-90% confluence. For this research, cells were cultured to reach 70-80% confluence before treated with the chemicals.

2.3. UV-VIS and Fluorescence Spectrum Detection

SpectraMax M5 Spectrophotometer was used to read the UV visible spectrum for doxorubicin, rhodamine 6G, silver (Ag) and gold (Au) nanoparticles (NPs). In addition, it was used to read the fluorescence spectrum for doxorubicin and Rhodamine. Table 1 describes the concentrations of the chemicals used in this method. Doxorubicin and Rhodamine were prepared at the same concentrations in methanol. Whereas Ag and Au NPs were diluted in Milli-Q water at different concentrations. The wavelength range of 200 – 800 nm was used to read UV spectrum for all chemicals. The fluorescence spectrum range was 400 - 800 nm for Doxorubicin and Rhodamine.

Table 1. Different concentrations of the chemicals were prepared to read the UV-VIS and fluorescence spectrums by spectrophotometer. Methanol was used to prepare the stock solutions of Doxorubicin and Rhodamine 6G at concentrations of 0.2 mM and 0.3 mM respectively. While Ag and Au NPs were diluted with Milli-Q water at different concentrations.

Spectrum Detection	Doxorubicin	Rhodamine 6G	Ag NPs	Au NPs
UV-VIS	1, 0.75, 0.5, 0.25, 0.1 μM	1, 0.75, 0.5, 0.25, 0.1 μM	100, 37.5, 25, 12.5, 5 mg/mL	100, 37.5, 25, 12.5, 5 mg/ml
Fluorescence	1, 0.75, 0.5, 0.25, 0.1 μM	1, 0.75, 0.5, 0.25, 0.1 μM	---	---

2.3. Detection and Quantification of Mass Spectrometry and UV Detection Limits

Quadruple Time of Flight Liquid Chromatography / Mass Spectrometry (Q-TOF LC/MS) (Bruker Impact II™ and Ultimate 3000 UPLC (Dionex) was used to detect and quantify the maximum and lower detection limits based on the mass spectra for both Doxorubicin and Rhodamine 6G. MS method was performed by direct injection of different concentrations of Doxorubicin and Rhodamine (Table 2), between every single injection, methanol HPLC grade was used to wash the LC tubing. For Q-TOF LC/MS method, Doxorubicin was prepared at different concentrations (Table 2) and eluted by using gradient of solvent (A) 0.1% formic acid in Milli-Q water and (B) 0.1% formic acid in acetonitrile. The flow rate was 0.3 mL/min, and the injection volume was 50 µL with a total acquisition time of 10 min. The reversed phase-high liquid chromatography (RP-HPLC) C18 column (Shimadzu 50 × 4.6mm, 3µm particle size) was used in the analysis. (Table 3) In addition, Rhodamine was also prepared at different concentrations (Table 2) and analyzed by using the isocratic elution method in 100% methanol and an injection volume of 50 µL (Fig 2). However, to quantify the limits of Doxorubicin and Rhodamine in the UV spectrum wavelength, analytical Hitachi HPLC was use. The gradient elution was conducted using mobile phase (A) 0.1% trifluoroacetic acid in Milli-Q water and (B) 0.1% trifluoroacetic acid in acetonitrile with the same gradients of Q- TOF method for Doxorubicin as shown in Table 3. Rhodamine was also analyzed with the isocratic method that has been used in Q- TOF.

Table 2. Rhodamine 6G and doxorubicin detectable concentrations for quantifying the mass and UV spectra by Q- TOF and HPLC.

Method	Rhodamine 6G	Doxorubicin
Q-TOF MS	5.0, 3.0, 2.5, 2.0, 1.5, 1.0, 0.5, 0.3, 0.2 nM.	5.0, 3.0, 1.5, 1µM, 500, 450, 300, 150 nM.
Q- TOF LC/MS	5.0, 3.0, 2.5, 2.0, 1.5, 1.0, 0.5, 0.3, 0.2 nM.	5.0, 3.0, 1.0µM, 500, 300, 150 nM.
HPLC-UV	5.0, 3.0, 2.5, 2.0, 1.5, 1.0, 0.5, 0.3, 0.2 nM.	5.0, 3.0, 1.0µM, 500, 300, 150 nM.

Table 3. RP-HPLC gradient for the separation of doxorubicin.

Time (min)	% A	% B	Flow Rate (mL/min)
0	95	5	0.3
0	95	5	0.3
1.5	95	5	0.3
6	5	95	0.3
7	5	95	0.3
7.1	95	5	0.3
9	95	5	0.3

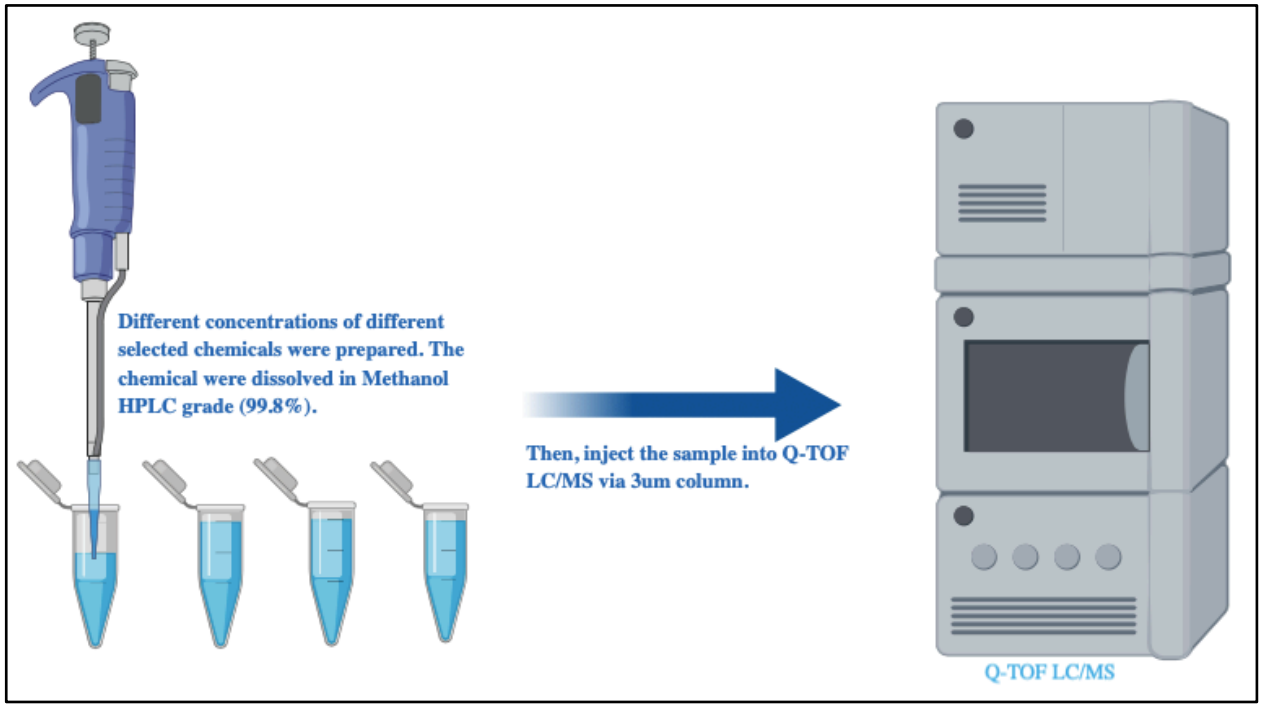

Figure 2. The sequence of steps for Q-TOF LC/MS.

2.4. Cell Treatment

Cells were seeded into sterilized 22x22 mm coverslip (globe Scientific Inc), in 6 well plate (Greiner bio-one CELLSTAR®, total volume of 2 mL at each well) under normal growth conditions until reached 70–80% confluency. The cells then were treated with 100 µL of the selected chemical at different concentrations ranging from 150 to 1 nM for Doxorubicin, 100 µM to 0.01 nM for Rhodamine 6G and 100 mg/mL for NPs (Table 4). The cells were treated for a total incubation time of 18 hrs. Then, cells were fixed for 10 min in fixing solution (2.5 mL PFA, 7.5 mL PBS and 0.2 g sucrose) at room temperature; afterward, cells were washed 3 times with PBS 5 min each time. After that, the coverslip was placed on the slide that contains 25 µL of Mounting Media overnight at room temperature (Fig 3).

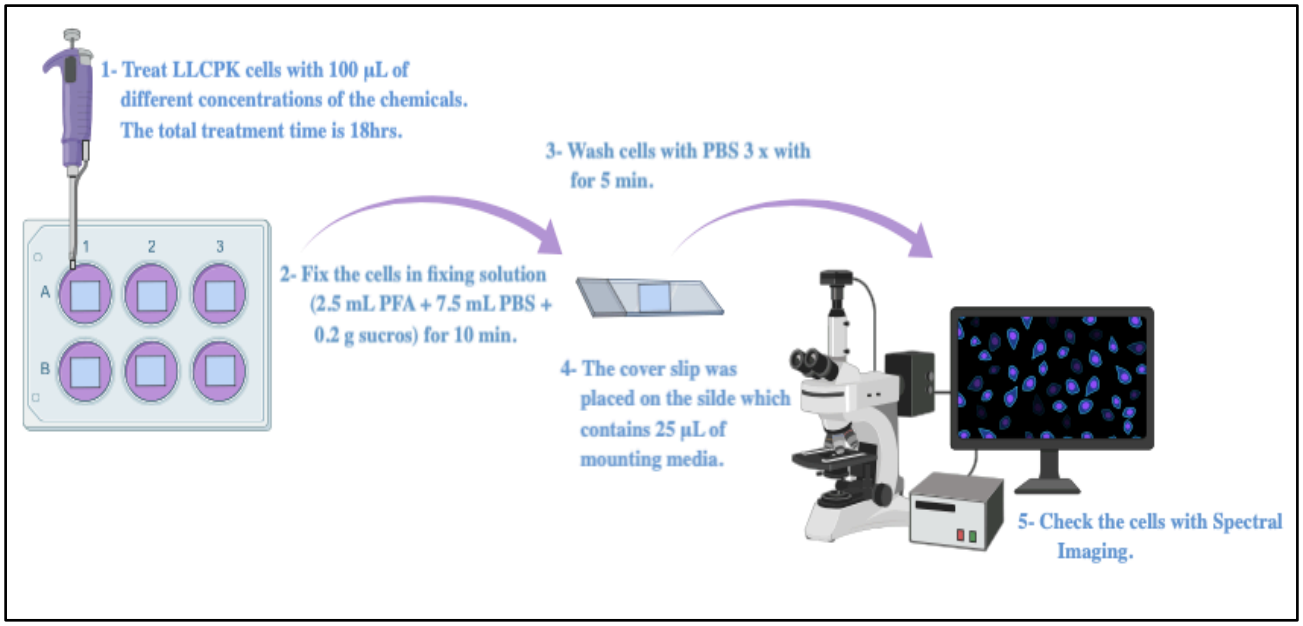

Figure 3. The sequence of steps for the cells treatments and analysis for spectral imaging.

Table 4. Selected chemical concentrations for spectral imaging

Spectral Imaging	Doxorubicin	Rhodamine 6G	NPs
Concentrations	150, 100, 10, 1 nM	100 μM, 0.2, 0.08, 0.01 nM	100mg/mL

2.5. Spectral Imaging

Spectral imaging instrument (ASI Spectral Imaging System, OLYMPUS) was used in this research. Manual image acquisition was conducted with 60× magnification fields. For spectral imaging data, the pure doxorubicin, rhodamine 6G, Ag and Au NPs spectral wavelengths were identified at the beginning. Then, we uploaded these spectrums as libraries for further cells analysis. Subsequently, images of the cells that treated with chemicals were captured randomly by using SKY and brightfield filters at least 10 capturing at each concentration. Afterward, we analyzed the captured image by using spectrum libraries of the chemicals and scanned all the interesting area to obtain the location that matched with spectrum wavelength library (Fig 4).

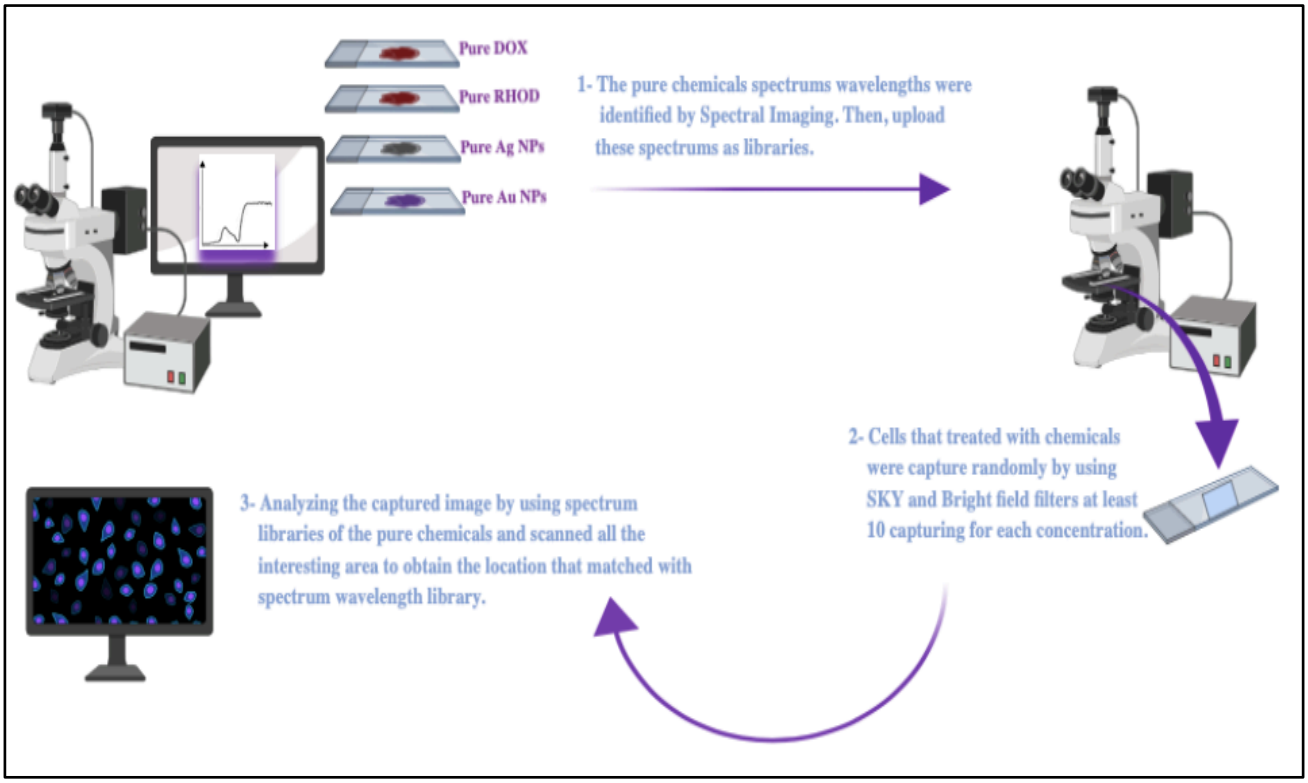

Figure 4. The sequence of steps for the spectral imaging data acquisition.

2.6. Statistical Analysis

Most of our statistical analysis was conducted by using Spectral Imaging software version 7.2.7.34276 and GraphPad Prism software version 8.0. Microsoft Excel software version 16 was also used for linear regression analysis to obtain a standard calibration curve and linear equation. Comparisons between two groups were analyzed with two-tailed student-t tests. Comparisons of three or more groups were done using ANOVA analysis followed by a posthoc test. BioRender software was also used to draw the figures in this research.

Chapter 3

RESULTS AND DISCUSSION

3.1. Spectrophotometer

The UV Spectra of Rhodamine 6G with concentration range 1 – 0.1 μM show excitation at ~ 530 nm, which was compared with previous studies and showed consistent results (Fig 5b). Using the scanning spectrophotometer we obtained a wavelength of fluorescence emission spectrum at ~580 nm, which is also consistent with previous researches (Chapman et al., 2016) (Fig 5a). We further conducted a linear regression analysis to evaluate the validity and the linearity of the concentration-dependent data. The relationships displayed in the scatterplots in Fig 6a and b of the coefficient of determination (R^2) of rhodamine 6G is linear between intensities at different concentrations and the wavelengths, at R^2= 0.99 and 0.95 for excitation and emission spectrum respectively. Doxorubicin excitation wavelength was found at ~483 nm for concentrations range 1 – 0.1 μM, which is consistent with previous studies (Liang et al., 2018) (Fig 7a). At the same concentrations, fluorescence emission wavelength was found ~592 nm (Fig 7b). In addition, linear regression analysis was conducted for excitation and emission spectrum data points. In the scatterplots in Fig 8a and b, the data point relationships showed linearity between intensities and the wavelengths at different concentrations of excitation and emission spectrum, at R^2= 0.96 and 0.89 respectively.

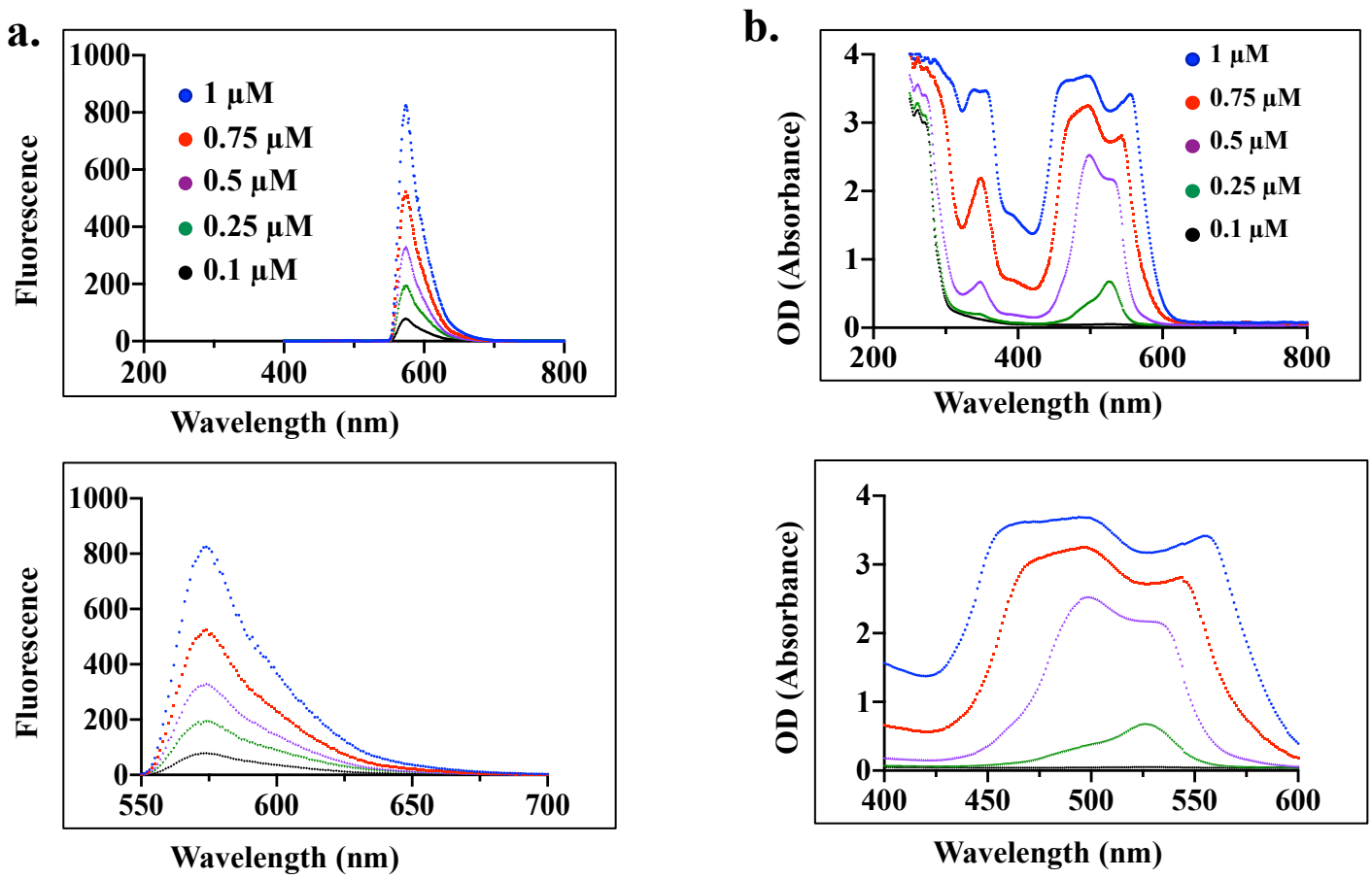

Figure 5. (a) Fluorescence emission wavelength of Rhodamine 6G with methanol at ~ 580 nm with each concentration. (b) Spectrophotometer excitation wavelength of Rhodamine 6G with methanol at ~ 530 nm with each concentration. The lower graphs of a and b are the enlarged scale of the area interested.

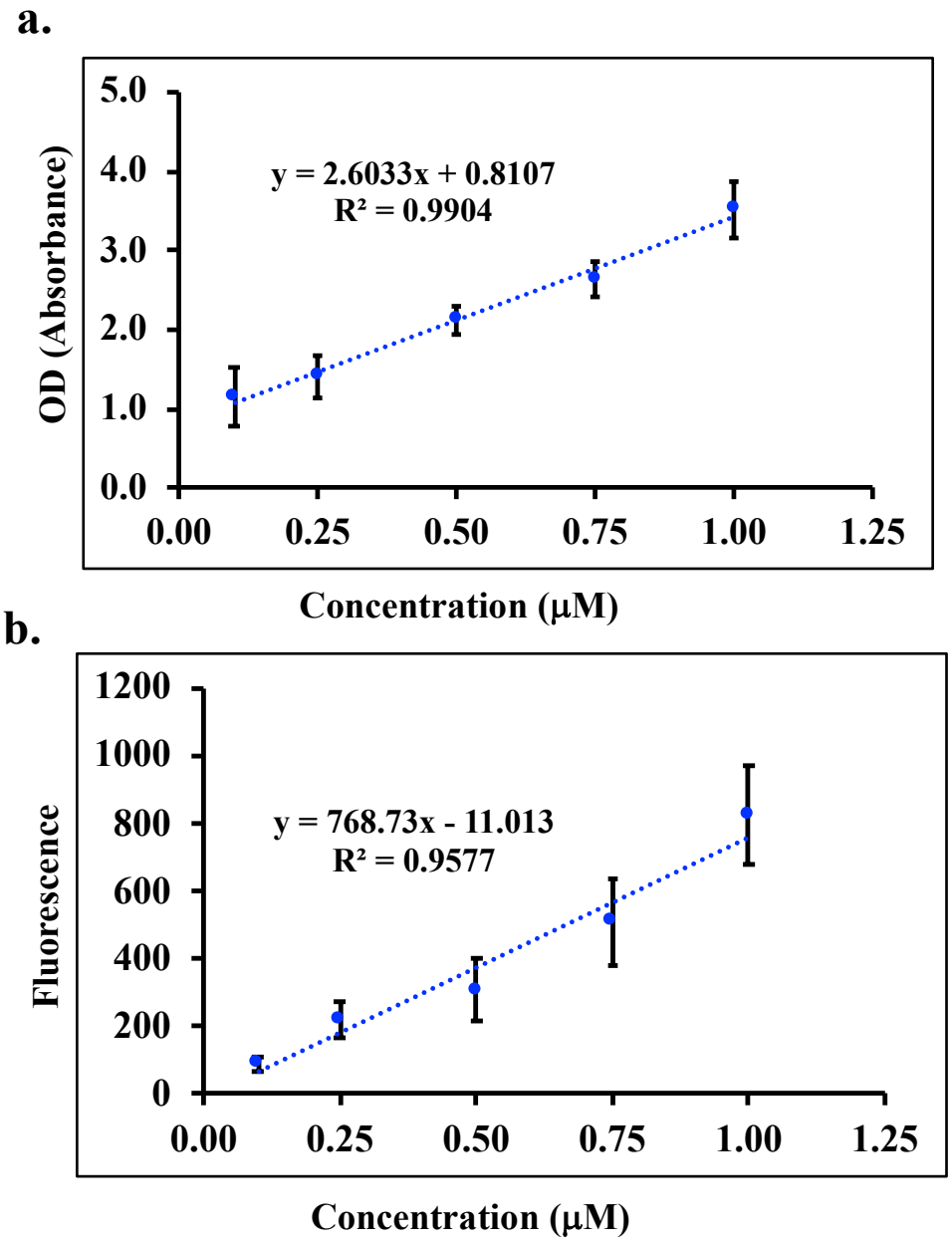

Figure 6. (a) Linear regression analysis of Rhodamine 6G excitation wavelength. X= concentrations range from 1 – 0.1 µM, y= average intensity. (b) Linear regression analysis of Rhodamine 6G emission wavelength (580 nm). X= concentrations range from 1 – 0.1 µM, y= average of intensity.

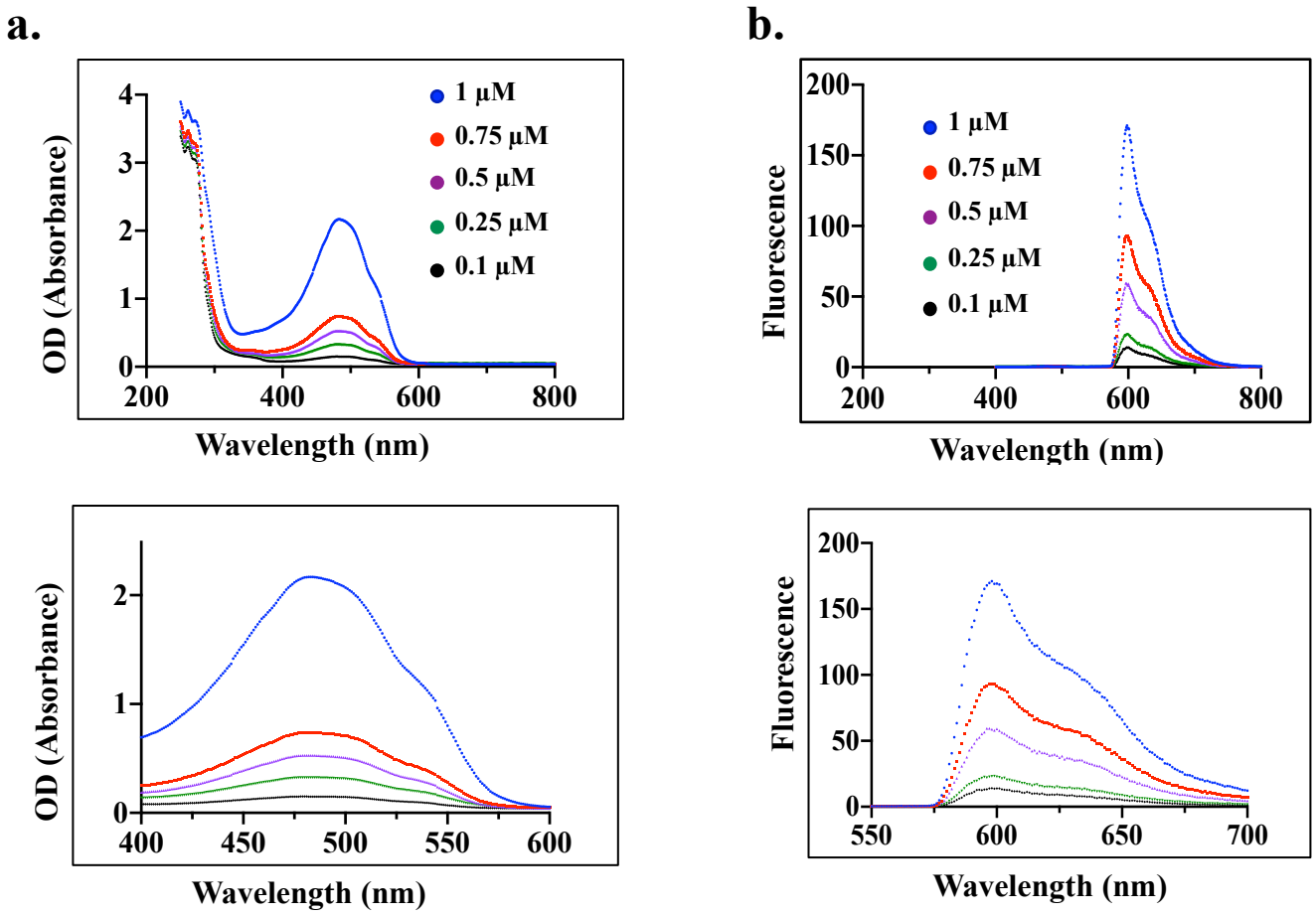

Figure 7. (a) Spectrophotometer excitation wavelength of Doxorubicin with methanol at ~483 nm with each concentration. (b) Spectrophotometer emission wavelength of Doxorubicin with methanol at ~592 nm with each concentration. The lower graphs of a and b are the enlarged scale of the area interested.

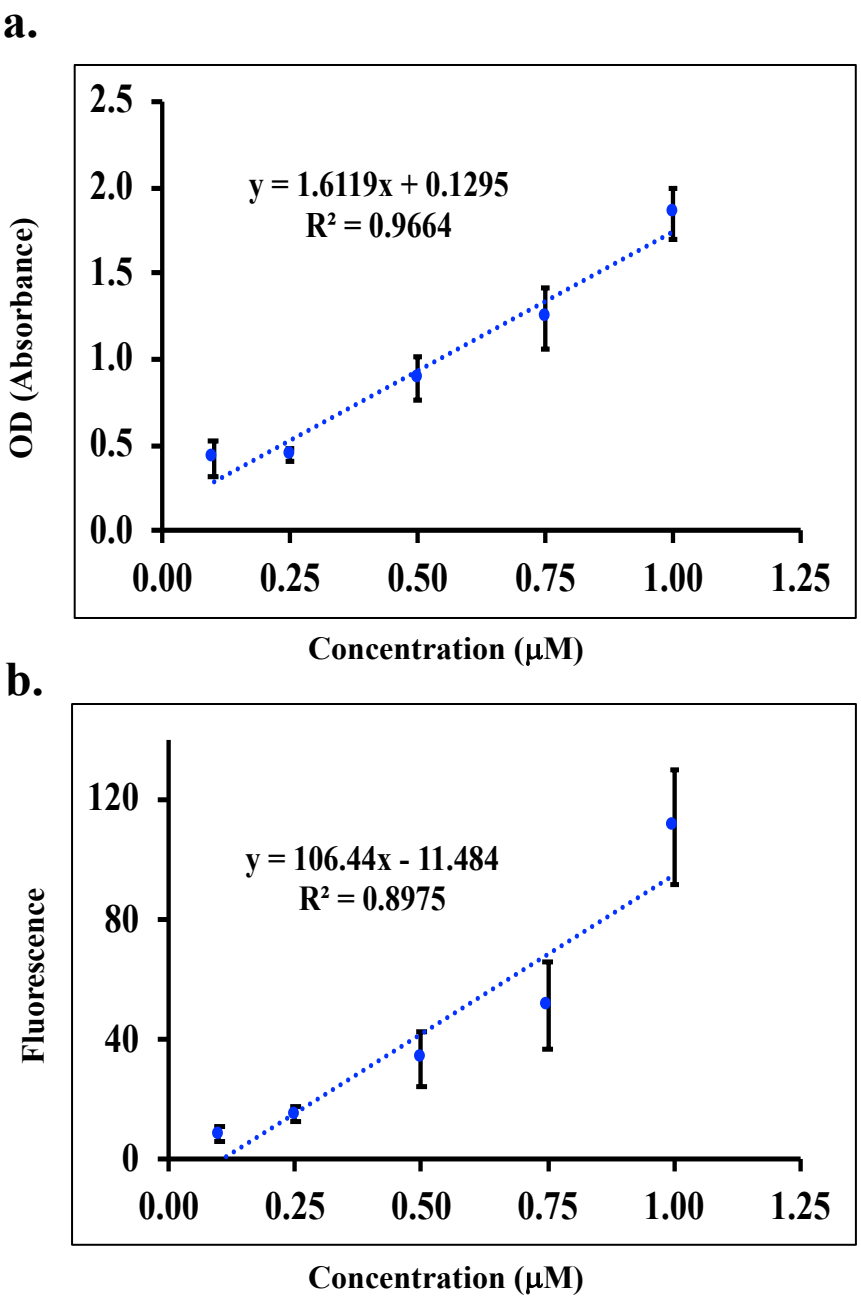

Figure 8. (a) Linear regression analysis of Doxorubicin excitation wavelength. X= concentrations range from 1 – 0.1 µM, y= average of intensities. (b) Linear regression analysis of Doxorubicin emission wavelength. X= concentrations range from 1 – 0.1 µM, y= average of intensities.

Further, Ag and Au NPs were scanned via spectrophotometer in 200 – 400 nm. AuNPs excitation wavelength was found at ~536 nm which is consistent with the expectation of previous researchers (between 520 and 580 nm, Haiss, Thanh, Aveyard, & Fernig, 2007) (Fig 9a). As well as Ag NPs excitation wavelength at ~ 420 nm that is also consistent with previous studies (Fayaz et al., 2010) (Fig 9b). In addition, linear regression analysis was perfumed for NPs. As shown in Fig 10a and b the scatterplots of NPs, there is a linear relationship between intensities and the wavelength at different concentrations of Au and AgNPs at R^2= 0.94, 0.97 respectively.

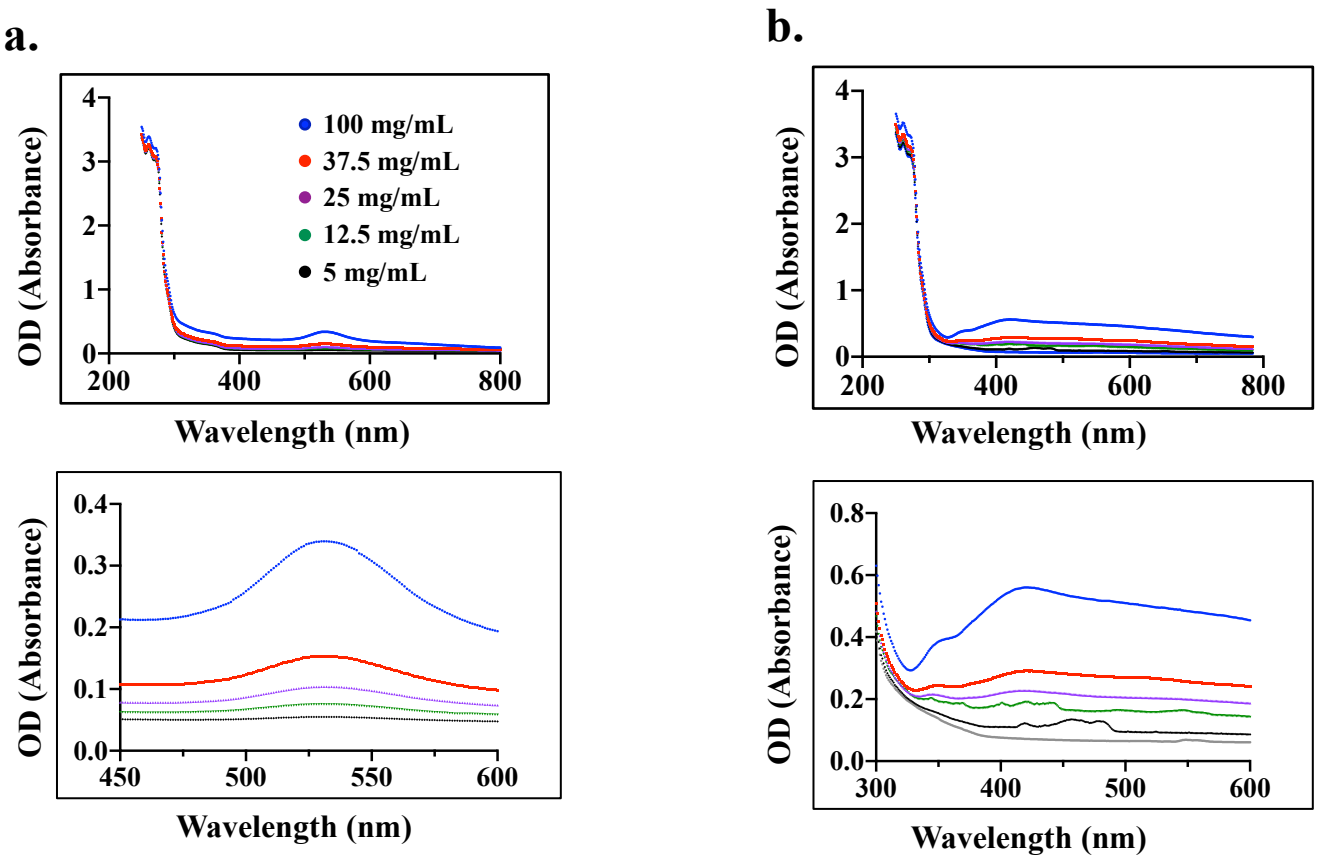

Figure 9. (a) Spectrophotometer excitation wavelength of gold NPs with Milli-Q water at ~ 536 nm with each concentration. (b) Spectrophotometer excitation wavelength of silver NPs with Milli-Q water at ~ 420 nm with each concentration. The lower graphs of a and b are the enlarged scale of the area interested.

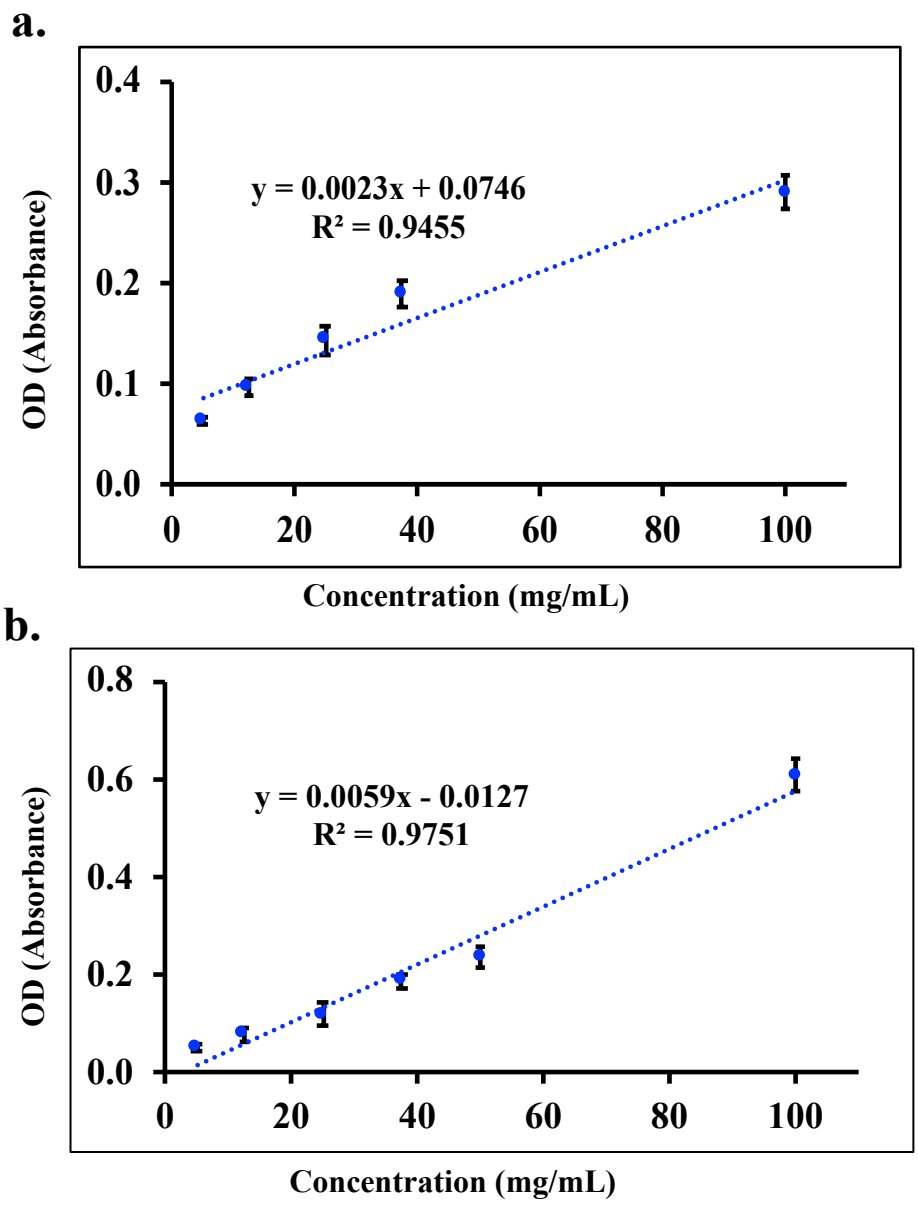

Figure 10. (a) Linear regression analysis of silver NPs excitation wavelength. X= concentrations range from 100 – 5 mg/mL, y= average of intensities. (b) Linear regression analysis of gold NPs excitation wavelength. X= concentrations range from 100 – 5 mg/mL, y= average of intensities.

3.2. Q- TOF MS and LC/MS

To quantify the maximum and minimum mass spectrometry concentrations limits of the selected chemicals, Q-TOF MS and LC/MS was conducted. For Q-TOF MS method, Rhodamine was by injected at different concentrations (Table 2) and by checking the molecular mass the maximum concentration limit to detect at 5 nM (Fig 11), while 0.2 nM is the minimum concentration with precursor ion at m/z 443 Da which consistent with previous studies (Ferreira et al., 2017) (Fig 12). Linear regression analysis was performed to check the validity of our MS data point. The scatterplot in Fig 13 showed the relationship between intensities and different concentrations at m/z 443 Da of MS data. There is linear relationship result between the MS data particularly from 0.2 to 2 nM at R^2= 0.9, from 2.5 to 5 nM the line becomes flat which it might be considering a sign of saturation. Furthermore, Q- TOF LC/MS was performed for Rhodamine at the same concentrations as Q-TOF MS method. The detection of LC/MS data was done by using 3 μm column via checking the molecular mass of the chemical at each concentration. The maximum and minimum concentrations of detectable limits of Rhodamine concentration were consistent with MS data, at 5 – 0.2 nM respectively (Fig 14, 15). The linear analysis also conducted on Q- TOF LC/MS data, and it showed a good linearity relationship between the area under the curve (AUC) of the intensities vs. concentrations, R^2= 0.98 (Fig 16). For a better comparison between spectral imaging and LC/MS data, UV quantification of Rhodamine 6G was also performed by using analytical HPLC. The limits concentrations detectable for rhodamine 6G UV peaks (at 530 nm) were consistent with Q- TOF MS and LC/MS data which at 5 – 0.2 nM (Fig 17, 18). The linearity of AUC for UV peaks and intensities shown in Fig 19, our data point showed a good linearity (R^2= 0.98) but because we set all the data at zero, it gave a lower linear relationship (R^2= 0.66) in comparing with Q- TOF MS and LC/MS data.

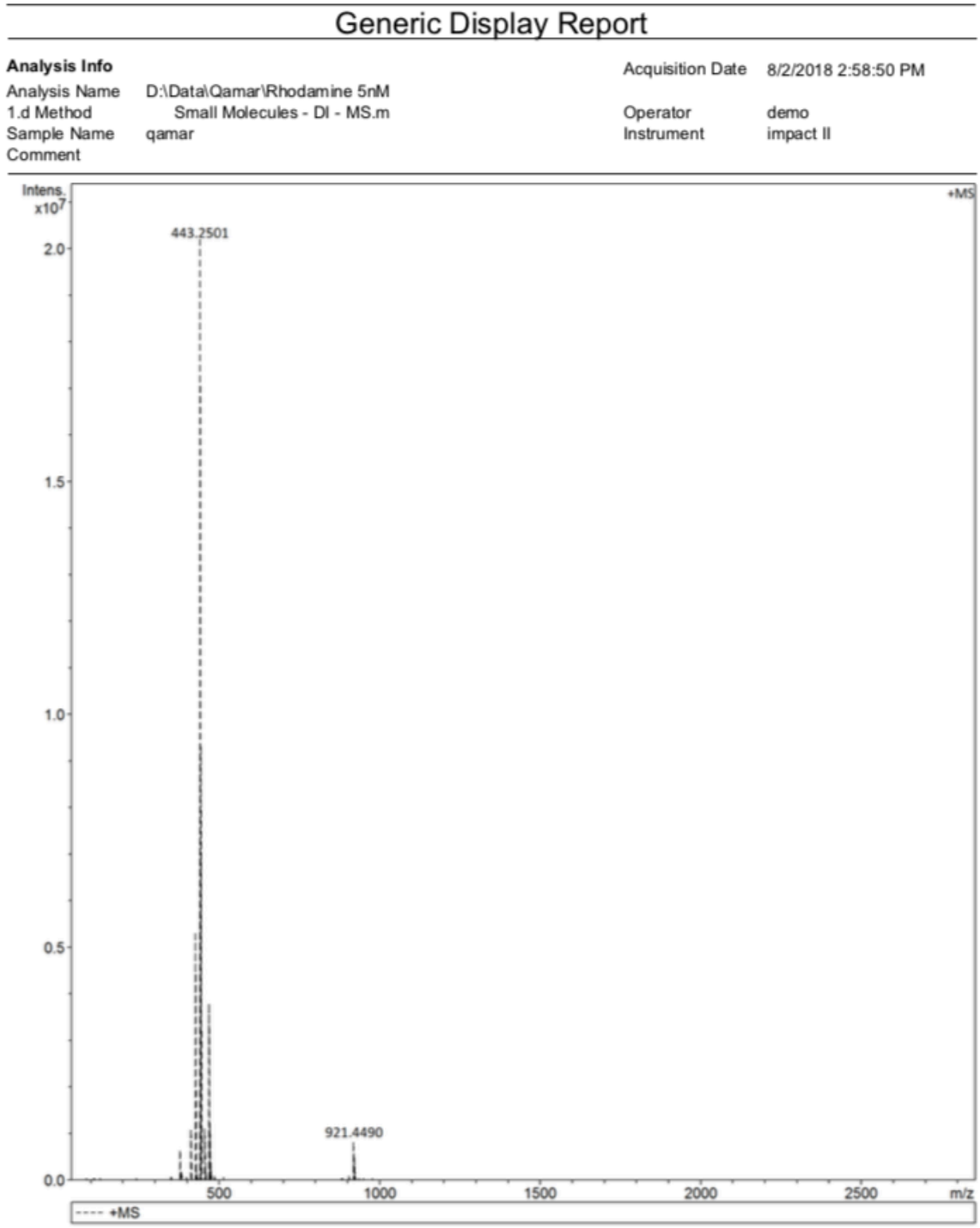

Figure 11. Q- TOF MS result for direct injection of Rhodamine 6G at the concentration of 5 nM (which is considered to be the maximum concentration limit), precursor ion at m/z 443 Da.

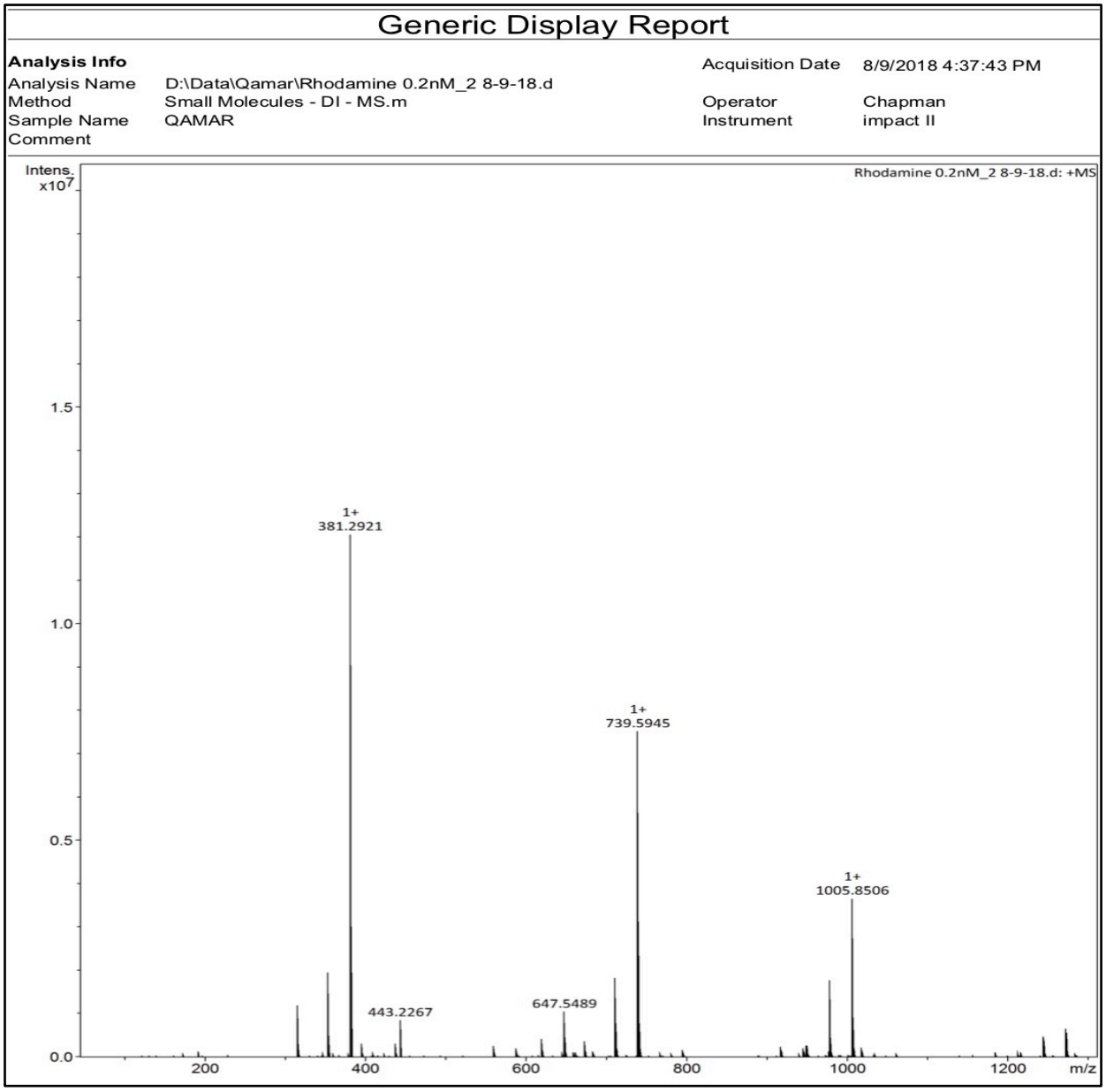

Figure 12. Q- TOF MS result for direct injection of Rhodamine 6G at the concentration of 0.2 nM (which is considered to be the minimum concentration limit), precursor ion at m/z 443 Da.

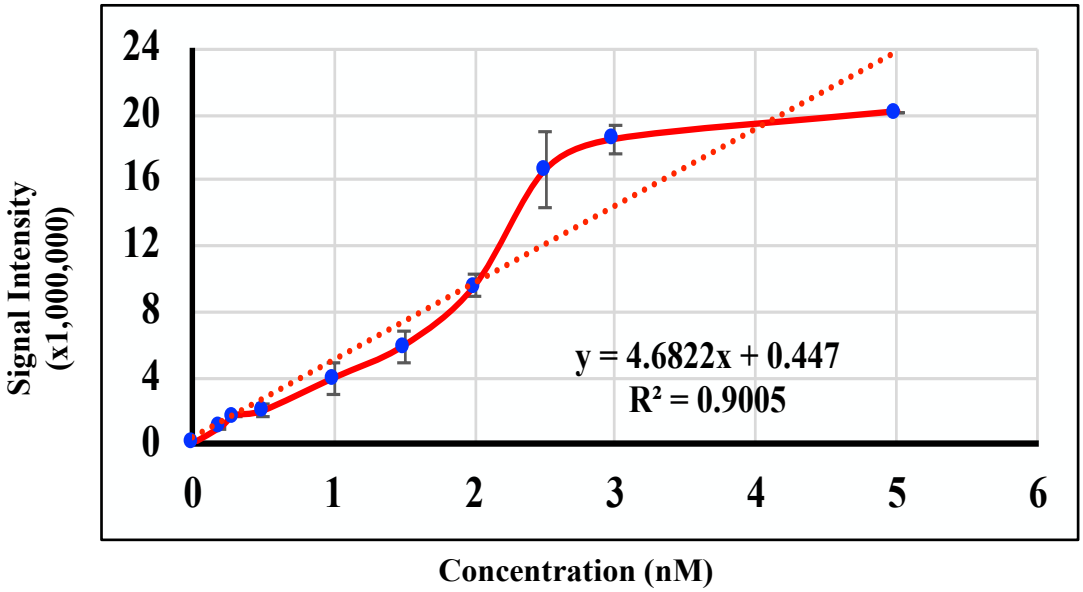

Figure 13. Linear regression analysis of Rhodamine Q-TOF MS data. X= concentrations range from 5 – 0.2 nM, y= average of intensities of m/z 443 Da.

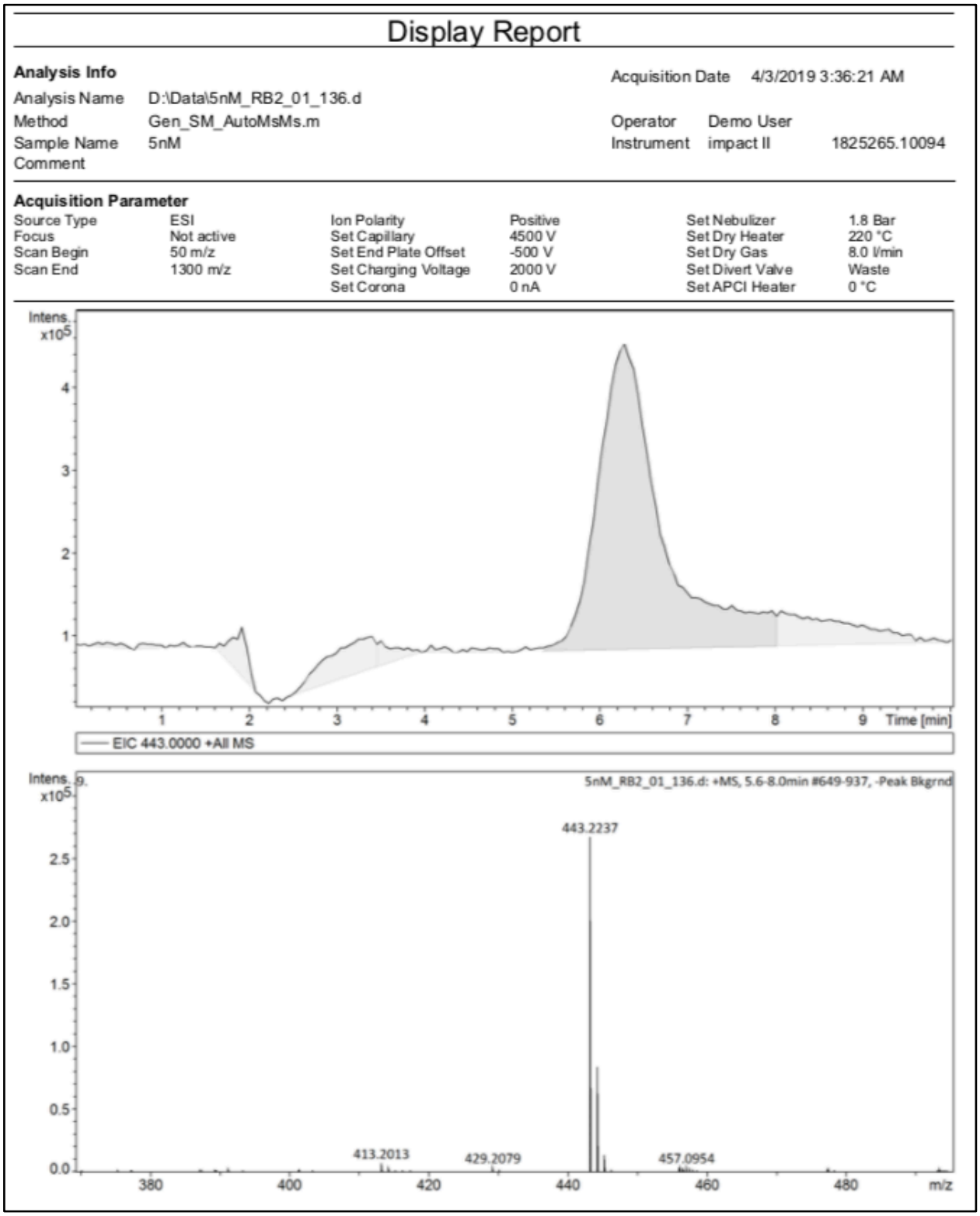

Figure 14. Q- TOF LC/MS result for the AUC of Rhodamine 6G at the concentration of 5 nM (which is considered to be the maximum concentration limit), precursor ion at m/z 443 Da.

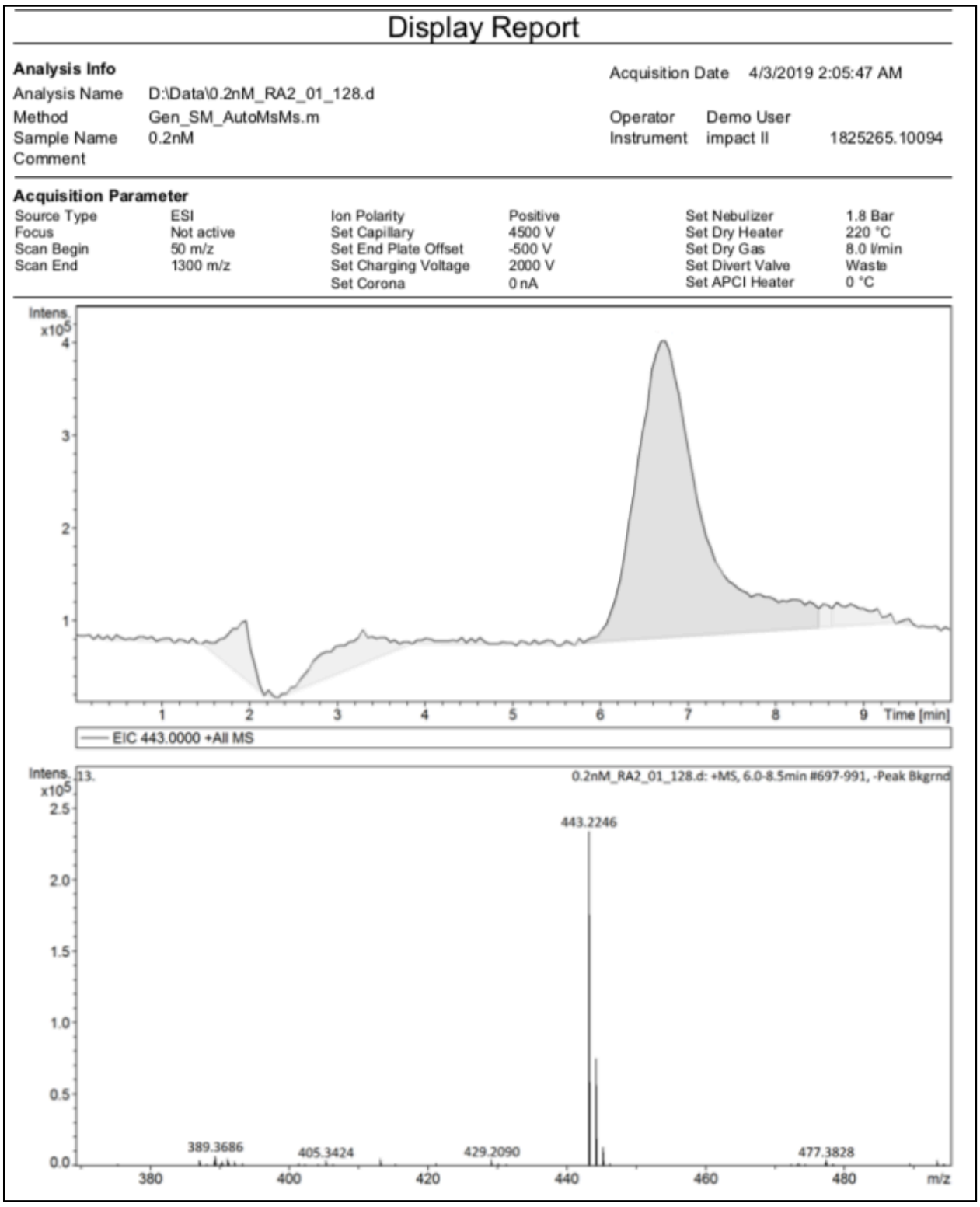

Figure 15. Q- TOF LC/MS result for the AUC of Rhodamine 6G at the concentration of 0.2 nM (which is considered to be the minimum concentration limit), precursor ion at m/z 443 Da.

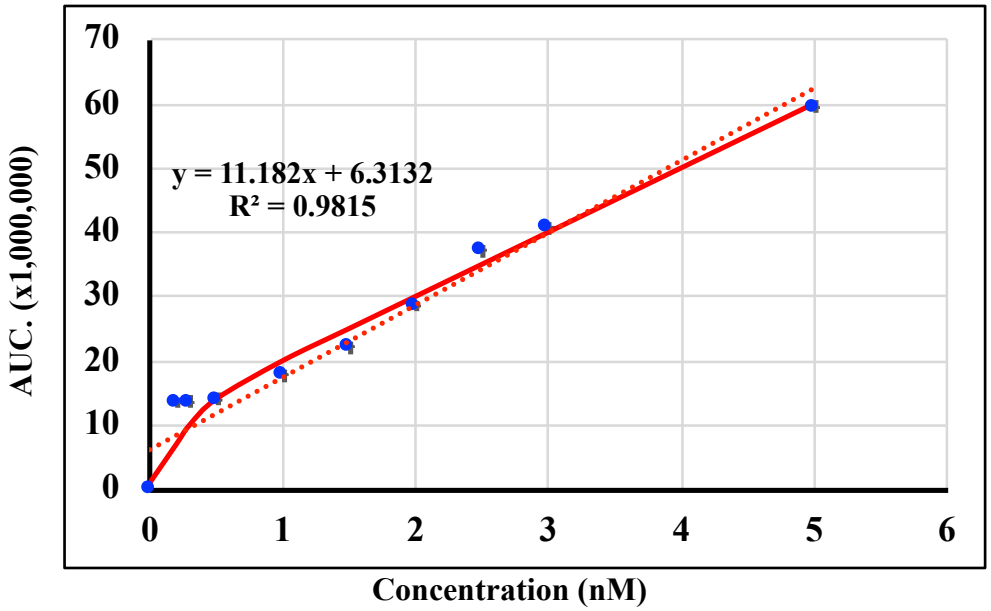

Figure 16. Linear regression analysis of Rhodamine Q-TOF LC/MS AUC data. X= concentrations range from 5 – 0.2 nM, y= average of intensities of m/z 443 Da.

Area % Report

Data File: C:\Users\UPLC system 2\Desktop\rhodamine 030419\5nM2019-04-04 13-21-36 (GMT -07-00).dat
Method: C:\Enterprise\Projects\Hitachi\Method\Rhodamine1.met
Acquired: 4/4/2019 1:22:53 PM (GMT -07:00)
Printed: 4/8/2019 11:10:35 AM (GMT -07:00)

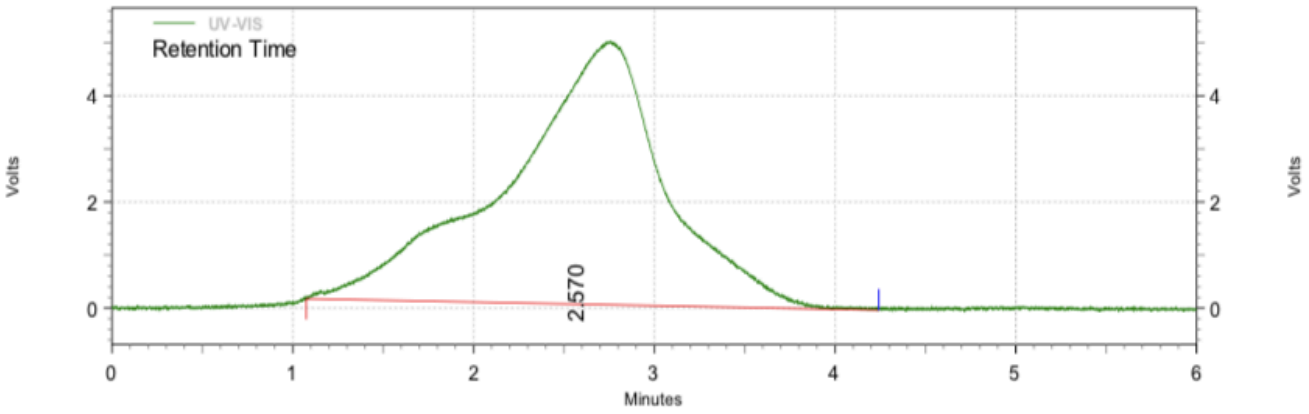

UV-VIS Results

Retention Time	Area	Area %	Height	Height %
2.570	1195854	100.00	16708	100.00
Totals	1195854	100.00	16708	100.00

Figure 17. Analytical HPLC chromatograph result for the AUC of Rhodamine 6G at the concentration of 5 nM (which is considered to be the maximum concentration limit), the UV detection at 530 nm.

Area % Report

Data File: C:\Users\UPLC system 2\Desktop\rhodamine 030419\0.2nM2019-04-04 13-29-04 -07-00).dat (GMT
Method:
Acquired: C:\Enterprise\Projects\Hitachi\Method\Rhodamine1.met
Printed: 4/4/2019 1:30:20 PM (GMT -07:00)

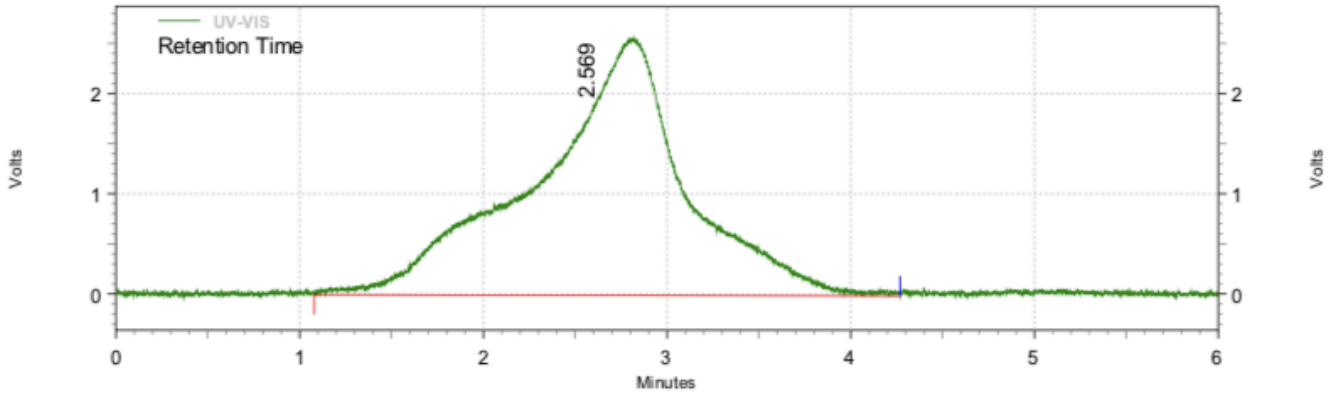

UV-VIS Results

Retention Time	Area	Area %	Height	Height %
2.569	452739	100.00	6987	100.00
Totals	452739	100.00	6987	100.00

Figure 18. Analytical HPLC chromatograph result for the AUC of Rhodamine 6G at the concentration of 0.2 nM (which is considered to be the minimum concentration limit), the UV detection at 530 nm.

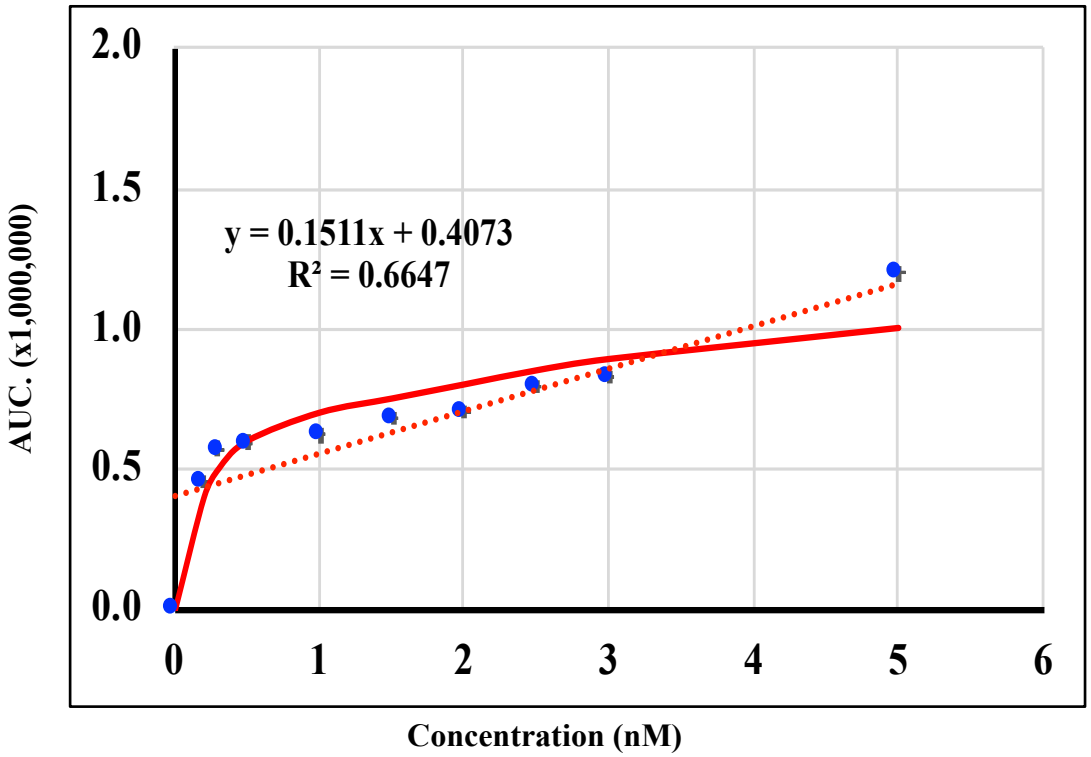

Figure 19. Linear regression analysis of rhodamine HPLC - UV AUC data. X= concentrations range from 5 – 0.2 nM, y= average of intensities of 530 nm.

Doxorubicin Q- TOF MS and LC/MS were also conducted to quantify the maximum and minimum mass spectrometry concentrations detectable limits and further compare it with the spectral imaging system. Doxorubicin was directly injected at different concentrations (Table 2) for Q-TOF MS analysis. By checking the molecular mass the maximum concentration limit to detect was determined at 5 μM (Fig 20), while the minimum detection limit is 150 nM (Fig 21). The precursor ion was found at m/z 544 Da which is consistent with previous researches (Sottani, Poggi, Melchiorre, Montagna, & Minoia, 2013). Linear regression analysis was done to check the validity of the Q-TOF MS data. The relationship between different concentrations at m/z 544 Da and the intensities of MS data is showing in the scatterplot in Fig 22. Linear relationship results between the MS data especially from 150 nM to 1 μM at R^2= 0.86, from 1.5 to 5 μM the line starts to become flat which could be considered a sign of saturation. Also, at the same concentrations of Q- TOF MS method, doxorubicin was prepared to perform Q- TOF LC/MS analysis. The detection of the data was conducted by using a 3 μm column through testing the molecular mass of the chemical at each concentration. The maximum and minimum concentrations detectable limits were consistent with MS data, at 5 μM – 150 nM respectively (Fig 23, 24). Linear consideration was conducted on Q- TOF LC/MS, it showed an excellent linearity relationship between the intensities and AUC of the concentrations, R^2= 0.99 (Fig 25). At the same way of Rhodamine, analytical HPLC analysis was performed for UV quantification of Doxorubicin in order to compare spectral imaging and LC/MS data. Doxorubicin UV peaks for the detectable concentrations limits (at 483 nm) were consistent with Q- TOF MS and LC/MS data which at 5 μM – 150 nM (Fig 26, 27). The linearity of the intensities and AUC- UV peaks are shown in the scatter plot, the result here also represent an excellent linear relationship between our data point (R^2= 0.99) (Fig 28).

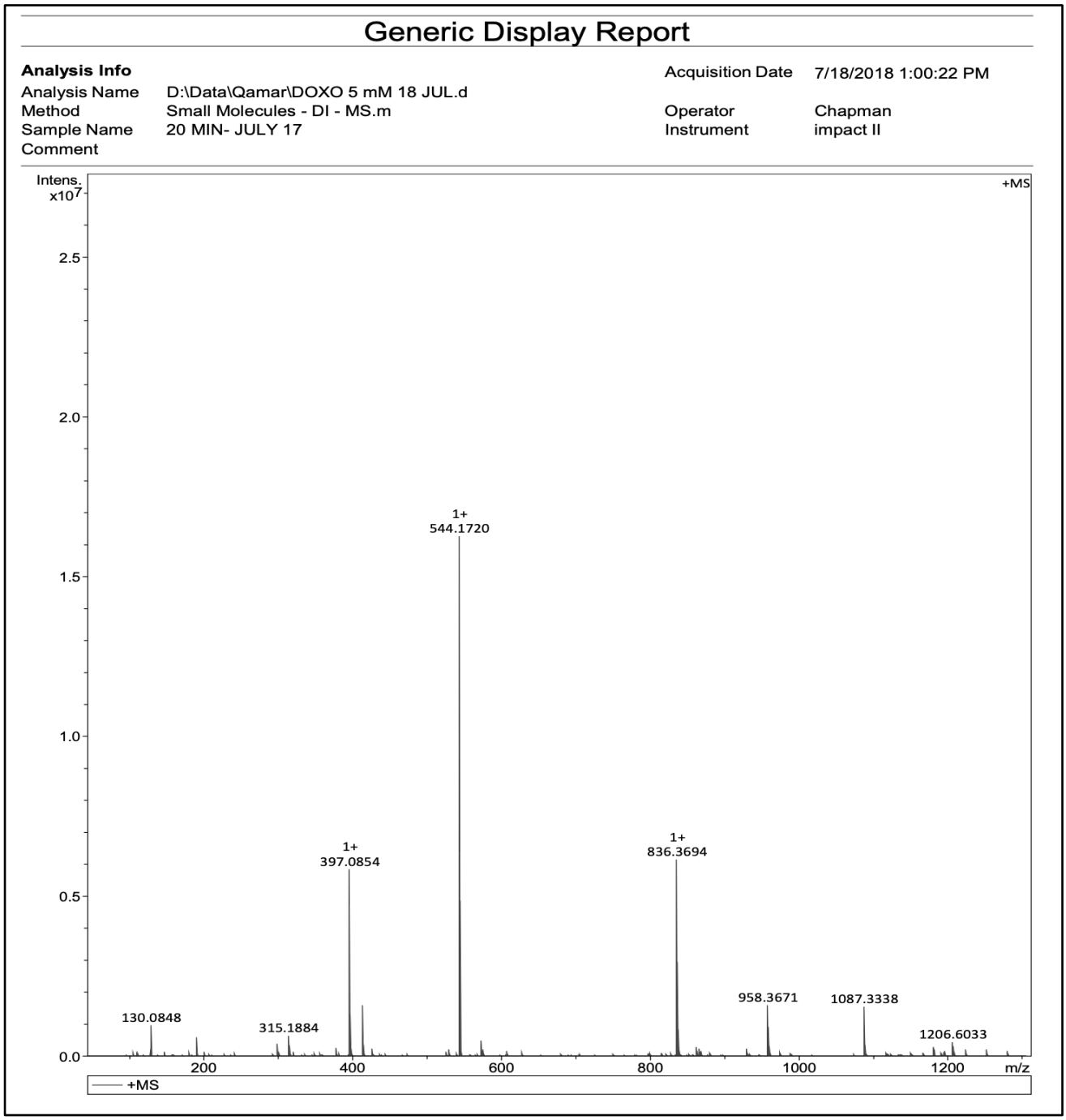

Figure 20. Q- TOF MS result for direct injection of Doxorubicin at the concentration of 5µM (which is considered to be the maximum concentration limit), precursor ion at m/z 544 Da.

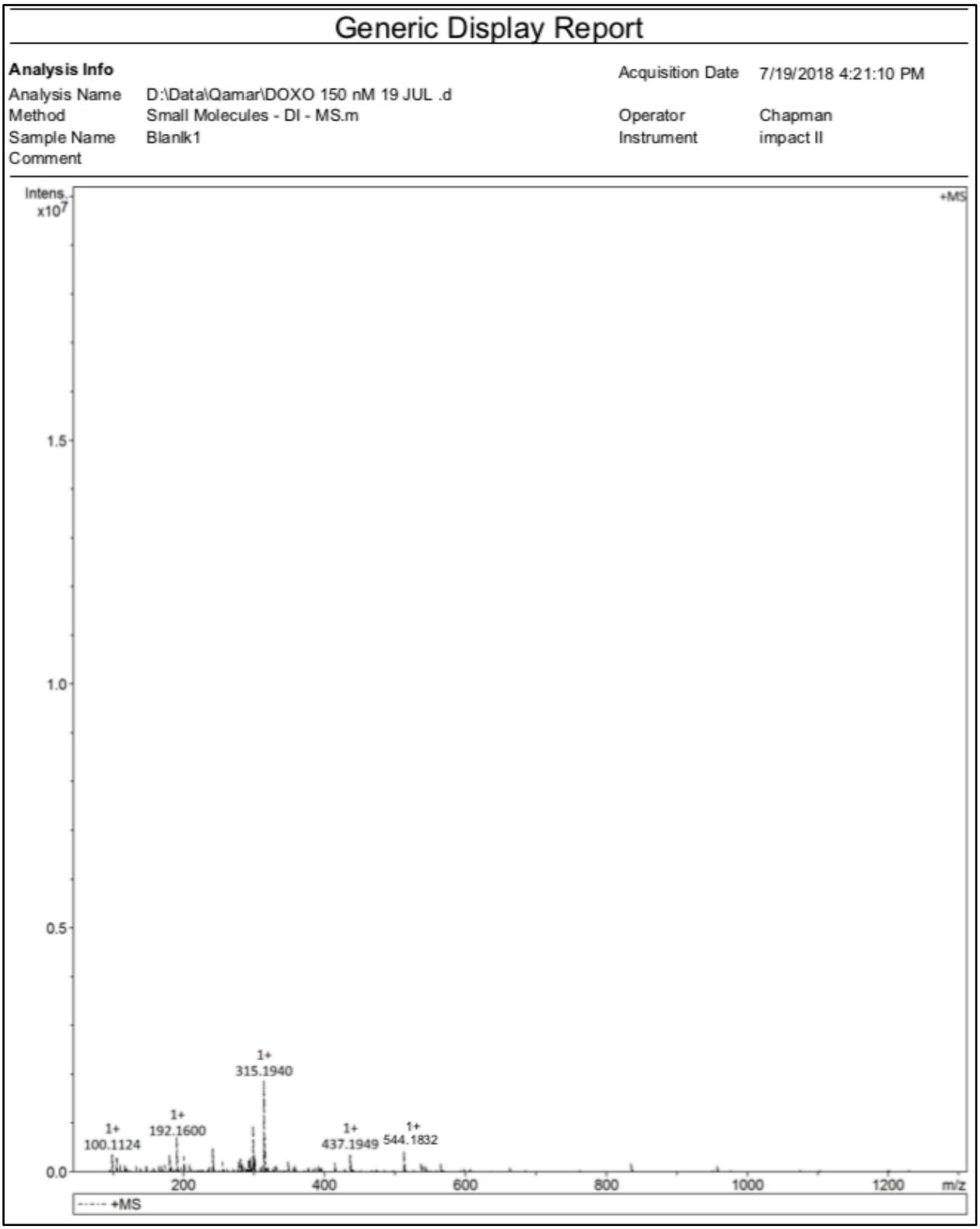

Figure 21. Q- TOF MS result for direct injection of Doxorubicin at the concentration of 150 nM (which is considered to be the minimum concentration limit), precursor ion at m/z 544 Da.

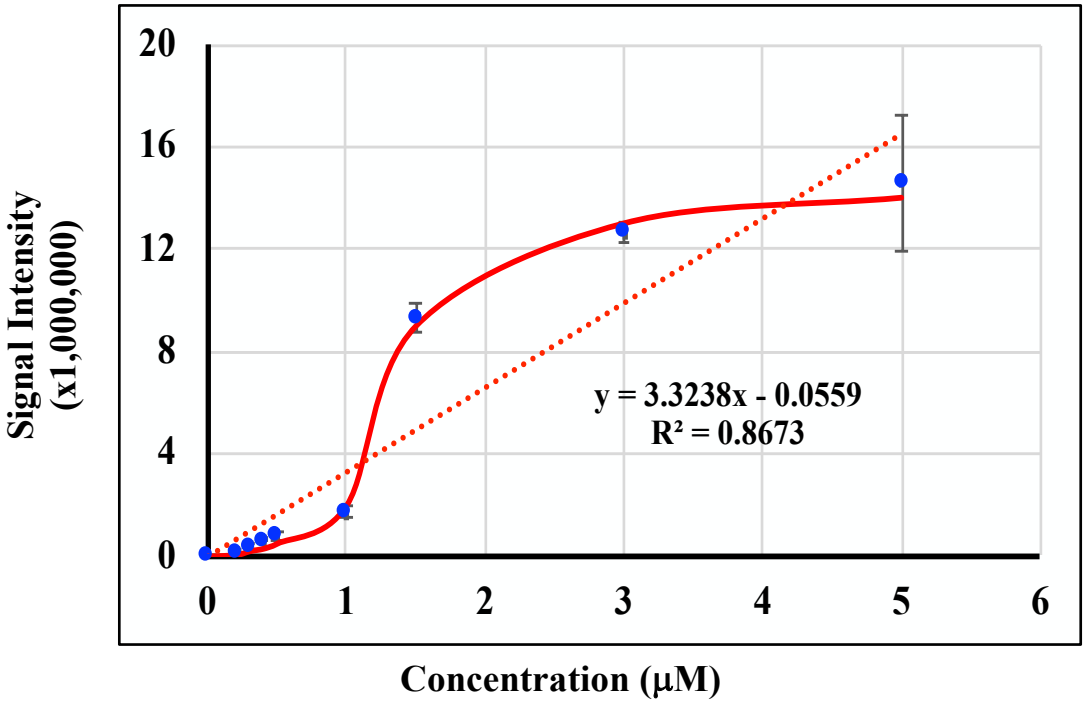

Figure 22. Q- TOF MS Linear regression analysis of Doxorubicin data. X= concentrations range from 5 µM – 150 nM, y= average of intensities of m/z 544 Da.

Figure 23. Q- TOF LC/MS result for the AUC of Doxorubicin at the concentration of 5 µM (which is considered to be the maximum concentration limit), precursor ion at m/z 544 Da.

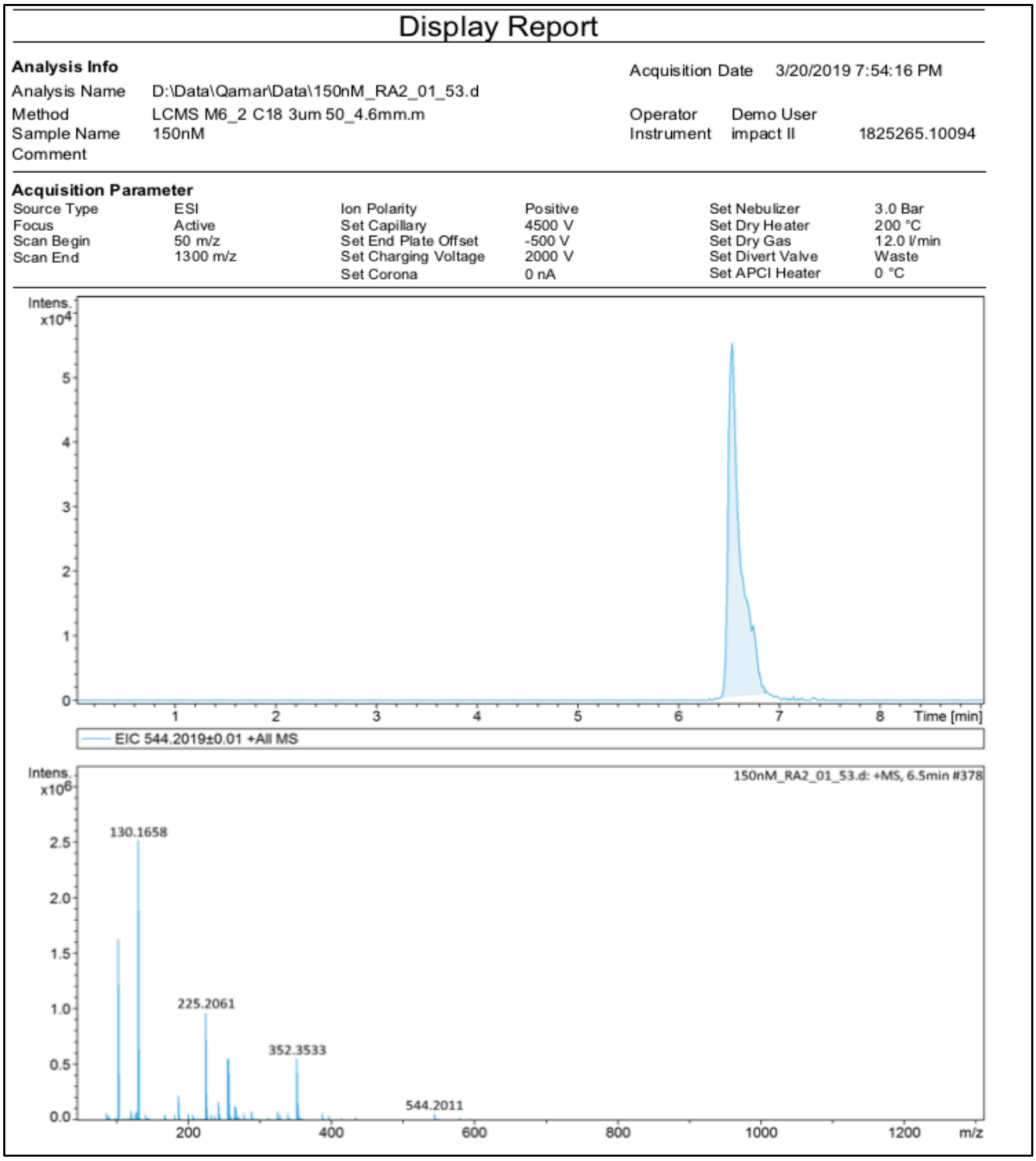

Figure 24. Q- TOF LC/MS result for the AUC of Doxorubicin at the concentration of 150 nM (which is considered to be the minimum concentration limit), precursor ion at m/z 544 Da.

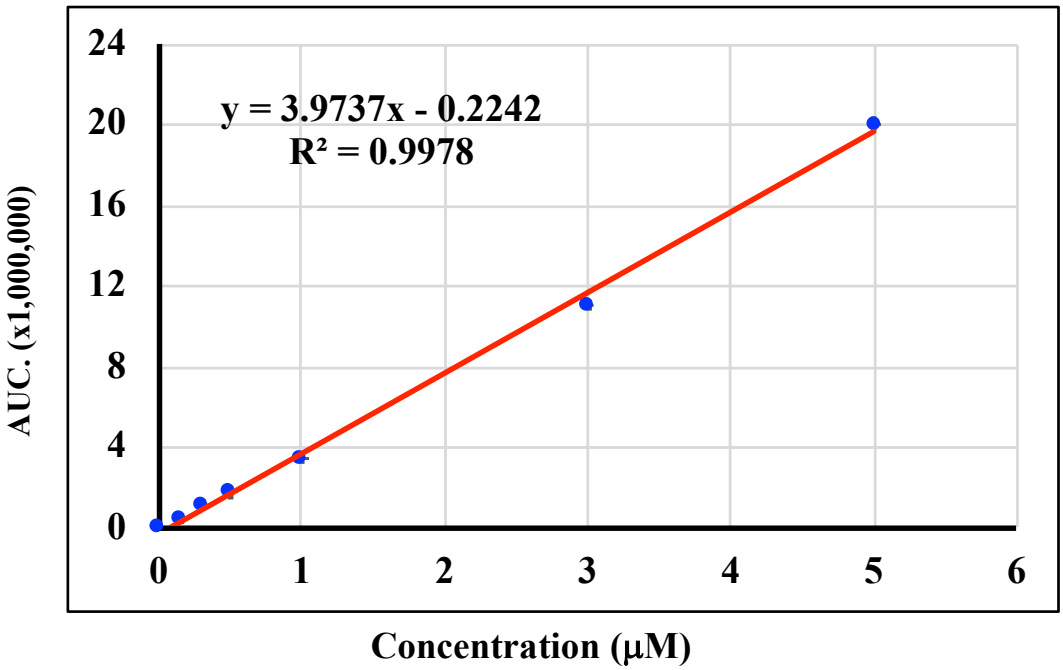

Figure 25. Q- TOF LC/MS AUC linear regression analysis of Doxorubicin data. X= concentrations range from 5 µM – 150 nM, y= average of intensities of m/z 544 Da.

Area % Report

Data File: C:\Users\UPLC system 2\Desktop\Qamar\5000nM2019-03-19 12-59-01 (GMT -07-00).dat
Method: C:\Enterprise\Projects\Hitachi\Method\Doxo_1.met
Acquired: 3/19/2019 1:00:16 PM (GMT -07:00)
Printed: 3/19/2019 3:09:08 PM (GMT -07:00)

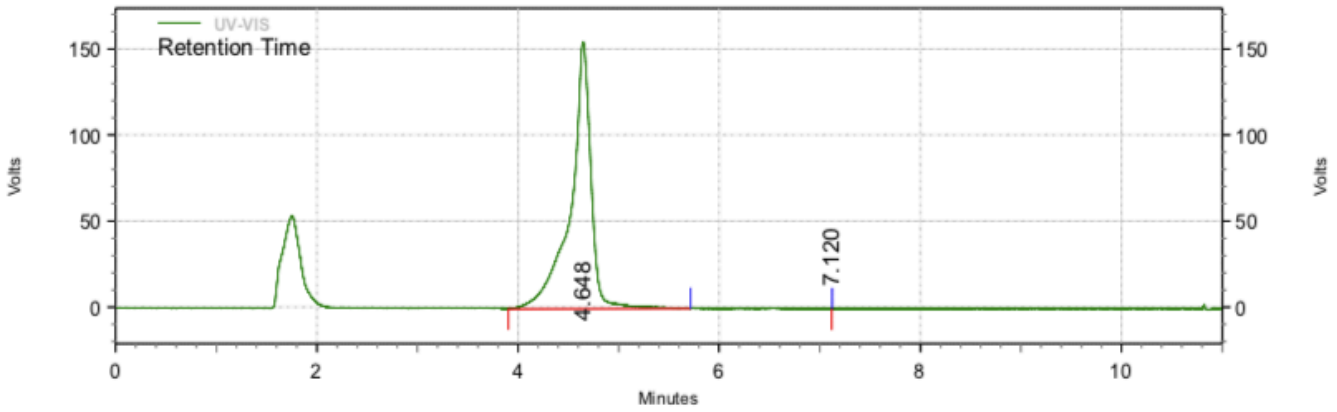

UV-VIS Results

Retention Time	Area	Area %	Height	Height %
4.648	8753330	100.00	620619	100.00
7.120	17	0.00	0	0.00
Totals	8753347	100.00	620619	100.00

Figure 26. Analytical HPLC chromatograph result for the AUC of doxorubicin at the concentration of 5µM (which is considered to be the maximum concentration limit), the UV detection at 483 nm.

Area % Report

Data File: C:\Users\UPLC system 2\Desktop\Qamar\150nM2019-03-19 10-53-22 (GMT -07-00).dat
Method: C:\Enterprise\Projects\Hitachi\Method\Doxo_1.met
Acquired: 3/19/2019 10:54:45 AM (GMT -07:00)
Printed: 3/19/2019 2:54:37 PM (GMT -07:00)

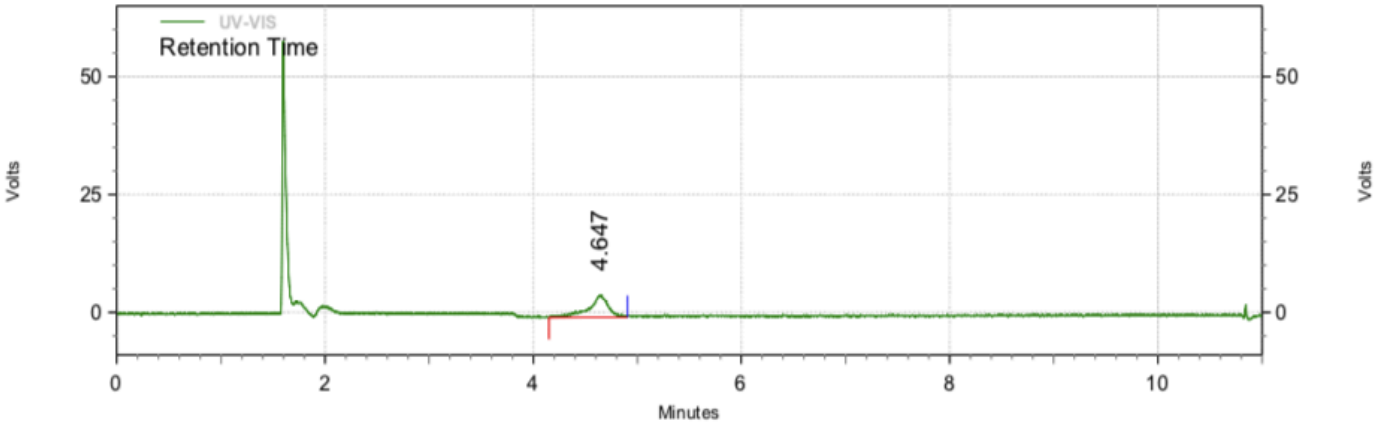

UV-VIS Results

Retention Time	Area	Area %	Height	Height %
4.647	253421	100.00	19015	100.00
Totals	253421	100.00	19015	100.00

Figure 27. Analytical HPLC chromatograph result for the AUC of doxorubicin at the concentration of 150 nM (which is considered to be the minimum concentration limit), the UV detection at 483 nm.

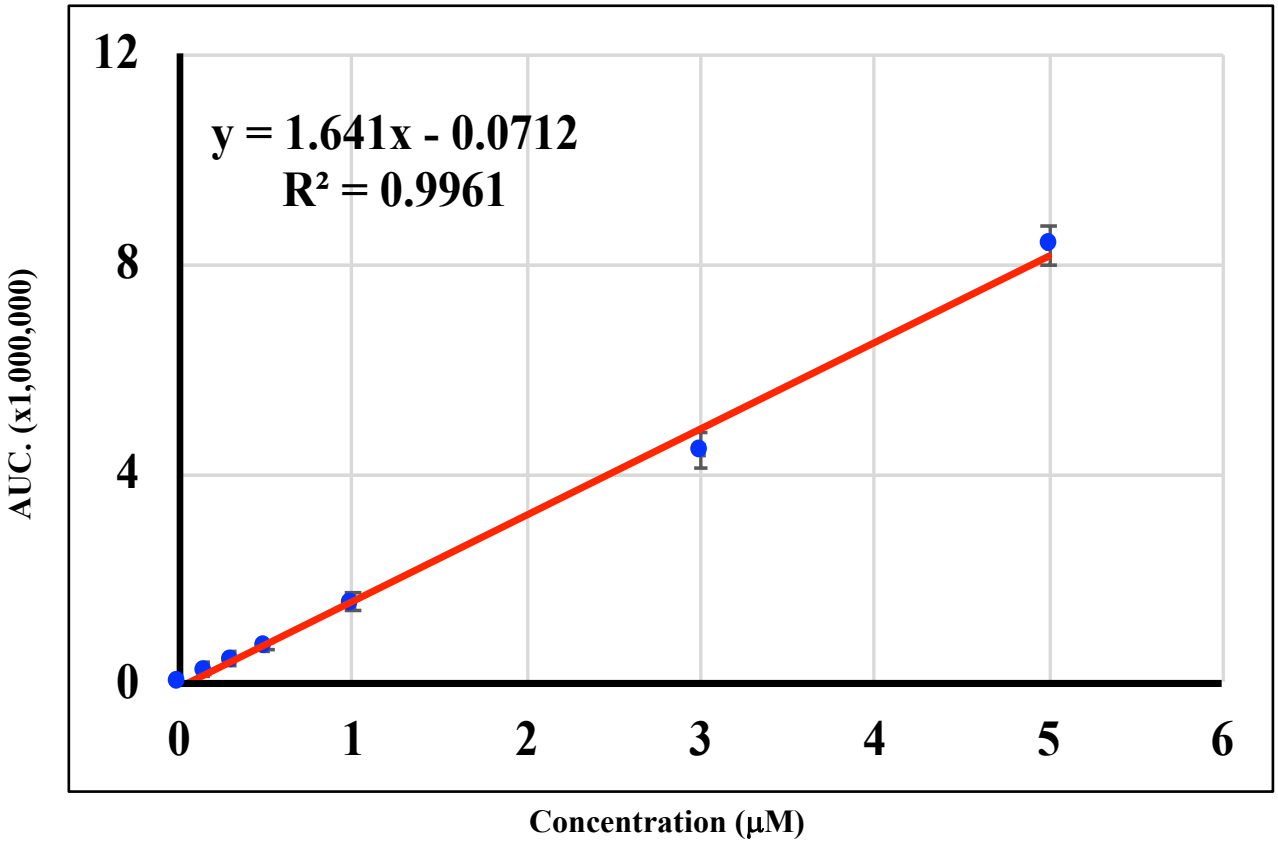

Figure 28. Linear regression analysis of doxorubicin HPLC - UV AUC data. X= concentrations range from 5 µM – 150 nM, y= average of intensities of 483 nm.

3.3 Spectral Imaging

3.3.1 Rhodamine Spectral Imaging result

The spectral imaging measurements were conducted by using SKY filter for pure rhodamine 6G fluorescence wavelength at ~ 580 nm which was detected using spectrophotometer. However, pure Rhodamine (dye alone) with spectral imaging system gives an additional wavelength peak at ~ 670 nm which we didn't identified yet (Fig 29b). These wavelengths were uploaded and saved as libraries for further treated cell analysis.

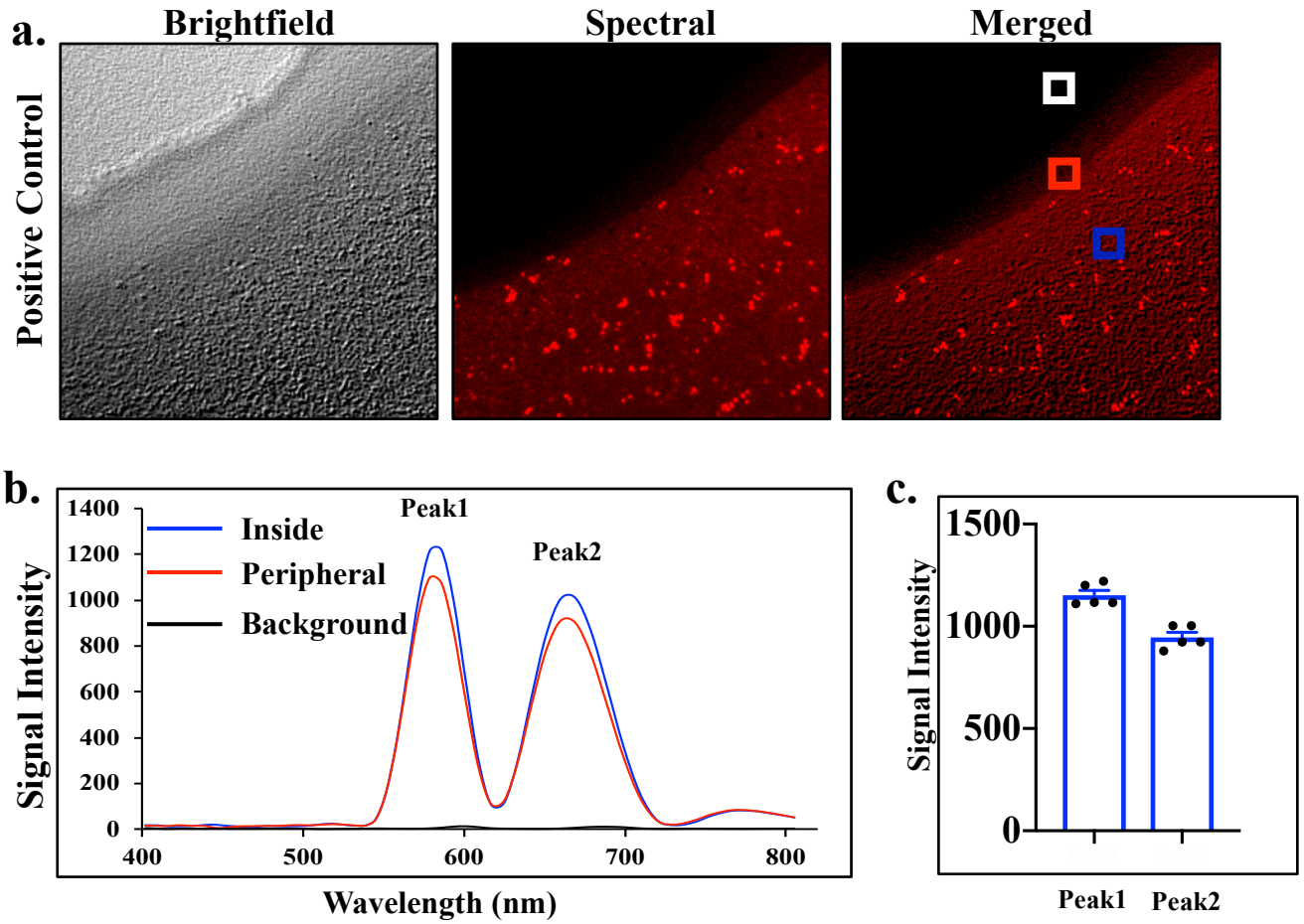

Figure 29. (a) Pure Rhodamine 6G brightfield image by using brightfield filter, spectral image by using SKY filter which represents the uploaded Rhodamine library analysis and merged image which is merged between brightfield and spectral images. (b) The graph represents pure Rhodamine 6G fluorescence wavelength at ~ 580 nm, 670 nm, X= wavelengths (580, 670 nm) and Y= signal intensity. Inside represents the area that contains brighter fluorescence dye and higher intensity in comparing with the peripheral zone, while background showed the wavelength of the background area of rhodamine. (c) The bars showed the intensity variation of the data point for peak1 which is higher than peak2.

Fig 29a showed the brightfield image of pure Rhodamine obtained by using brightfield filter, a spectral image which was done by using SKY filter. Its represent the uploaded wavelength library analysis, and merged image that merged between brightfield and spectral images. The graph in Fig 29b represents different fluorescence wavelengths of pure rhodamine 6G at ~ 580 nm, 670 nm. The inside showed the area that has brighter fluorescence dye and higher wavelength intensity in comparison to the peripheral area, background showed the wavelength intensity of the chemical background. In addition, the bars (Fig 29c) illustrate the intensity data point variation of peak1 which is higher than peak2. Furthermore, analysis of the cell that treated with rhodamine 6G was also conducted in this research. Cells were treated at different concentrations starting with 0.2 nM as the minimum concentration detectable by Q- TOF (Table 4) for 18 hrs and then the cells were fixed for spectral imaging analysis. Fig 30a represented the brightfield, spectral and merged images of the negative control which is untreated cells. Fig 30b showed the difference between cytoplasm and nucleoplasm wavelength which are considered to be background in compare with the positive control (pure dye). In order to show the saturation area inside the cells, 100 μM of Rhodamine 6G was used to treat the cells for 18 hrs. Fig 31a showed the brightfield image, a spectral image (by using SKY filter) which is the result of the uploaded libraries of pure Rhodamine and merged images of the cells that treated with 100 μM of the dye. The spectral image also showed the rhodamine location in the cell which is specified in the cytoplasm. Fig 31b illustrates different fluorescence wavelengths of 100 μM treated cells at ~ 580 nm, 670 nm, which are consistent with pure dye results. However, there is an additional small peak at ~ 530 nm which we didn't identify it yet. Blue wavelength represented the cytoplasm rhodamine spectrum, and red wavelength showed the spectrum of rhodamine in the cell nucleoplasm. The bars **(Fig 31c)** illustrate the

intensity data point diversity of peak1 which is higher than peak2, and this diversity was consistent with peaks variations of the pure rhodamine.

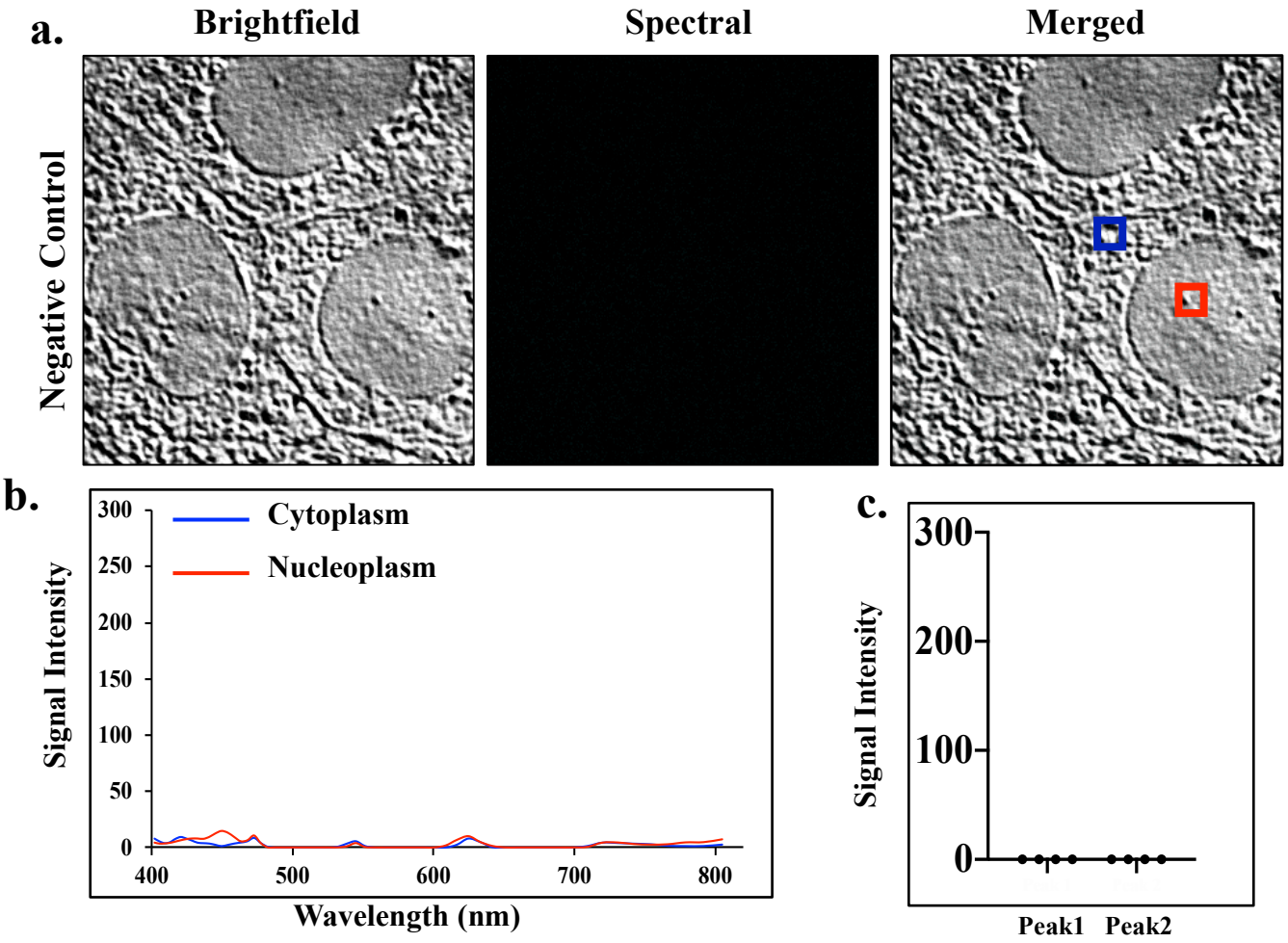

Figure 30. (a) Negative control of the untreated cells brightfield image by using brightfield filter, spectral image by using SKY filter and merged image which is merged between brightfield and spectral images. (b) The graph represents negative control fluorescence wavelengths which are considered to be a background in comparing with the positive control, X= wavelengths and Y= signal intensity. (c) The bars showed the intensity variation of the data point for untreated cells.

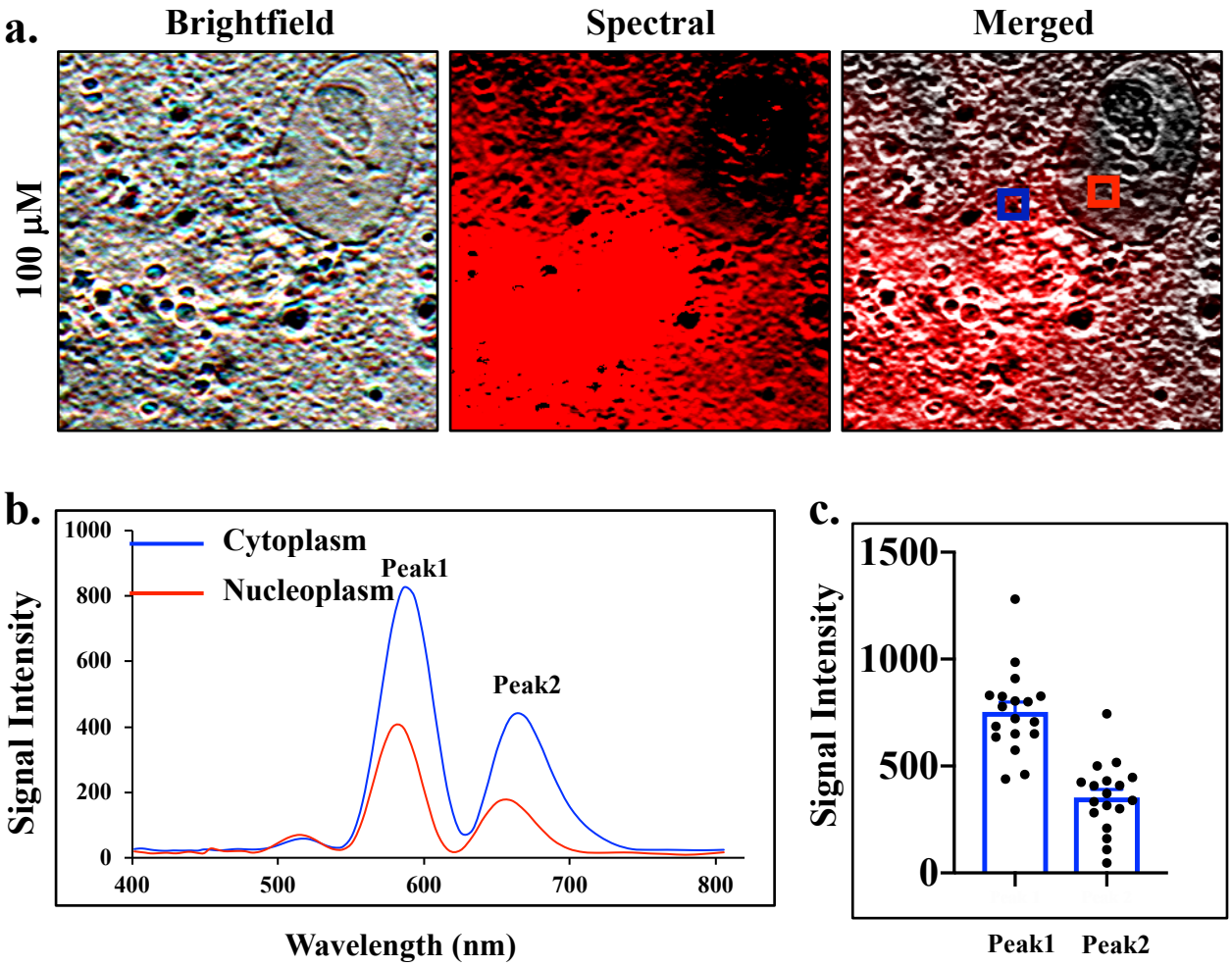

Figure 31. (a) Brightfield image of treated cells with 100 µM of Rhodamine 6G image by using brightfield filter, spectral image by using SKY filter which represented the result of uploaded Rhodamine library and the saturation area is showing in the lower left part of the image. The spectral image also showed the rhodamine location in the cell which is specified in the cytoplasm. The merged image which is a combination of brightfield and spectral images. (b) The graph represented Rhodamine 6G fluorescence wavelength at ~ 580 nm, 670 nm inside the cells, X= wavelengths and Y= signal intensity. The blue wavelength shows the area that contains Rhodamine fluorescence which is in the cytoplasm, while the red wavelength represents the spectrum of the area in the cell nucleoplasm. (c) The bars showed the intensity variation of the data point for peak1 which is higher than peak2, and this variation in consistent with pure dye data pint results.

Forward, we treated the cells with 0.2 nM of rhodamine which is considered to be the maximum limit to detect this dye in comparison with Q- TOF. Fig 32a demonstrated the brightfield image, spectral image which is the result of the uploaded libraries of pure Rhodamine and merged images of the cells that treated with 0.2 nM of the dye. Fig 32b showed different fluorescence wavelengths of 0.2 nM treated cells at ~ 580 nm, 670 nm, which are consistent with pure and 100 μM dye results. The blue wavelength represents the cytoplasm spectrum of Rhodamine and red wavelength showed the spectrum of the cell nucleoplasm. The bars in Fig 32c explained the variety of intensity data point of peak1 which is higher than peak2, and this variation consistent with peaks variations of the pure and 100 μM rhodamine results. In addition, the intensities at this concentration become lower than pure and 100 μM Rhodamine samples which are expected since we prepare lower concentrations. Since rhodamine can be detectable at a concentration of 0.2 nM, we treated cells with much lower concentration at 0.08 nM. Fig 33a showed the brightfield image by brightfield filter, spectral image which is the result analysis of the uploaded libraries of pure Rhodamine (the system also showed rhodamine location in the cell which is in the cell cytoplasm) and merged images of the cells that were treated with 0.08 nM of the dye. Fig 33b demonstrated different fluorescence wavelengths of 0.08 nM treated cells at ~ 580 nm, 670 nm, which are consistent with pure, 100 μM and 0.2 nM dye results. Blue wavelength clarifies the cytoplasm spectrum of Rhodamine and red wavelength showed the spectrum of the nucleoplasm of the sample. The bars in Fig 33c interpreted the data point intensity variation of peak1 which is higher than peak2, this variation consistent with peaks variations of the pure, 100 μM and 0.2 nM Rhodamine results.

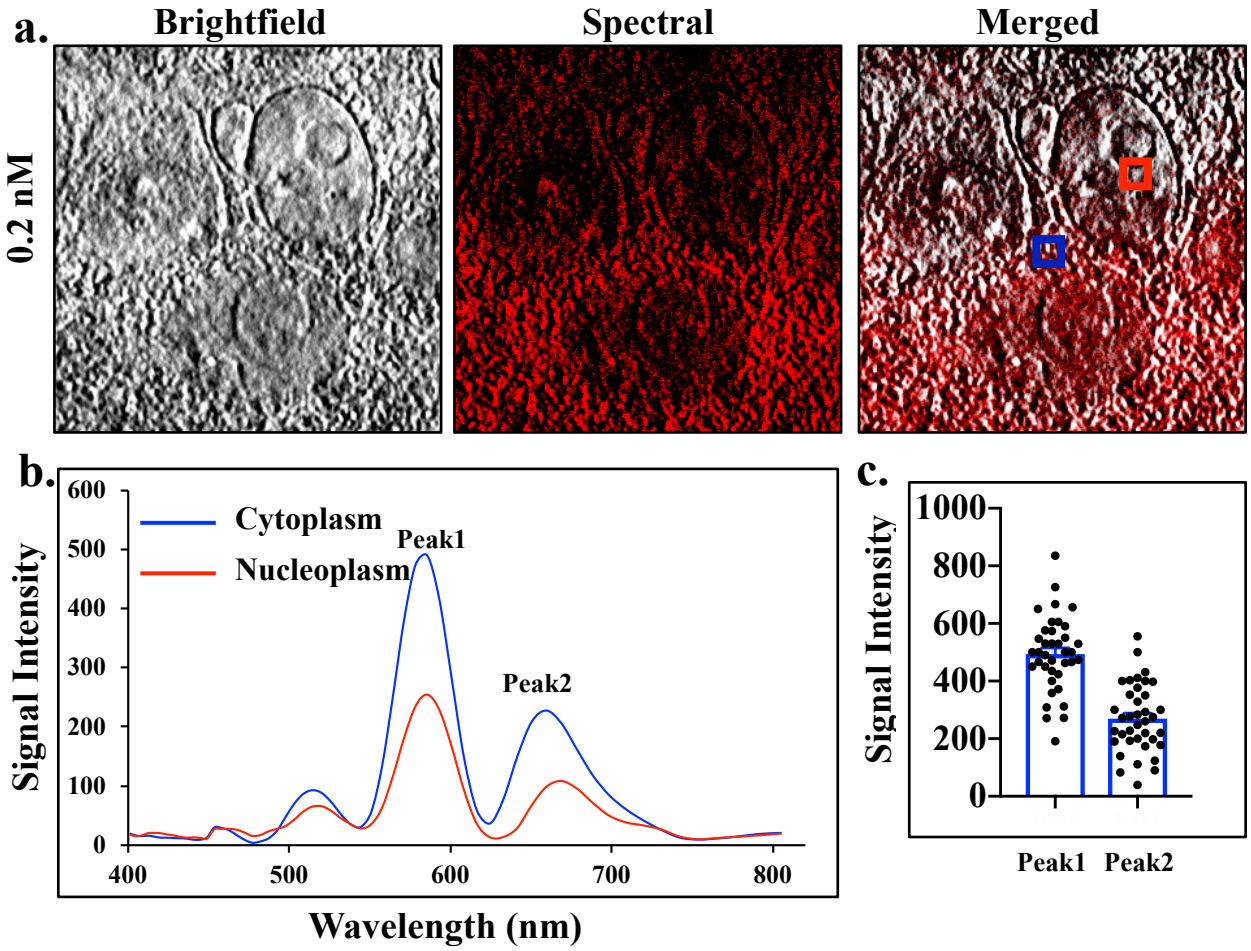

Figure 32. (a) Cells treated with 0.2 μM of Rhodamine 6G brightfield image by using brightfield filter, spectral image by using SKY filter which represented the result of uploaded rhodamine library and merged image which is a combination of brightfield and spectral images. (b) The graph represented Rhodamine 6G fluorescence wavelength at ~ 580 nm, 670 nm inside the cells, X= wavelengths and Y= signal intensity. The blue wavelength explained the area that contains Rhodamine fluorescence which is in the cytoplasm, while red wavelength showed the spectrum of the area which was in cell nucleoplasm. (c) The bars showed the intensity variation of the data point for peak1 which is higher than peak2, and this variation in consistent with pure dye data pint results. The intensities here become lower in comparing with pure and 100 μM rhodamine since we prepared lower concentration.

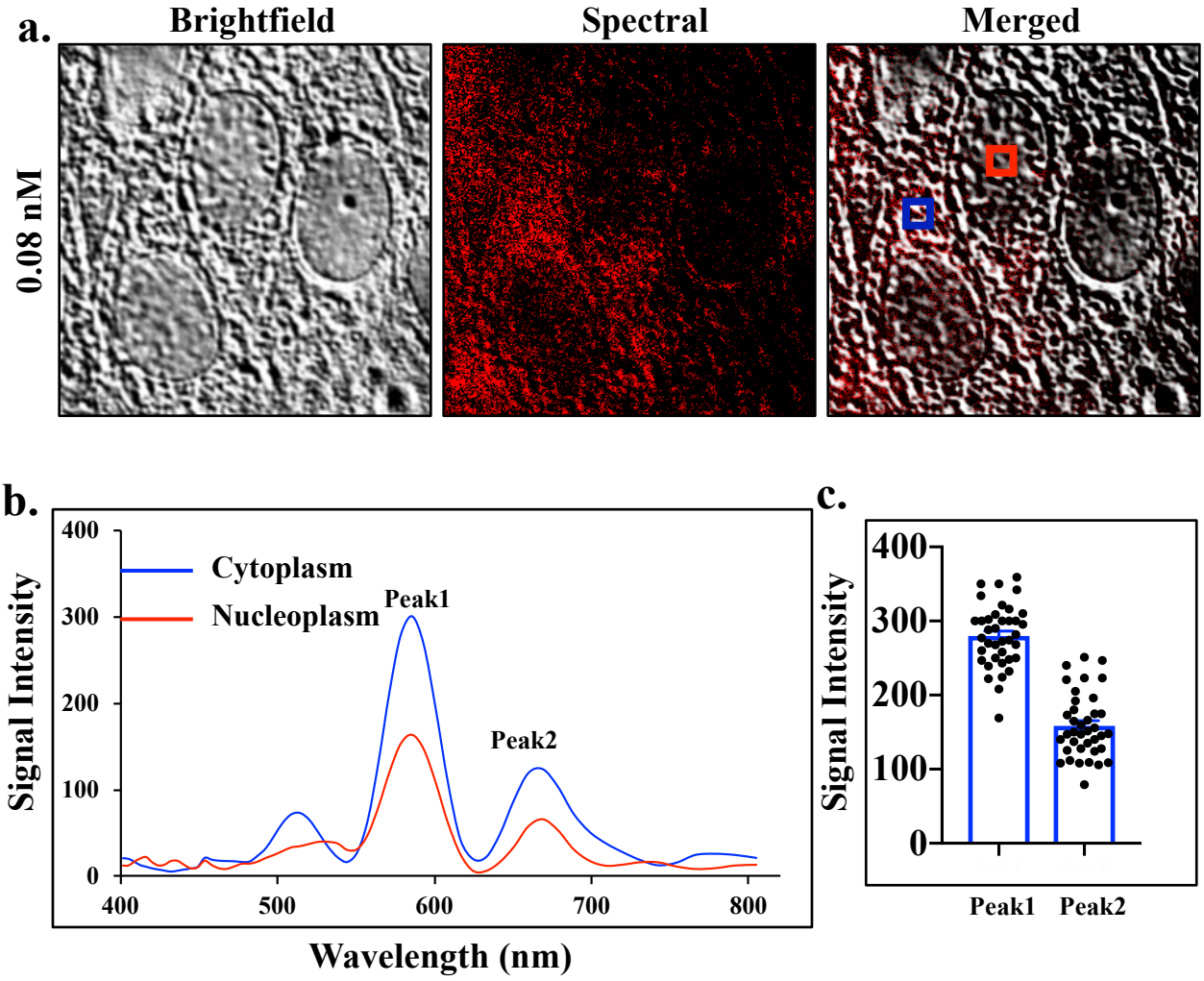

Figure 33. (a) Brightfield image of the cells that treated with 0.08 µM of Rhodamine 6G by using brightfield filter, spectral image by using SKY filter which represented the result of uploaded Rhodamine library and merged image which is a combination of brightfield and spectral images. (b) The graph represented Rhodamine 6G fluorescence wavelength at ~ 580 nm, 670 nm inside the cells, X= wavelengths and Y= signal intensity. The blue wavelength showed the area that contains Rhodamine fluorescence which is in the cytoplasm, while red wavelength explained the spectrum of the cell nucleoplasm. (c) The bars illustrated the data point intensity variation of peak1 which is higher than peak2, this variation consistent with peaks variations of the pure, 100 µM and 0.2 nM rhodamine results. The intensities here become lower in comparing with pure and 100 µM rhodamine since we prepare lower concentration.

Then, we treated cells with 0.01 nM of rhodamine for further analysis. Fig 34a interpreted the brightfield image which has been done by brightfield filter, a spectral image which is considered to be the result analysis of the uploaded libraries of pure Rhodamine. The spectral image also illustrates the dye location in the cell which is in the cytoplasm. The merged image is a combination of spectral and brightfield images of 0.01 nM Rhodamine. Fig 34b showed different fluorescence wavelengths of 0.01 nM treated cells at ~ 580 nm, 670 nm, which are consistent with pure, 100 μM, 0.2 and 0.08 nM dye results. The blue wavelength illustrated the spectrum of cytoplasm which contains rhodamine, and the red wavelength showed the spectrum of the cell nucleoplasm. The bars in Fig 34c demonstrated the diversity of intensity data point of peak1 which is higher than peak2, this variety consistent with peaks variations of the pure, 100 μM 0.2 and 0.08 nM rhodamine data. The intensities here become much lower in compare with higher concentration points. Therefore, 0.01 nM consider being be the minimum detectable concentration of rhodamine 6G by the spectral imaging system in comparing with 0.2 nM which is the minimum concentration to detect by Q- TOF system. Furthermore, we conducted a linear regression analysis to check the validity of our data point of Rhodamine 6G. Fig 35a represented the linearity result of the average intensities of peak 1 vs log of different concentrations in M, the data showed a good linear relationship result at R^2= 0.85. Therefore, we can consider it as a stander peak for Rhodamine in this research. While Fig 35b illustrated the linear relationship between the average intensities of peak 2 and the log of concentrations in M, it showed less linearity in comparing with peak 1 at R^2= 0.72. Fig 35c demonstrated the linearity of the ratio of average intensities for peak 1/peak 2, the linear relationship between these data point is less in comparing with peak 1 and peak 2 at R2= 0.17.

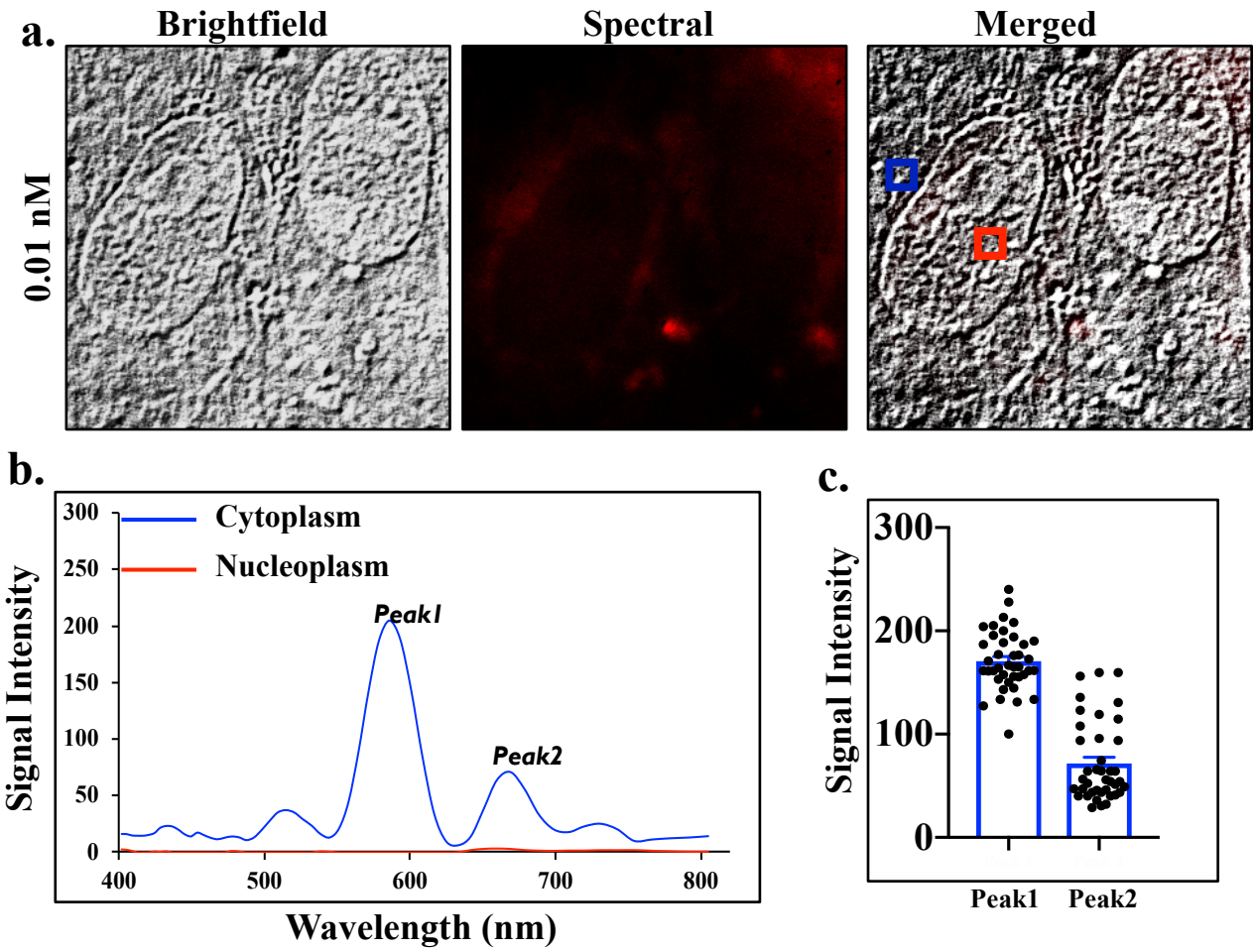

Figure 34. (a) Cells treated with 0.01 µM of Rhodamine 6G brightfield image by using brightfield filter, spectral image by using SKY filter which clarified the result of uploaded Rhodamine library and merged image of both brightfield and spectral images. (b) The graph showed Rhodamine 6G fluorescence wavelength at ~ 580 nm, 670 nm in the cells, X= wavelengths and Y= signal intensity. The blue wavelength described the area that has Rhodamine fluorescence which is the cytoplasm, while red wavelength demonstrated the spectrum of the nucleoplasm. (c) The bars interpret the data point intensity variation of peak1 which is higher than peak2, this diversity consistent with peaks variations of the pure, 100 µM, 0.2 and 0.08 nM Rhodamine data. The intensities here also become lower in comparing with higher concentrations of rhodamine. Therefore, 0.01 nM consider being be the minimum detectable concentration of rhodamine by spectral imaging.

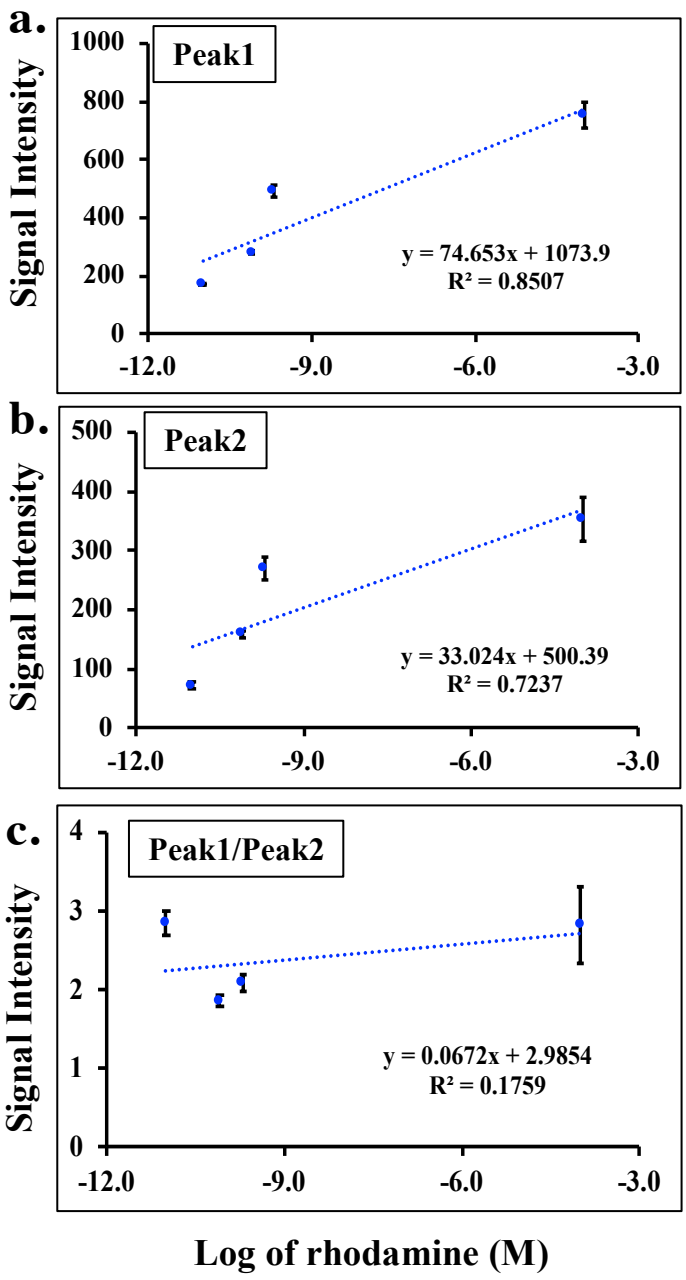

Figure 35. Linear regression analysis of Rhodamine 6G data by spectral imaging. X= log of concentrations in M, Y= average of signal intensity. (a) The graph represented the average intensities of peak 1 (~ 580 nM) vs the concentrations, and here we can consider peak 1 because of its show good linearity at R^2= 0.85. (b) This graph demonstrated the peak 2 average intensities, it showed less linearity in comparing with peak 1 at R^2= 0.72. (c) illustrated the ratio of average intensities for peak 1/peak 2, which has less linearity in comparing with peak 1 and peak 2 at R^2= 0.17.

3.3.2. Doxorubicin Spectral Imaging Result

Since spectral imaging system was able to identify the amount and location of Rhodamine 6G within cell samples, we further tested another chemical with the same approach. To check pure Doxorubicin fluorescence wavelength, spectral imaging was conducted by using SKY filter to have the spectrum at ~ 592 nm which is consistent with the spectrophotometer fluorescence spectrum. However, an additional wavelength peak at ~ 670 nm also appears with Doxorubicin which we didn't identify this peak yet (Fig 36b). For cell analysis, these wavelengths were uploaded and saved as libraries files. As shown in Fig 36a brightfield filter was used to capture brightfield image of pure Doxorubicin, used SKY filter to capture the spectral image, it represent the analysis of uploaded wavelengths library and merged image that combined between brightfield and spectral images. The graph in Fig 36b illustrated pure Doxorubicin fluorescence wavelength at ~ 592 nm, 670 nm. The inside interprets the area that contains higher wavelength intensity based on brighter chemical fluorescence in comparing with the peripheral area which contains less. The background showed the wavelength intensity of the chemical background area, which should be any spectrum but not doxorubicin spectrum. In addition, the bar graph Fig 36c showed the variety of intensity data point result of peak1 which is higher than peak2. Next, we treated the cells with different concentrations of Doxorubicin, starting with 150 nM since it was the maximum detectable concentration limit by Q- TOF. Fig 37a displayed the negative control images which are untreated cells, starting with brightfield image by brightfield filter, spectral image by SKY filter and merged images. Fig 37b showed wavelength differences between cytoplasm and nucleoplasm which reflect the background in comparing with the positive control (pure Doxorubicin).

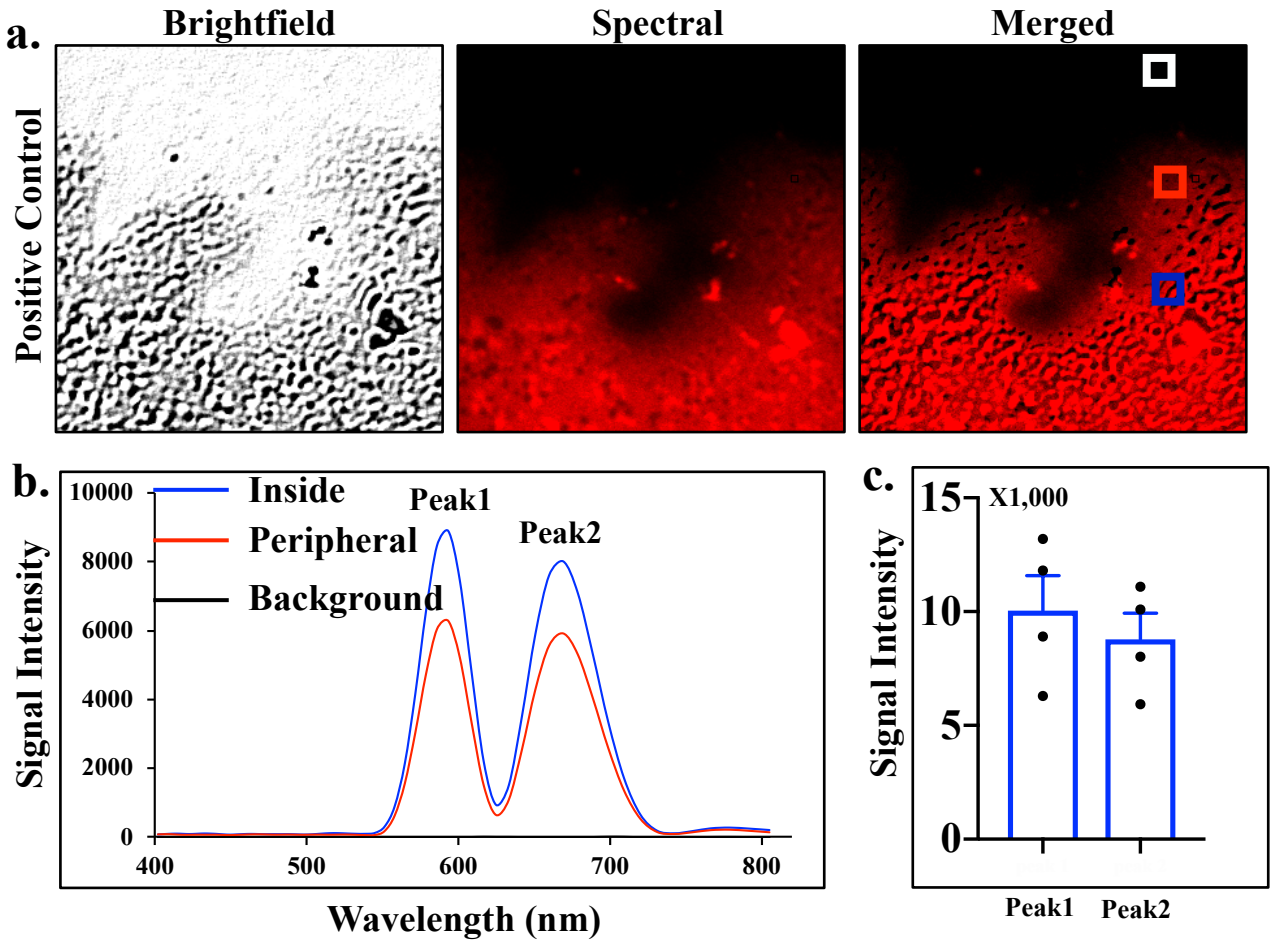

Figure 36. (a) Brightfield image of pure Doxorubicin by using brightfield filter, spectral image by using SKY filter which exemplified the analysis of uploaded library and merged image which combines between brightfield and spectral images. (b) The graph demonstrated the fluorescence wavelength of pure Doxorubicin at ~ 592 nm, 670 nm, X= wavelengths, and Y= signal intensity. Inside showed the area that covers higher intensity and brighter chemical fluorescence in comparing with the peripheral zone whereas background displayed Doxorubicin wavelength of the background region. (c) The bar graph exhibited the variation of the intensity data point result for peak1 which is higher than peak2.

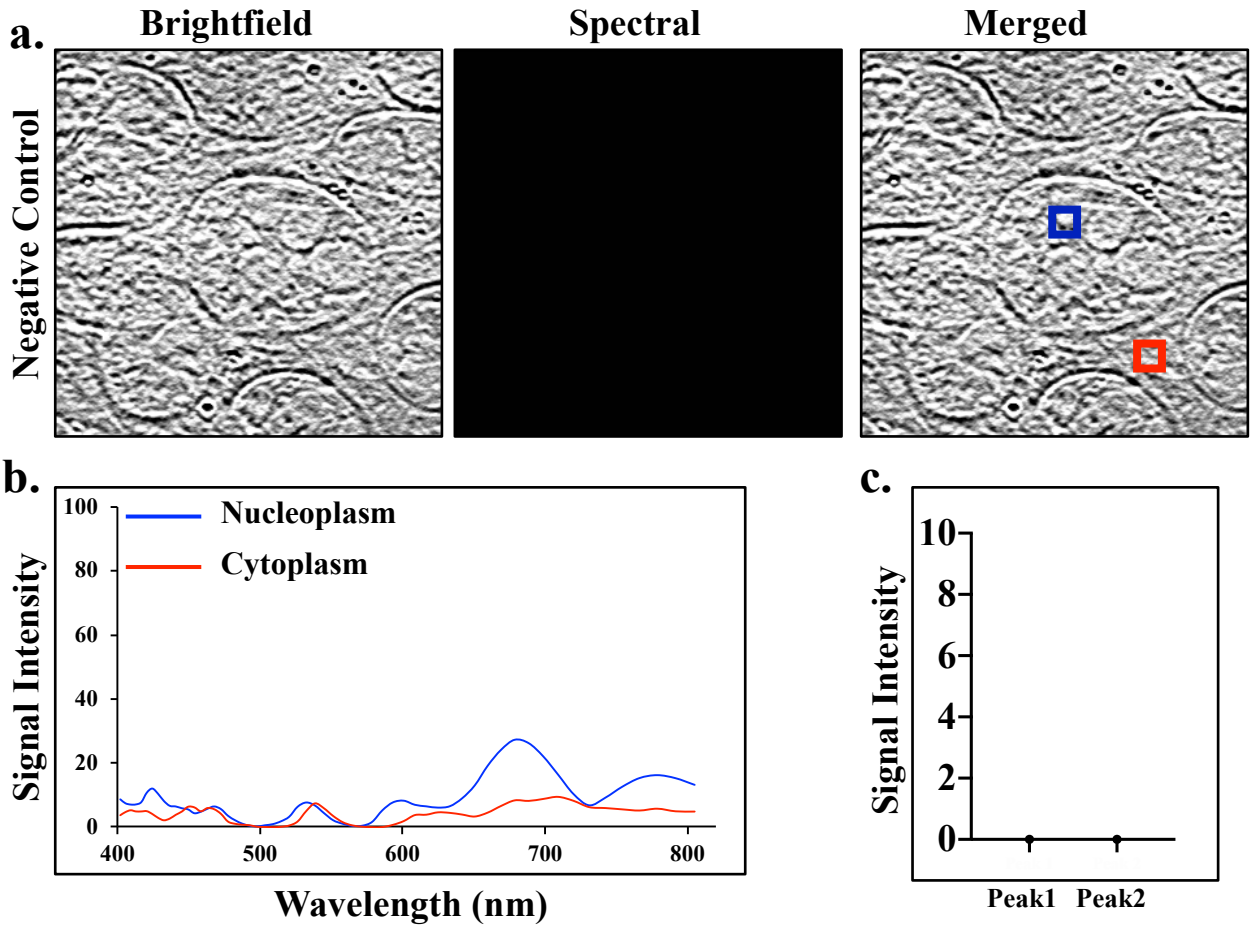

Figure 37. (a) Untreated cells which are considered to be the negative control in the study. The brightfield image captured by using brightfield filter, spectral image by using SKY filter and merged image which combined between brightfield and spectral images. (b) The graph illustrated the fluorescence wavelengths of the negative control which reflect the background in comparing with positive control. X= wavelengths and Y= signal intensity. (c) The bars indicated the data point of the intensity variation for untreated cells.

Cells treated with 150 nM of Doxorubicin are shown in Fig 38a as brightfield image which was taken with brightfield filter, spectral image by SKY filter which is the result of the uploaded libraries of pure Doxorubicin and merged of brightfield and spectral images. The spectral image revealed Doxorubicin location in the cell which is specified in the nucleoplasm. Fig 38b exhibited different fluorescence wavelengths of 150 nM treated cells at ~ 592, 670 nm, which are consistent with the pure chemical results. However, there is an additional small peak at ~ 520 and we didn't yet identify this peak. The blue wavelength represents the nucleoplasm spectrum of Doxorubicin, and red wavelength showed the background spectrum which is cell cytoplasm. The bar graph in Fig 38c illustrated the variety of intensity data point results of peak1 which is higher than peak2, this variety consistent with peaks variations of the pure Doxorubicin. Furthermore, we treated cells with lower concentrations of Doxorubicin, 100 nM Fig 39, 10 nM Fig 40 and 1 nM fig 41. At all of these figures, (a) represented the brightfield image that captured by brightfield filter, a spectral image which is the results of uploaded library analysis done by using SKY filter and merged image which is combine between spectral and brightfield images. (b) The graph showed different wavelength intensities of 592 and 670 nm based on the location. The blue spectrum displayed the area that has Doxorubicin in the sample, and the red spectrum exhibits the background region which is cytoplasm. (c) The bars explained the intensity data point variation for peak 1 that is higher than peak 2, the variation consistent with pure, 150 nM of doxorubicin. In general, within cell samples, the intensities become lower at each concentration 150 – 1 nM in comparing with pure Doxorubicin.

Linear regression analysis performed to check the validity of our data point of Doxorubicin. Fig 42a showed the linearity result of the average intensities of peak1 vs log of different concentrations, the data displayed an excellent linear relationship result at R^2= 0.93. Therefore, we can consider it as a standard peak for Doxorubicin in this study. While Fig 42b demonstrated the linear relationship between the average intensities of peak 2 and the log of concentrations. It displayed less linearity in comparison with peak 1 at R^2= 0.76. In addition, Fig 43a illustrated the linearity of the ratio of average intensities for peak 1/peak 2, the linear relationship between these data point is less as compared with peak1 and peak2 at R^2= 0.62. The graph in Fig 43b showed the percentage of the abnormal cells (specifically abnormal nucleoplasm) of the samples, this done by counting the abnormal nucleoplasm at each sample image, the percentage of the abnormality increases with higher concentrations of Doxorubicin.

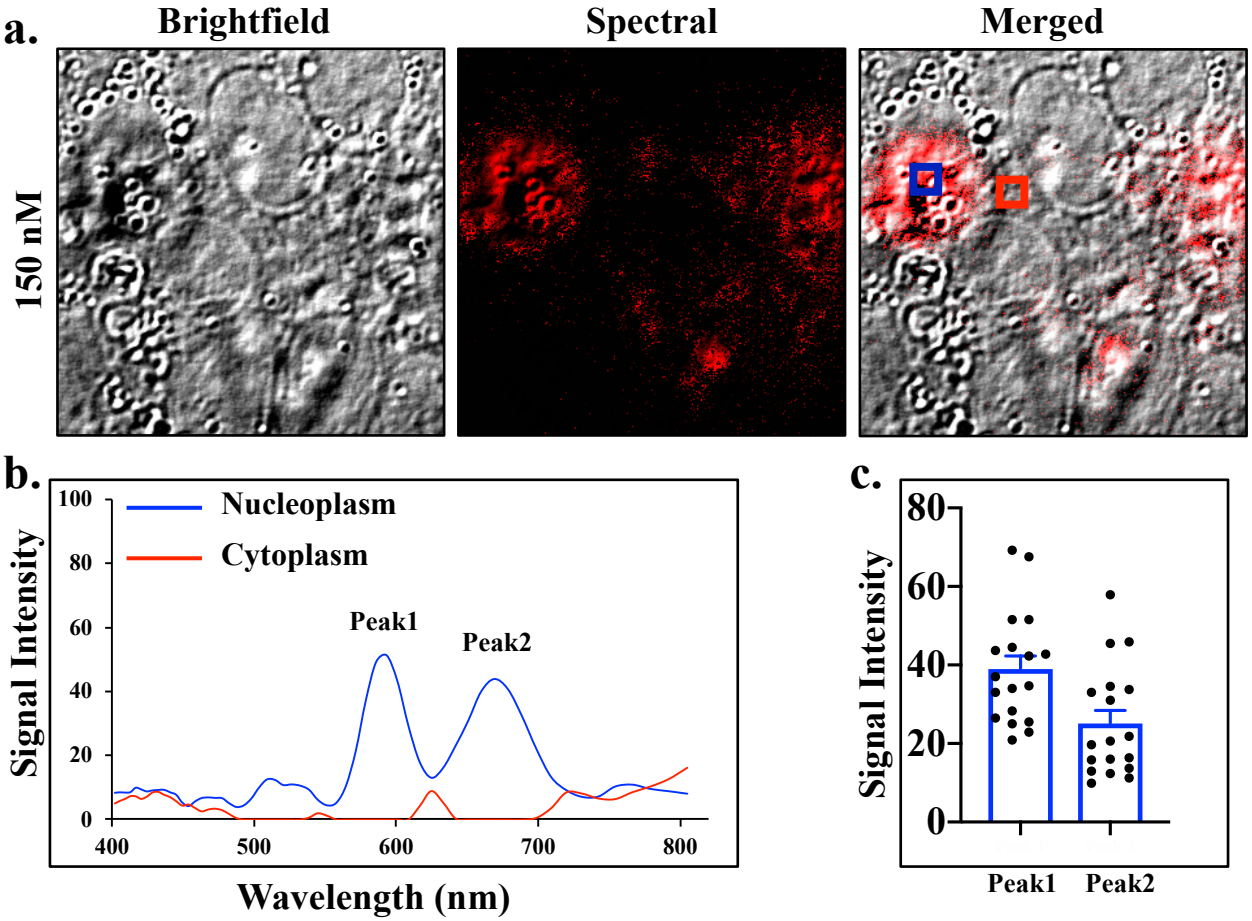

Figure 38. (a) Brightfield image of the cells which are treated with 150 nM of Doxorubicin by using brightfield filter, spectral image by using SKY filter which displayed the result of uploaded doxorubicin library and merged image of brightfield and spectral images. (b) The graph represented Doxorubicin fluorescence wavelength at ~ 592 nm, 670 nm inside the cells, X= wavelengths and Y= signal intensity. The blue wavelength shows the region that contains Doxorubicin fluorescence which is in the nucleoplasm, whereas red wavelength illustrated the spectrum of the background area which is cell cytoplasm. (c) The bar graph explained the intensity data point variety for peak1 which is higher than peak2 and this variation in consistent with pure Doxorubicin data results. The intensities here become lower in comparing with pure Doxorubicin since we prepared lower concentration.

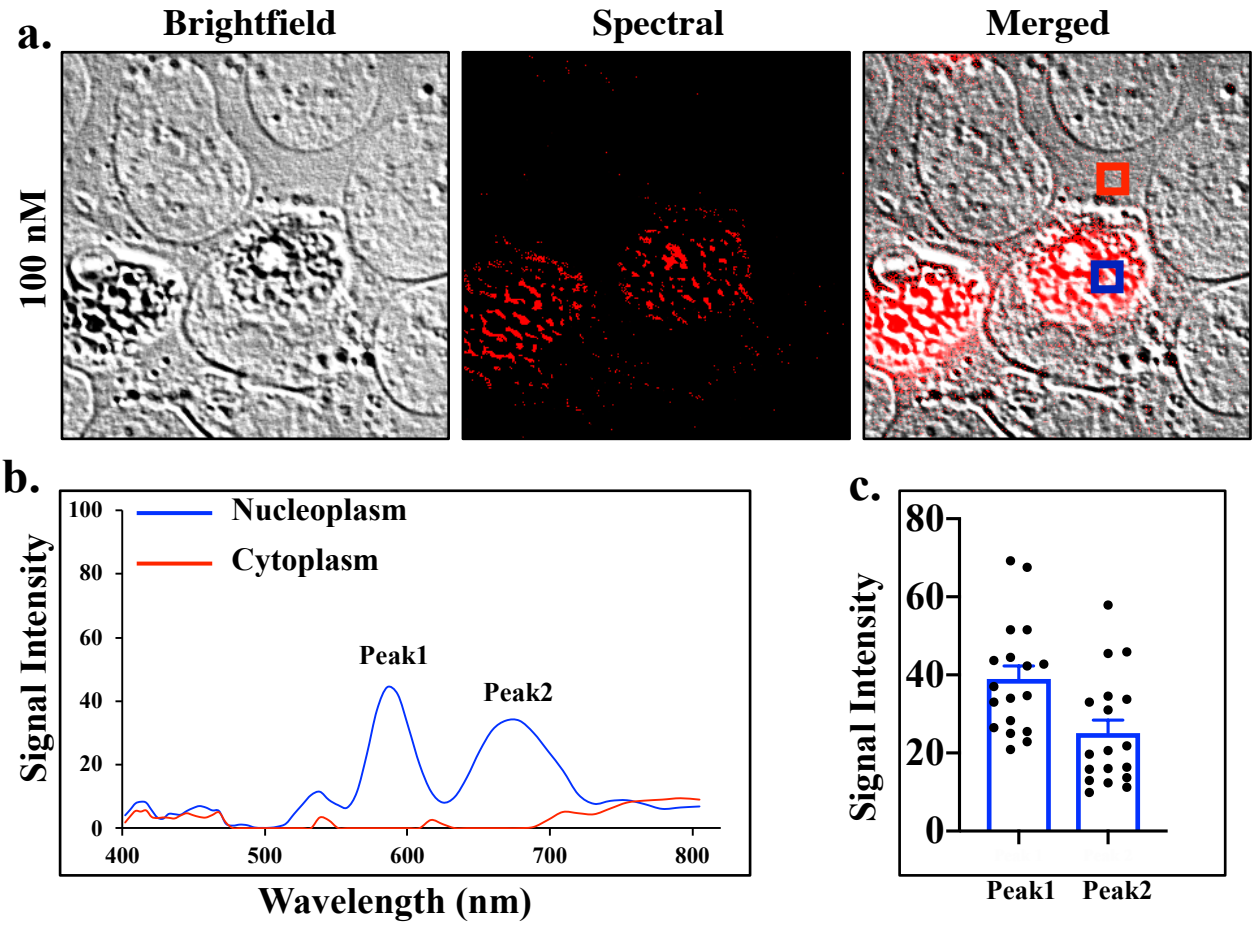

Figure 39. (a) Cell samples that treated with 100 nM of Doxorubicin, brightfield image done by using brightfield filter, spectral image by SKY filter which showed the result of uploaded Doxorubicin library and merged image between of brightfield and spectral images. (b) The graph illustrated Doxorubicin fluorescence wavelength at ~ 592 nm, 670 nm inside the cells, X= wavelengths and Y= signal intensity. The blue wavelength displays the area that contains Doxorubicin fluorescence which is in the nucleoplasm, while red wavelength showed the spectrum of the background region which is cell cytoplasm. (c) The bar graph explained the intensity data point variation for peak1 which is higher than peak2, and this variation in consistent with pure, 150 nM of Doxorubicin results. The intensities here become lower in comparing with pure, 150 nM Doxorubicin.

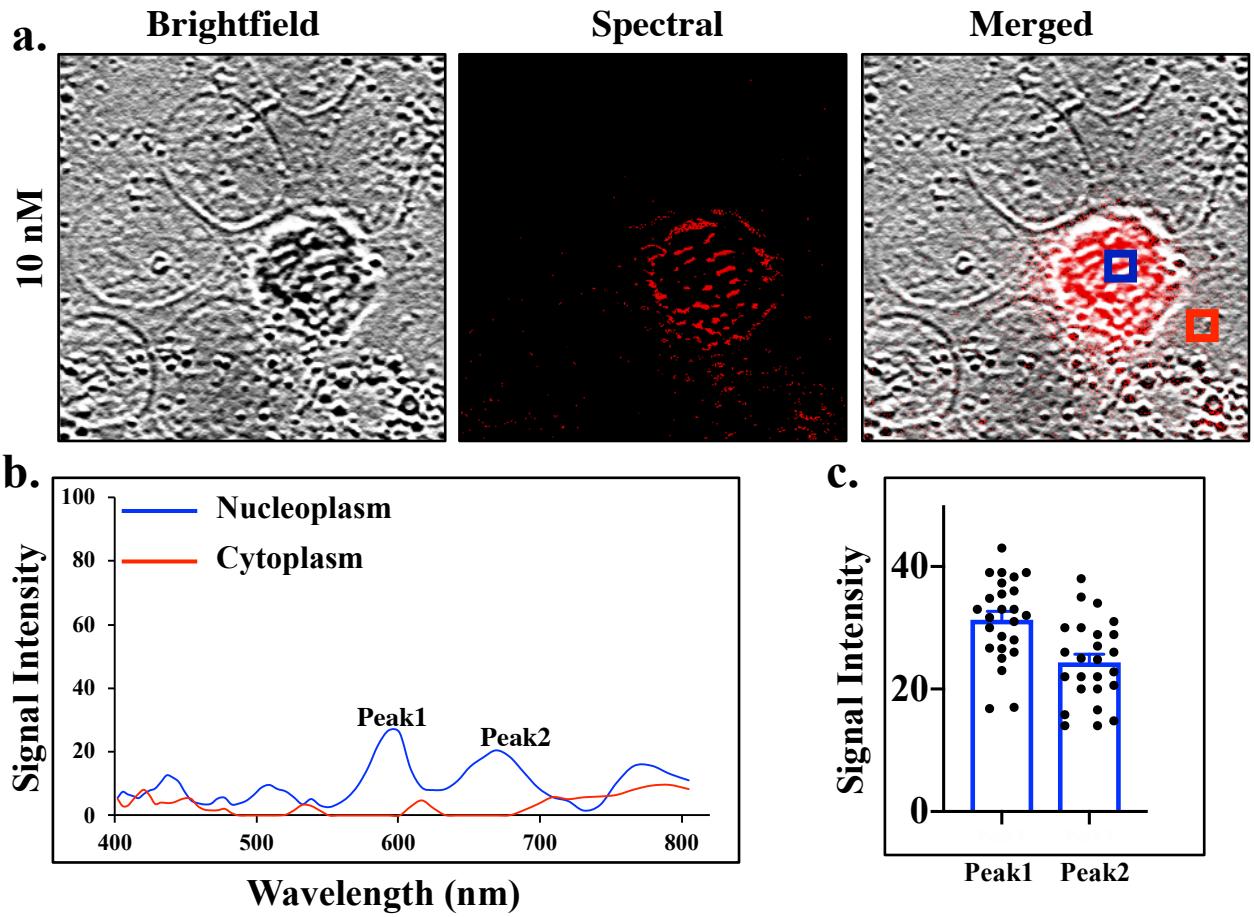

Figure 40. (a) Brightfield image is done by brightfield filter of cells that treated with 10 nM of Doxorubicin, spectral image by SKY filter which displayed the uploaded Doxorubicin library result and merged image of brightfield and spectral images. (b) The graph showed Doxorubicin fluorescence wavelength at ~ 592 nm, 670 nm inside the cells, X= wavelengths and Y= signal intensity. The blue wavelength illustrated the area that contains Doxorubicin fluorescence which is in the nucleoplasm, while red wavelength showed the spectrum of the background area which is in the cytoplasm. (c) The bar graph displayed the variation of intensity data point for peak1 that is higher than peak2, this variation in consistent with pure, 150, 100 nM of Doxorubicin results. The intensities here become lower in comparing with pure, 150, 100 nM Doxorubicin.

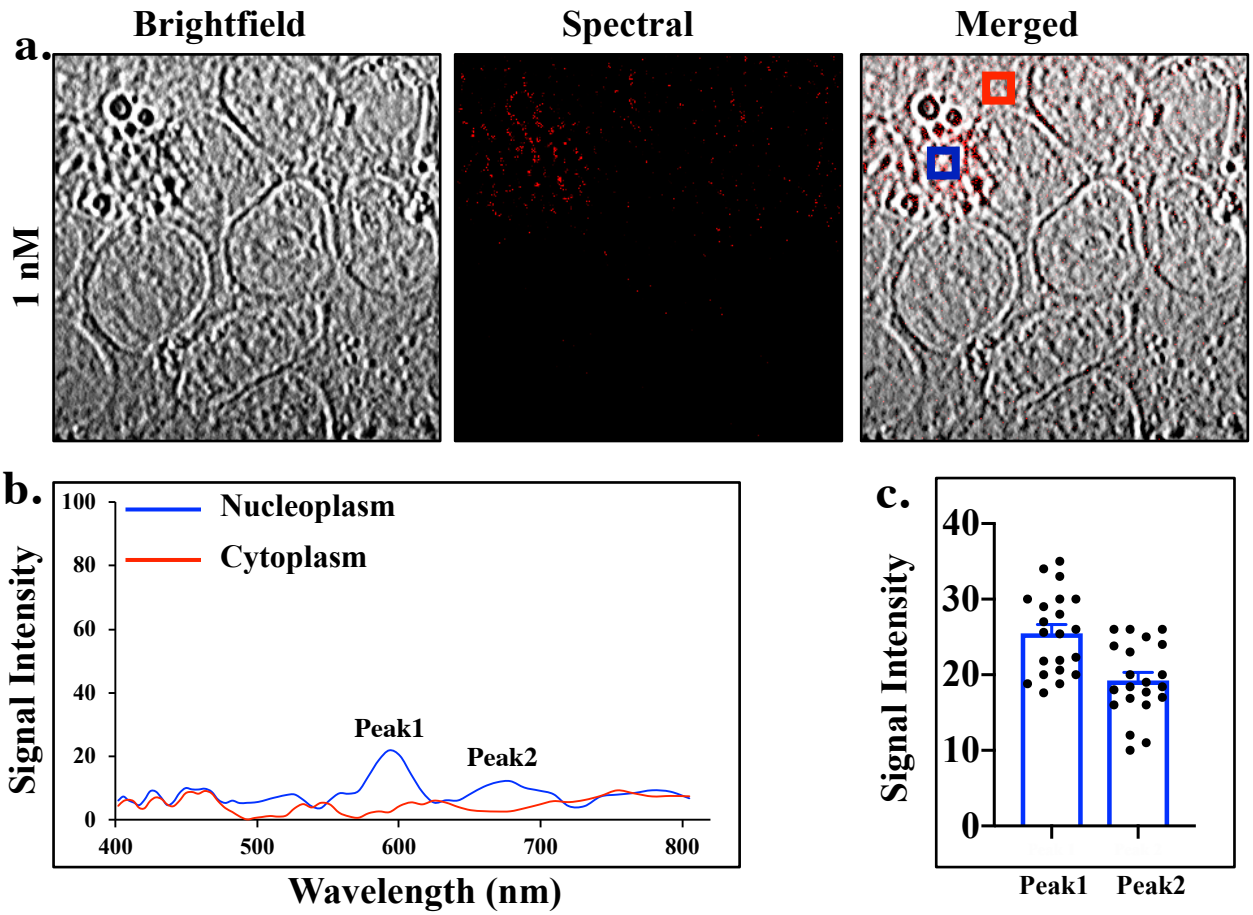

Figure 41. (a) Cells that treated with 10 nM of Doxorubicin, brightfield image by brightfield filter, spectral image by SKY filter which showed the result of uploaded Doxorubicin library and merged image of brightfield and spectral images. (b) The graph illustrated Doxorubicin fluorescence wavelength at ~ 592 nm, 670 nm inside the cells, X= wavelengths and Y= signal intensity. The blue wavelength displayed the region that contains Doxorubicin fluorescence which is in the nucleoplasm, while red wavelength explained the spectrum of the background area which is cell cytoplasm. (c) The bar graph exhibited the intensity data point variety of peak1 that is higher than peak2, this variety in consistent with pure, 150, 100, 10 nM of Doxorubicin results. The intensities here also become lower in comparing with pure, 150, 100, 10 nM Doxorubicin.

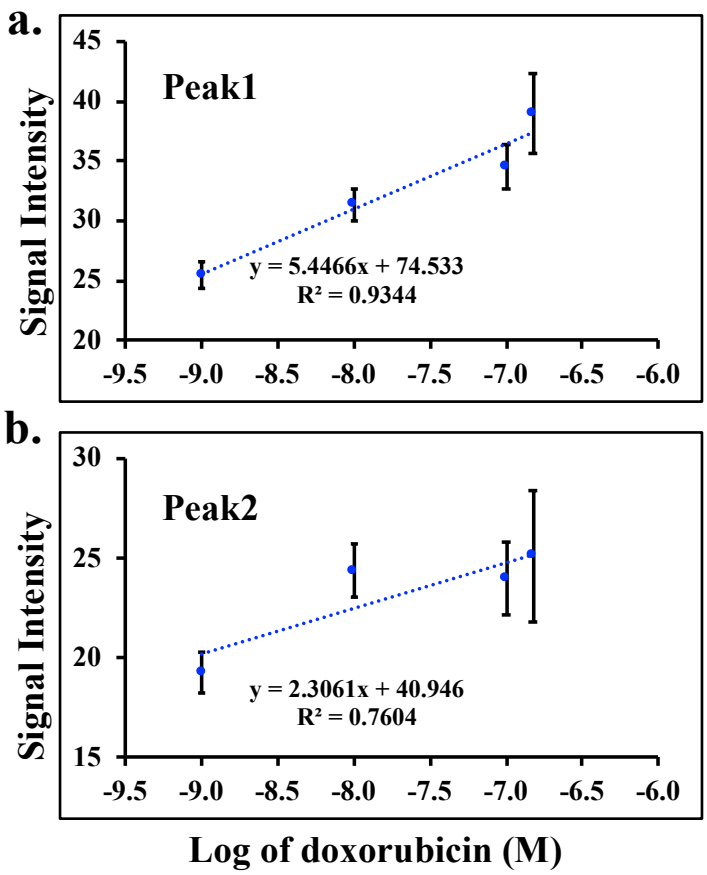

Figure 42. Linear regression analysis of Doxorubicin data by spectral imaging. X= log of concentrations in M, Y= average of signal intensity. (a) The graph illustrated the average intensities of peak 1 (~ 592 nM) vs the concentrations, here we can consider peak 1 because of its show excellent linearity at R^2= 0.9. While graph (b) explained peak 2 average intensities, it showed less linearity in comparing with peak 1 at R^2= 0.76.

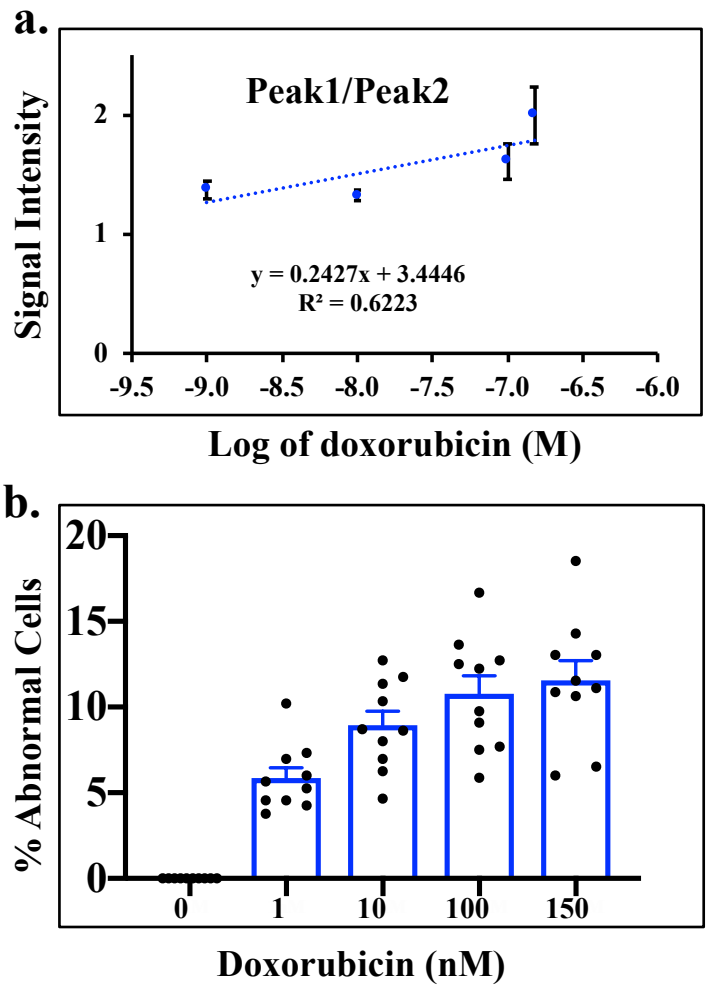

Figure 43. Linear regression analysis of Doxorubicin data by spectral imaging. X= log of concentrations in M, Y= average of signal intensity. (a) The graph demonstrated the ratio of average intensities for peak 1/peak 2, which has less linearity in comparing with peak 1 and peak 2 at R^2= 0.62. (b) The graph displayed the percentage of the abnormal cells (specifically abnormal nucleoplasm) of the samples, the percentage increase with higher concentrations of Doxorubicin.

3.3.3. Au and Ag NPs Spectral Imaging Result

For the reason that NPs have no fluorescence, spectral imaging system was conducted by using brightfield filter for pure Au and Ag NPs at ~ 536 nm and 420, respectively. These wavelengths are in consistent with Spectrophotometer results, and the wavelengths were uploaded and saved as libraries files for cell analysis. For Au NPs results, Fig 44a showed the brightfield image which was performed by brightfield filter, the spectral image which represents the analysis of uploaded wavelengths library of the brightfield image and merged image that combined between brightfield and spectral images. The graph in Fig 44b demonstrated the pure Au NPs wavelength at ~ 536 nm. The blue wavelength interpreted the area that contains higher wavelength intensity based on brighter NPs analysis (bigger particle size) in comparison with a red wavelength which showed the region that contains less (smaller particle size). The background displayed the wavelength intensity of the NPs background area, which is exhibited by black color spectrum. In addition, the bar graph in Fig 44c illustrated the intensity data point variation of Au NPs peak. Fig 45a showed the untreated cells images which are negative control, starting with brightfield image by brightfield filter, the spectral image which is the result for library analysis of brightfield image and merged images between them. Fig 45b showed wavelengths differences between many areas in the cell sample which reflect the background in comparing with the positive control (pure Au NPs). Forwards, we treat the cells with 100 mg/mL of Au NPs for 18 hrs. Fig 46a explained the brightfield image which was done by brightfield filter, a spectral image which is the result of the uploaded libraries for the pure Au NPs of brightfield image and merged between brightfield and spectral images. Brightfield image revealed Au NPs location in the cell which is in both nucleoplasm and cytoplasm. Fig 46b exhibited different wavelengths of the treated cells with 100 mg/mL at ~ 536 nm, which are consistent with pure Au NPs results. The blue wavelength

represented the region that has higher intensity based on brighter NPs analysis (bigger particle size), whereas the red spectrum showed the area that contains less (smaller particle size). Background displayed as a black color wavelength of the NPs background area. Fig 46c illustrated the intensity data point variation of the peak, here we might have an intensity that higher than one in the pure result, this is because we work with NPs which are not depending on the concentrations anymore; instead, it depends on the particles size. The chart in Fig 47 summarized the Au NPs results, the data for spectrum intensity of the pure Au NPs are higher than the negative control (untreated cells) sample. However, in the cells which treated with 100 mg/mL of Au NPs, we have in some points higher intensity in comparing with pure. This is because the analysis depend on the NPs size. The most interesting step when we treated the cells with 100 mg/mL of Ag NPs, Fig 48a illustrated the brightfield image which was performed by brightfield filter, the spectral image which showed the analysis of uploaded wavelengths library of the brightfield image and merged image of between brightfield and spectral images. The graph in Fig 48b displayed the pure Ag NPs wavelengths at ~ 420 nm, 762 nm. The pink wavelength interpreted the area that contained the core of Ag NPs, while the yellow wavelength showed the region that included shell of Ag NPs. Both at the same wavelength but different spectrum shape. The background was showed as a black spectrum of the area which contains no Ag NPs. In addition, the bar graph in Fig 48c illustrated the intensity data point variation of peak1 which is higher than peak2. As well as Fig 49a showed the negative control of untreated cells images, the brightfield image performed by brightfield filter, spectral image is the result for library analysis of brightfield image and merged image between brightfield and spectral images. Fig 49b displayed wavelengths intensity at ~ 455, 777 nm of different areas in the cell sample which reflect the background in comparing with the positive control (pure Ag NPs). Fig 49c the bar graph represented the different background intensity

between peak1 and peak2 which is the highest. Moreover, we treated the cells with 100 mg/mL of Ag NPs. Fig 50a illustrated the brightfield image which was conducted by brightfield filter, the spectral image which is the uploaded libraries result for the pure Ag NPs of brightfield image and merged image of brightfield and spectral images. Brightfield image explained Ag NPs location in the cell sample which is in the nucleoplasm and cytoplasm. Fig 50b displayed wavelengths differences (at ~ 420, 762 nm) between the core spectrum in pink color and the shell in yellow within the cell sample, the black spectrum reflected the background area of the NPs. Fig 50c the bar graph displayed the intensity wavelengths differences between peak1 which is higher than peak2, these data also consistent with pure Ag NPs results. The chart in Fig 51 summarized the Ag NPs results, (a) illustrated the average differences between peak1 of pure Ag NPs (at ~420 nm), negative control (~ 455 nm) and cells that treated with Ag NPs (at 420 nm). Peak2 of pure Ag NPs (at ~762 nm), negative control (~ 777 nm) and cells were treated with Ag NPs (~ 762 nm). While (b) explained the results of the intensity average of peak1/peak1 of pure Ag NPs which are higher than Ag NPs within the cells and negative control.

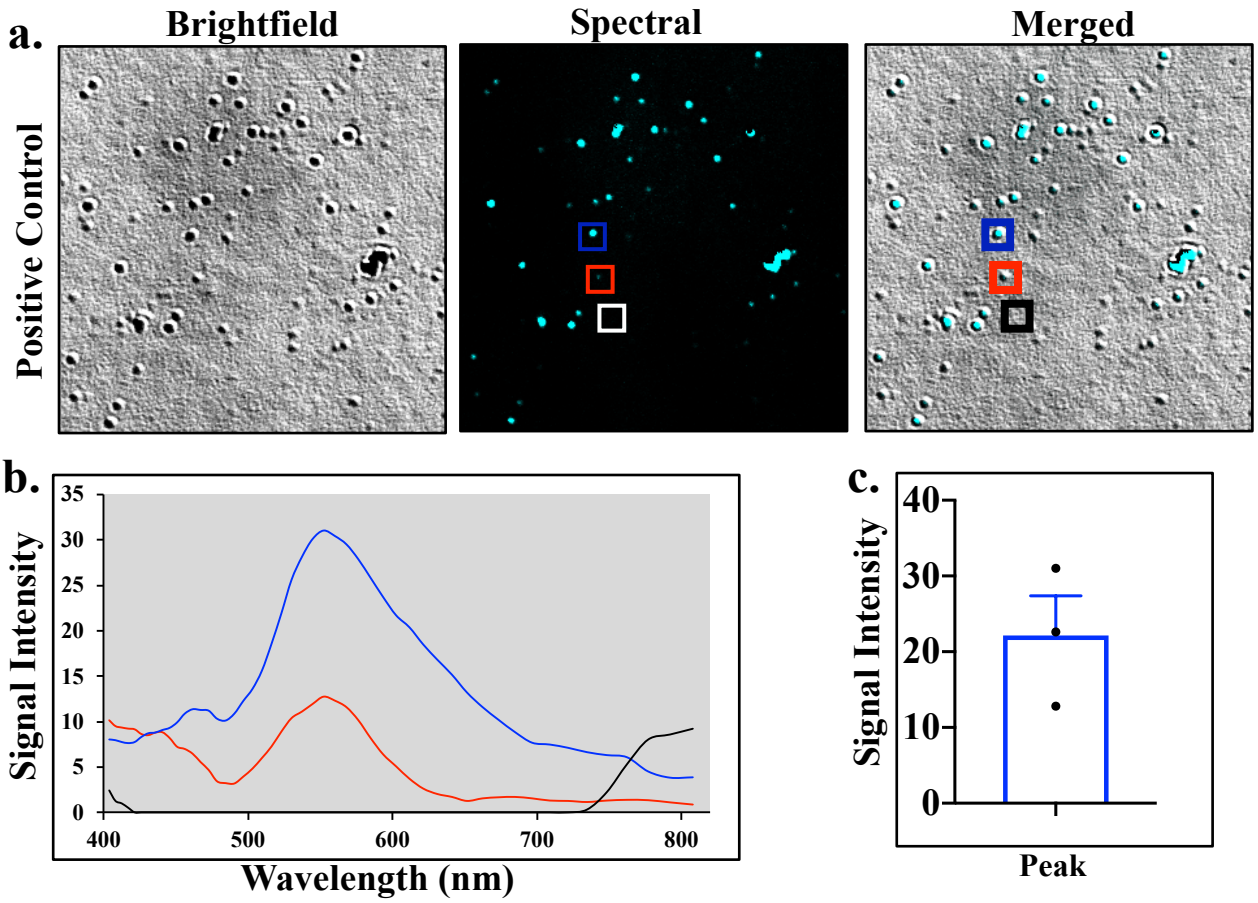

Figure 44. (a) Brightfield image of pure Au NPs done by using brightfield filter, the spectral image which is the result for the uploaded library analysis of brightfield image and merged image which combine between brightfield and spectral images. (b) The graph demonstrated the wavelengths of pure Au NPs at ~ 536 nm, X= wavelengths, and Y= signal intensity. The blue wavelength displayed the area that contains higher wavelength intensity based on brighter NPs analysis (bigger particle size), while red wavelength showed the region that includes less (smaller particle size). Background exhibited as a black color wavelength of the NPs background area. (c) The bar graph exhibited the intensity data point variation result for Au NPs peak.

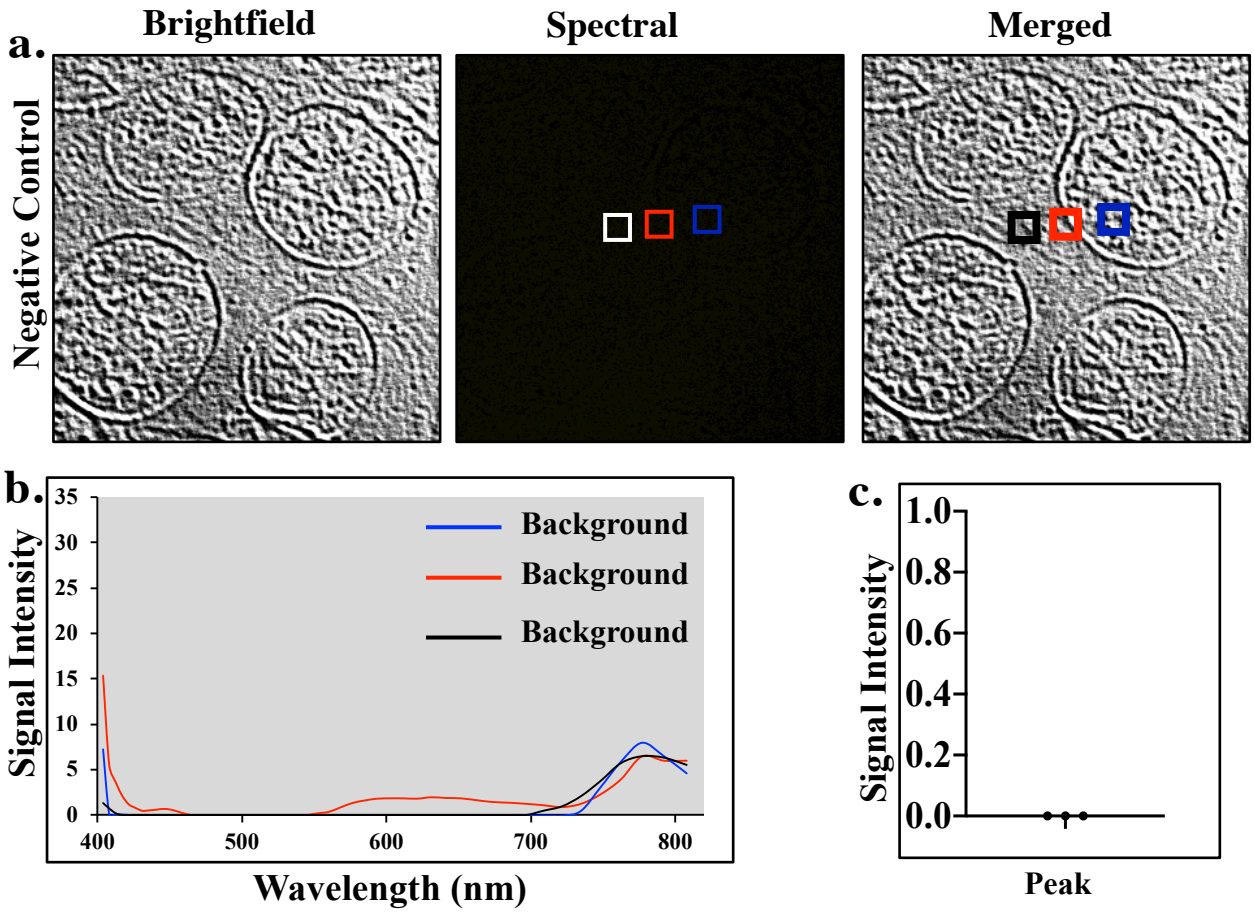

Figure 45. (a) Negative control of untreated cells. The brightfield image captured by using brightfield filter, spectral image is the result of library analysis of brightfield image and merged image which combined between brightfield and spectral images. (b) The graph demonstrated the wavelengths of the negative control which reflect the background in comparing with the positive control (pure Au NPs). X= wavelengths and Y= signal intensity. (c) The bars indicated the intensity variation of the data point for untreated cells.

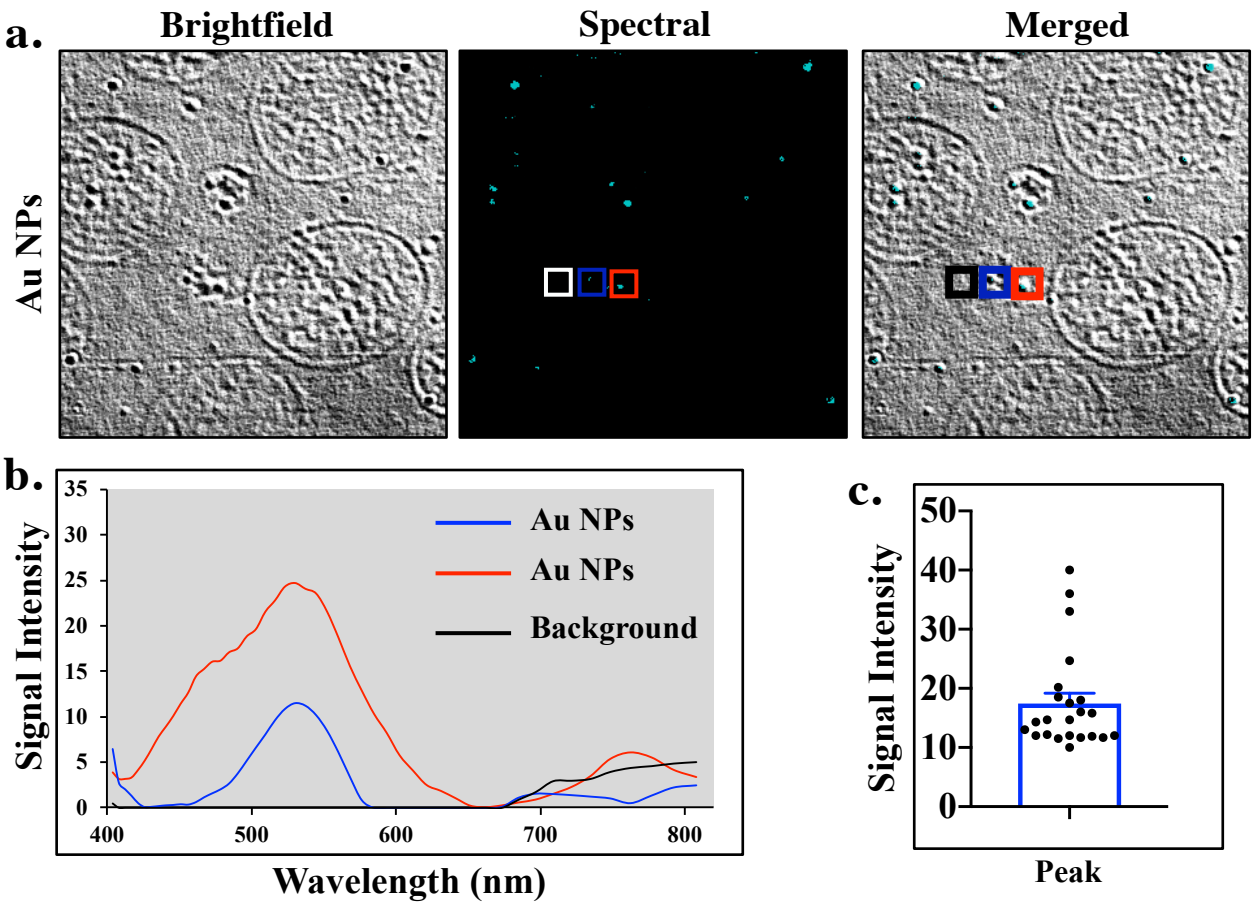

Figure 46. (a) Cell samples which are treated with 100 mg/mL of pure Au NPs, brightfield image done by using brightfield filter, the spectral image which showed the result of uploaded Au NPs library of brightfield image and merged image between the brightfield and spectral images. (b) The graph demonstrated Au NPs wavelength at ~ 536 nm inside the cells, X= wavelengths, and Y= signal intensity. The blue wavelength displayed the area that contains high intensity wavelength (bigger particle size), while the red wavelength showed less intensity (smaller particle size). (c) The bar graph explained the intensity data point variation for Au NPs peak, we may have higher intensity data because it depend on the particle size.

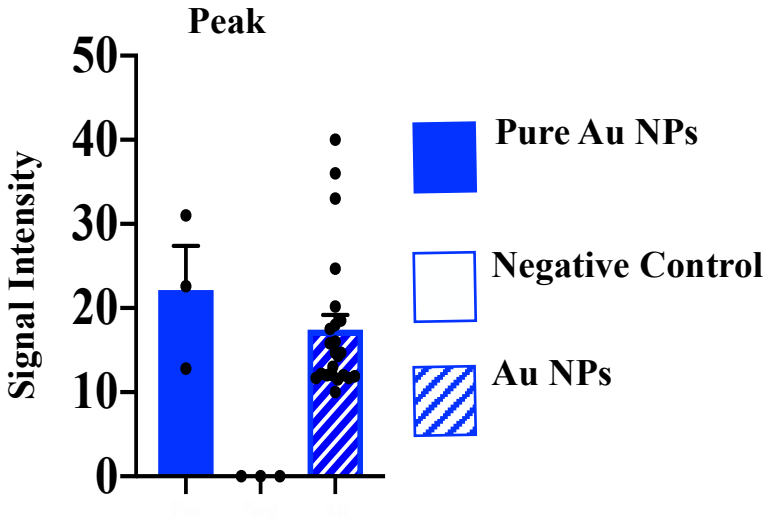

Figure 47. The chart summarized the Au NPs data results analysis. As is shown, the data for the wavelength intensity of the pure Au NPs is higher than the negative control. However, in the cells which treated with 100 mg/mL of Au NPs, we have in some points higher intensity in comparing with pure. This is because we work with NPs which are dependent on the particle size.

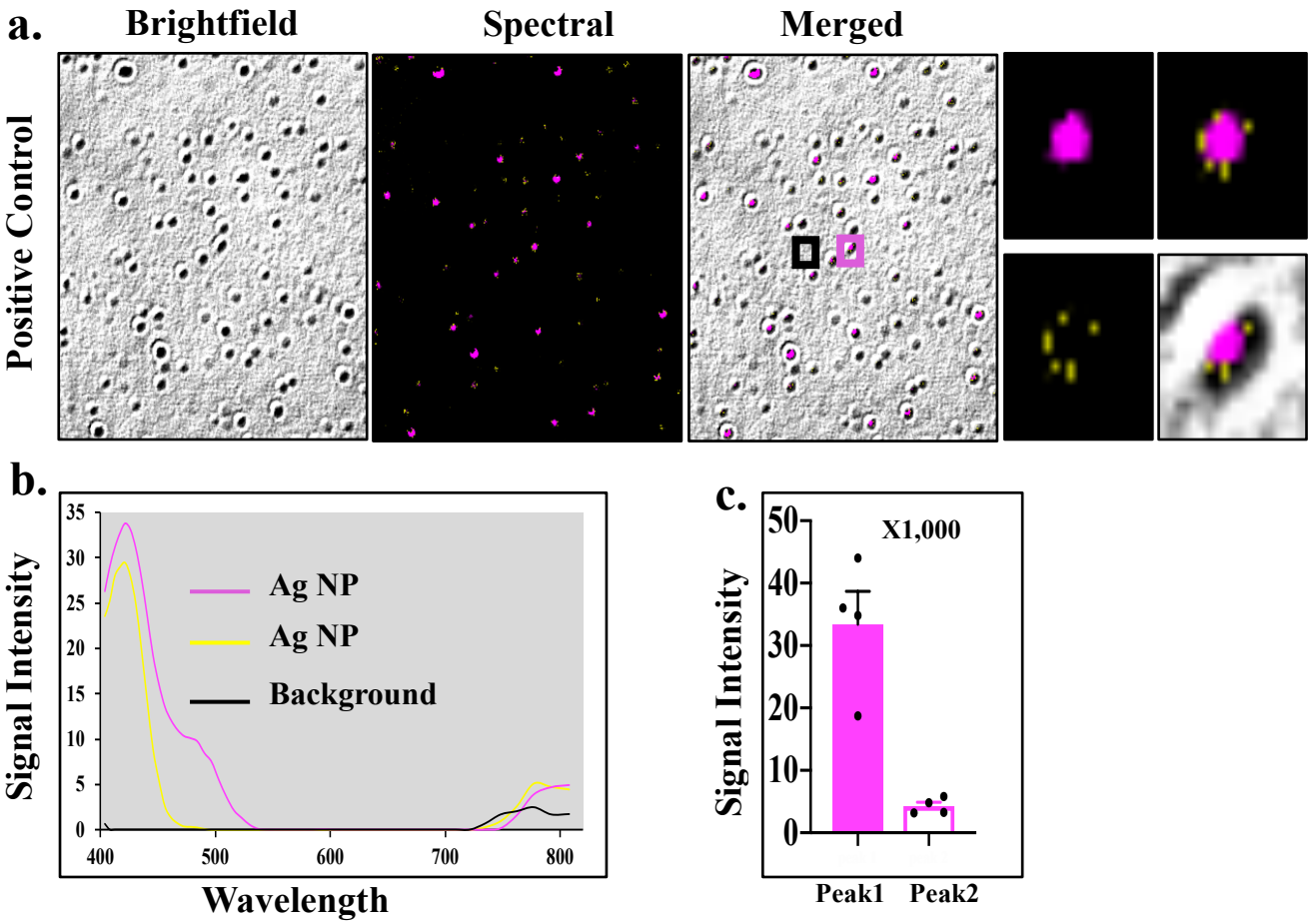

Figure 48. (a) Brightfield image of pure Ag NPs done by brightfield filter, the spectral image which is the analysis result for the uploaded library of brightfield image and merged image of brightfield and spectral images. (b) The graph illustrated the wavelengths of pure Au NPs at ~ 420, 762 nm, X= wavelengths, and Y= signal intensity. The pink wavelength displayed the intensity of the core area of Ag NPs, while the yellow wavelength showed the shell region. Background exhibits as a black color spectrum of the NPs background area. (c) The bar graph exhibited the intensity data point variation result for peak1 which is higher than peak2.

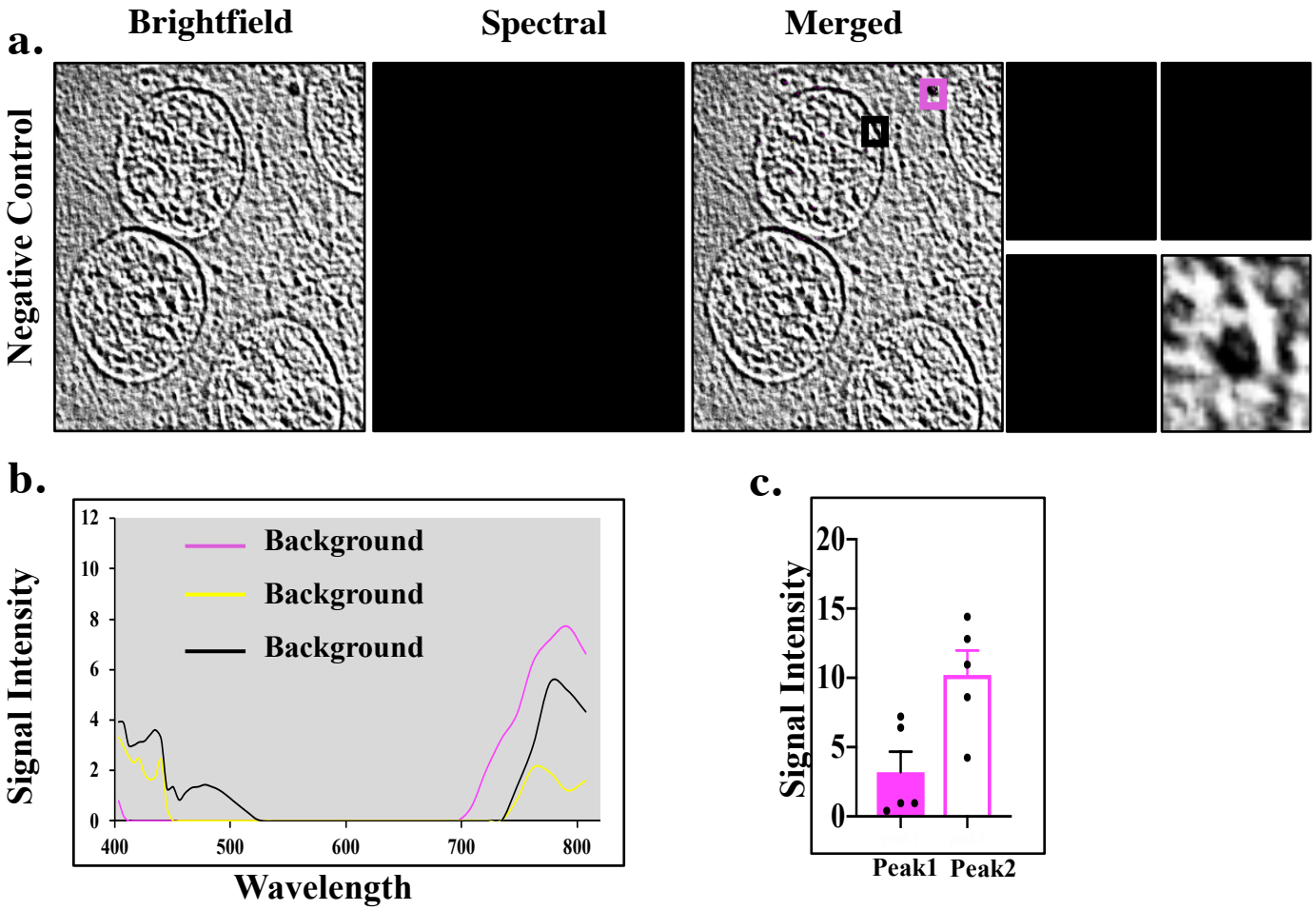

Figure 49. (a) Negative control of untreated cells, brightfield image by brightfield filter, the spectral image which is the result for the uploaded library analysis of brightfield image and merged image of brightfield and spectral images. (b) The graph illustrated the wavelengths of the negative control at ~ 455, 777 nm which we consider it as a background, X= wavelengths, and Y= signal intensity. (c) The bar graph exhibited the intensity data point variation for peak1 which is lower than peak2.

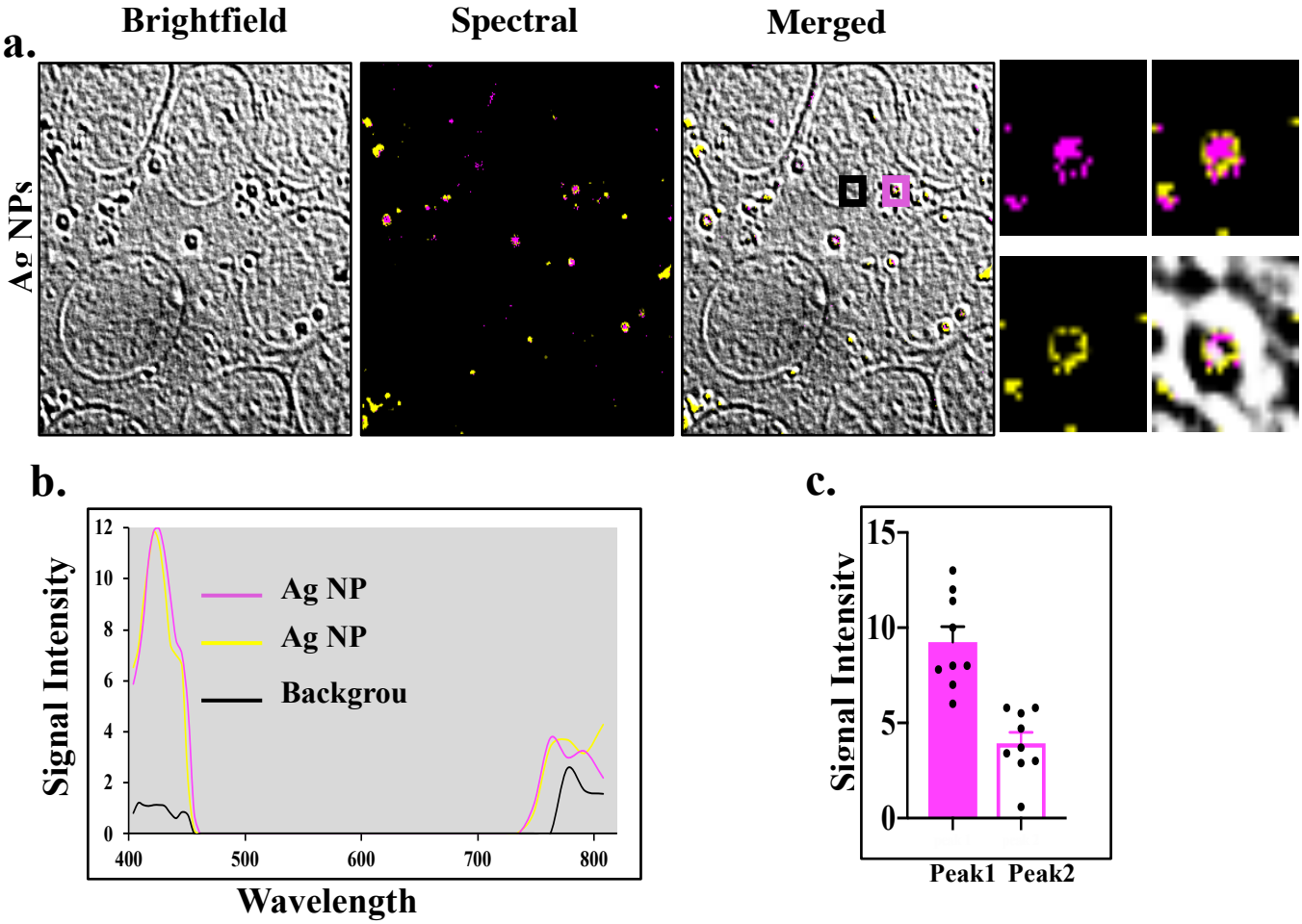

Figure 50. (a) Cells that treated with 100 mg/mL of Ag NPs, the brightfield image done by brightfield filter, the spectral image which is the analysis result for the uploaded library of brightfield image and merged image of brightfield and spectral images. (b) The graph illustrated the wavelengths of pure Au NPs at ~ 420, 762 nm, X= wavelengths, and Y= signal intensity. The pink wavelength demonstrated the intensity of the core area of Ag NPs, whereas yellow wavelength displayed the shell region. Background exhibited as a black color spectrum of the NPs background area. (c) The bar graph show the intensity data point variation for peak1 which is higher than peak2. This variation result is consistent with pure Ag NPs results.

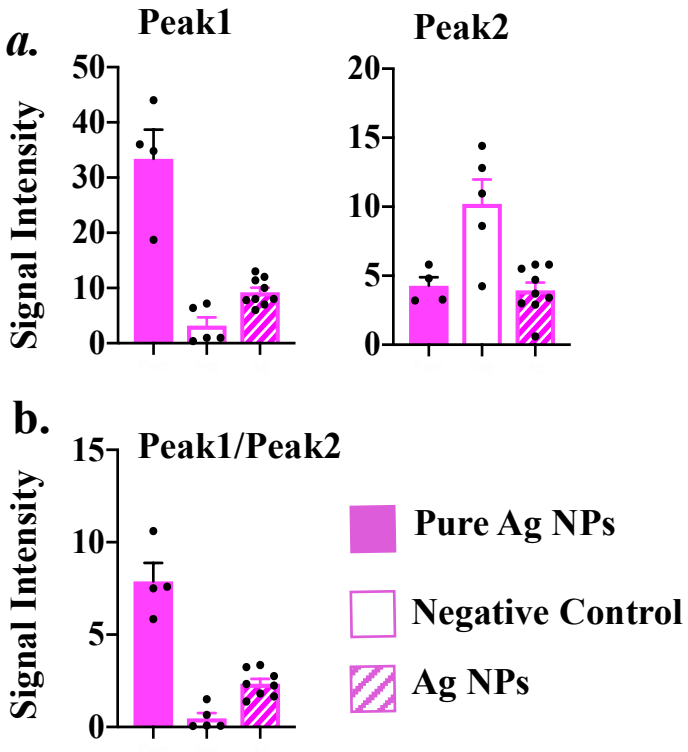

Figure 51. Summarized the Ag NPs analysis results, (a) explained the average differences between peak1 of pure Ag NPs (at ~420 nm), negative control (~ 455 nm) and cells that treated with 100 mg/mL of Ag NPs (at 420 nm). Peak2 of pure Ag NPs (at ~762 nm), negative control (~ 777 nm) and treated cells (~ 762 nm). While chart (b) demonstrated the results of the peak1/peak1 average of pure Ag NPs, which are higher than Ag NPs within the cells and negative control.

Chapter 4

CONCLUSION

The spectral imaging is a powerful technique which can capture the image of the sample and displays a spectrum at each pixel of our target. This feature provides the researchers with full and details information about the samples in a way that can help to enhance the understanding of many topics and questions. For instance, it allows the identification of the exact location and quantity of our sample in the cells. In this study, spectral imaging was conducted to test many chemicals including rhodamine 6g, doxorubicin, Au NPs and Ag NPs. Spectral imaging was able to identify each sample by the spectrum of the molecule; this done by uploading each spectrum of the pure chemicals as a library and use it for cells analysis. In addition, spectral imaging was capable to identify each molecule within cells by the library of the molecule wavelength. However, we observed extra peaks which are not consistent with the spectrophotometer and need to be identified.

References

Chapman, M., Mullen, M., Novoa-Ortega, E., Alhasani, M., Elman, J. F., & Euler, W. B. (2016). Structural Evolution of Ultrathin Films of Rhodamine 6G on Glass. *The Journal of Physical Chemistry C*, *120*(15), 8289–8297. https://doi.org/10.1021/acs.jpcc.6b01669

DaCosta, R. S., Wilson, B. C., & Marcon, N. E. (2007). Fluorescence and spectral imaging. *TheScientificWorldJournal*, *7*, 2046–2071. https://doi.org/10.1100/tsw.2007.308

Fayaz, A. M., Balaji, K., Girilal, M., Yadav, R., Kalaichelvan, P. T., & Venketesan, R. (2010). Biogenic synthesis of silver nanoparticles and their synergistic effect with antibiotics: a study against gram-positive and gram-negative bacteria. *Nanomedicine: Nanotechnology, Biology and Medicine*, *6*(1), 103–109. https://doi.org/10.1016/j.nano.2009.04.006

Ferreira, B. R. V., Correa, D. N., Eberlin, M. N., Vendramini, P. H., Ferreira, B. R. V., Correa, D. N., Vendramini, P. H. (2017). Fragmentation Reactions of Rhodamine B and 6G as Revealed by High Accuracy Orbitrap Tandem Mass Spectrometry. *Journal of the Brazilian Chemical Society*, *28*(1), 136–142. https://doi.org/10.5935/0103-5053.20160156

Garini, Y., Young, I. T., & McNamara, G. (2006). Spectral imaging: principles and applications. *Cytometry. Part A: The Journal of the International Society for Analytical Cytology*, *69*(8), 735–747. https://doi.org/10.1002/cyto.a.20311

Haiss, W., Thanh, N. T. K., Aveyard, J., & Fernig, D. G. (2007). Determination of Size and Concentration of Gold Nanoparticles from UV−Vis Spectra. *Analytical Chemistry*, *79*(11), 4215–4221. https://doi.org/10.1021/ac0702084

Li, Q., He, X., Wang, Y., Liu, H., Xu, D., & Guo, F. (2013). Review of spectral imaging technology in biomedical engineering: achievements and challenges. *Journal of Biomedical Optics*, *18*(10), 100901. https://doi.org/10.1117/1.JBO.18.10.100901

Liang, J., Zhang, Z., Zhao, H., Wan, S., Zhai, X., Zhou, J., … Lin, G. (2018). Simple and rapid monitoring of doxorubicin using streptavidin-modified microparticle-based time-resolved fluorescence immunoassay. *RSC Advances*, *8*, 15621–15631. https://doi.org/10.1039/C8RA01807C

Sottani, C., Poggi, G., Melchiorre, F., Montagna, B., & Minoia, C. (2013). Simultaneous measurement of doxorubicin and reduced metabolite doxorubicinol by UHPLC-MS/MS in human plasma of HCC patients treated with TACE. *Journal of Chromatography. B, Analytical Technologies in the Biomedical and Life Sciences*, *915–916*, 71–78. https://doi.org/10.1016/j.jchromb.2012.12.012

Appendices

Rhodamine 3nM MS result

Generic Display Report

Analysis Info

Analysis Name	D:\Data\Qamar\Rhodamine 3nM.d	Acquisition Date	8/6/2018 1:14:40 PM
Method	Small Molecules - DI - MS.m	Operator	bsyed
Sample Name	qamar	Instrument	impact II
Comment			

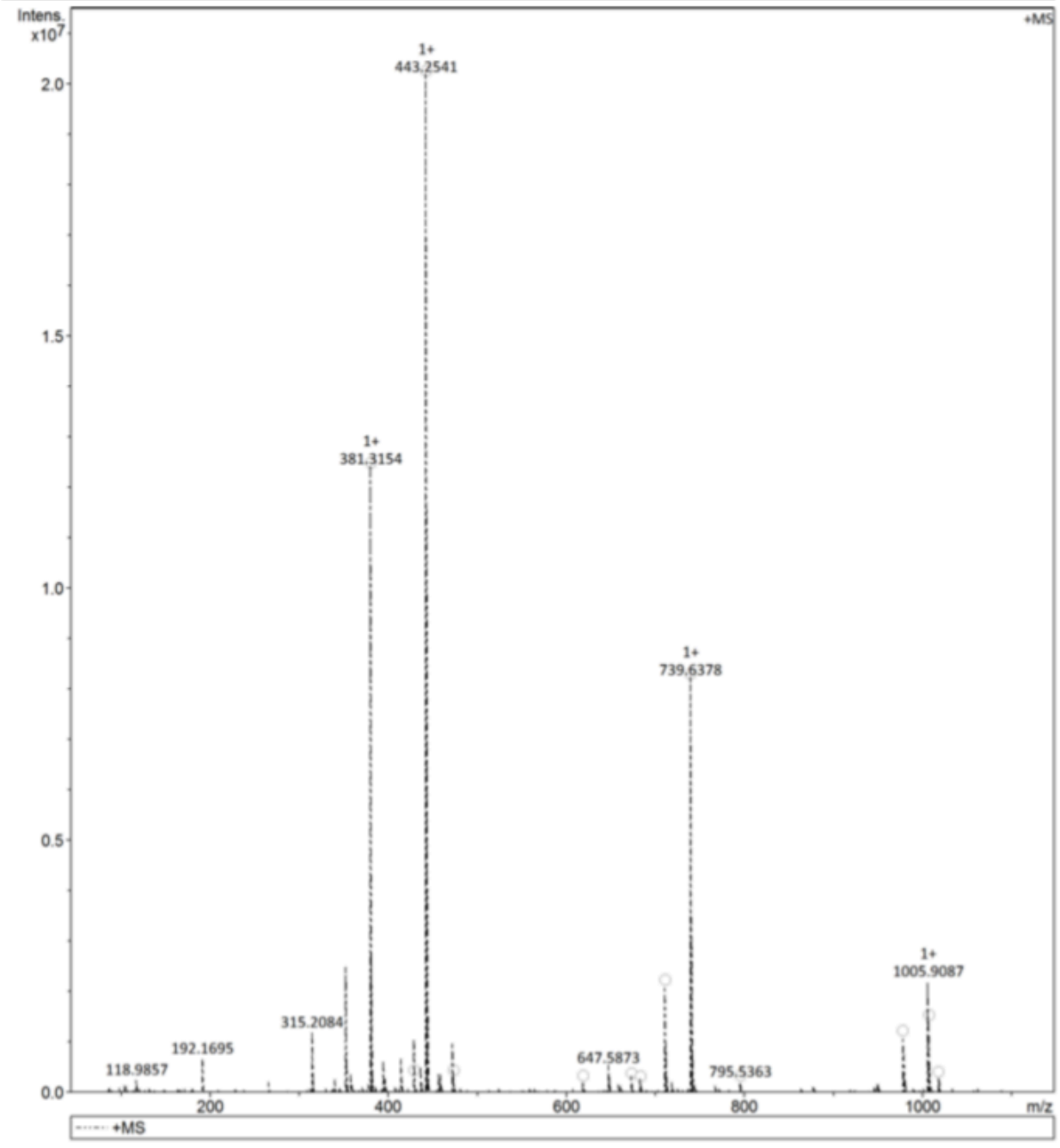

Rhodamine 2.5nM MS result

Generic Display Report

Analysis Info

Analysis Name	D:\Data\Qamar\Rhodamine 2.5nM_3 8-10-18.d	Acquisition Date	8/10/2018 2:31:14 PM
Method	Small Molecules - DI - MS.m	Operator	Chapman
Sample Name	QAMAR	Instrument	impact II
Comment			

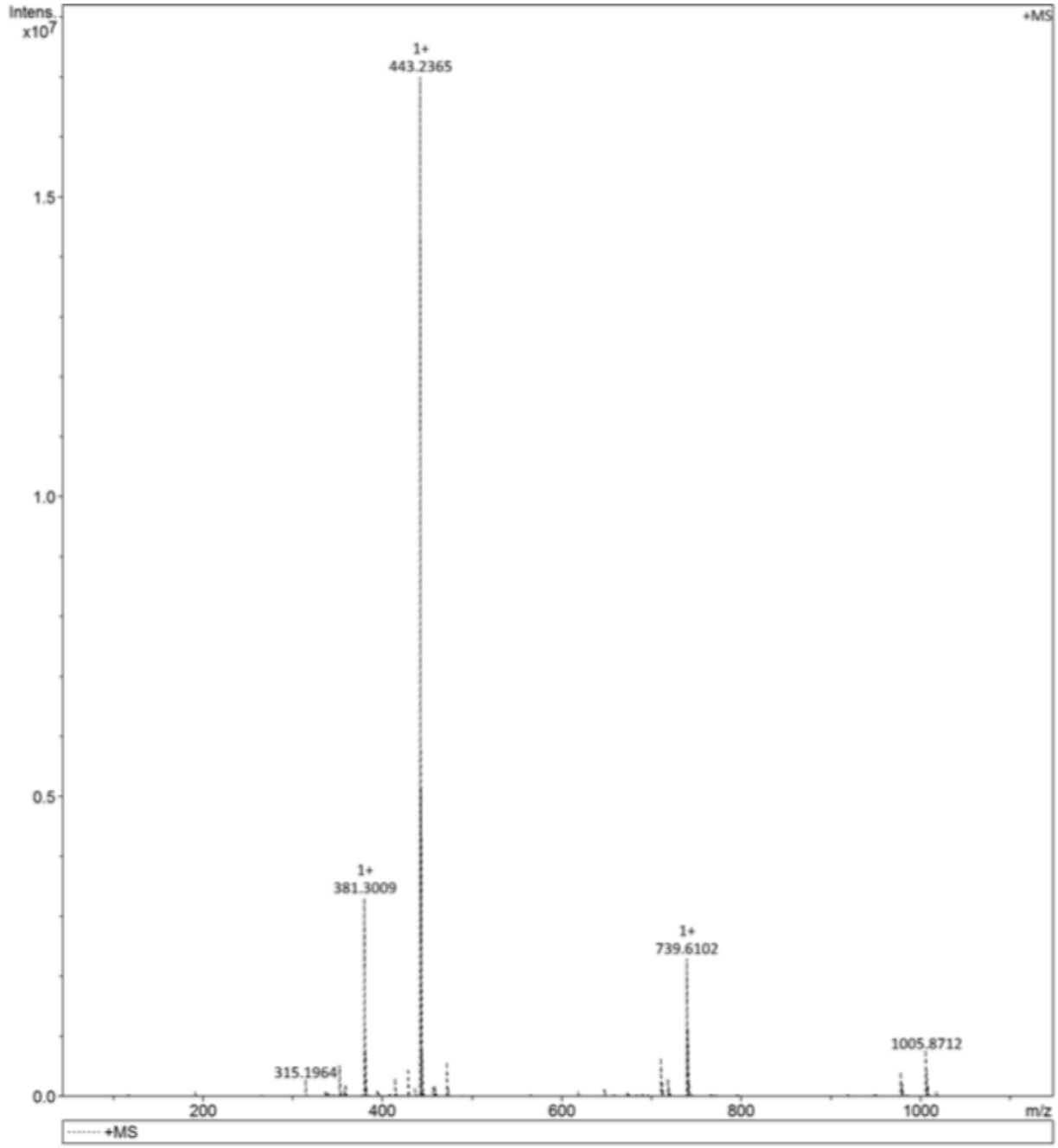

Rhodamine 2nM MS result

Generic Display Report

Analysis Info

Analysis Name	D:\Data\Qamar\Rhodamine 2nM_1 8-10-18.d	Acquisition Date	8/10/2018 2:53:18 PM
Method	Small Molecules - DI - MS.m	Operator	Chapman
Sample Name	QAMAR	Instrument	impact II
Comment			

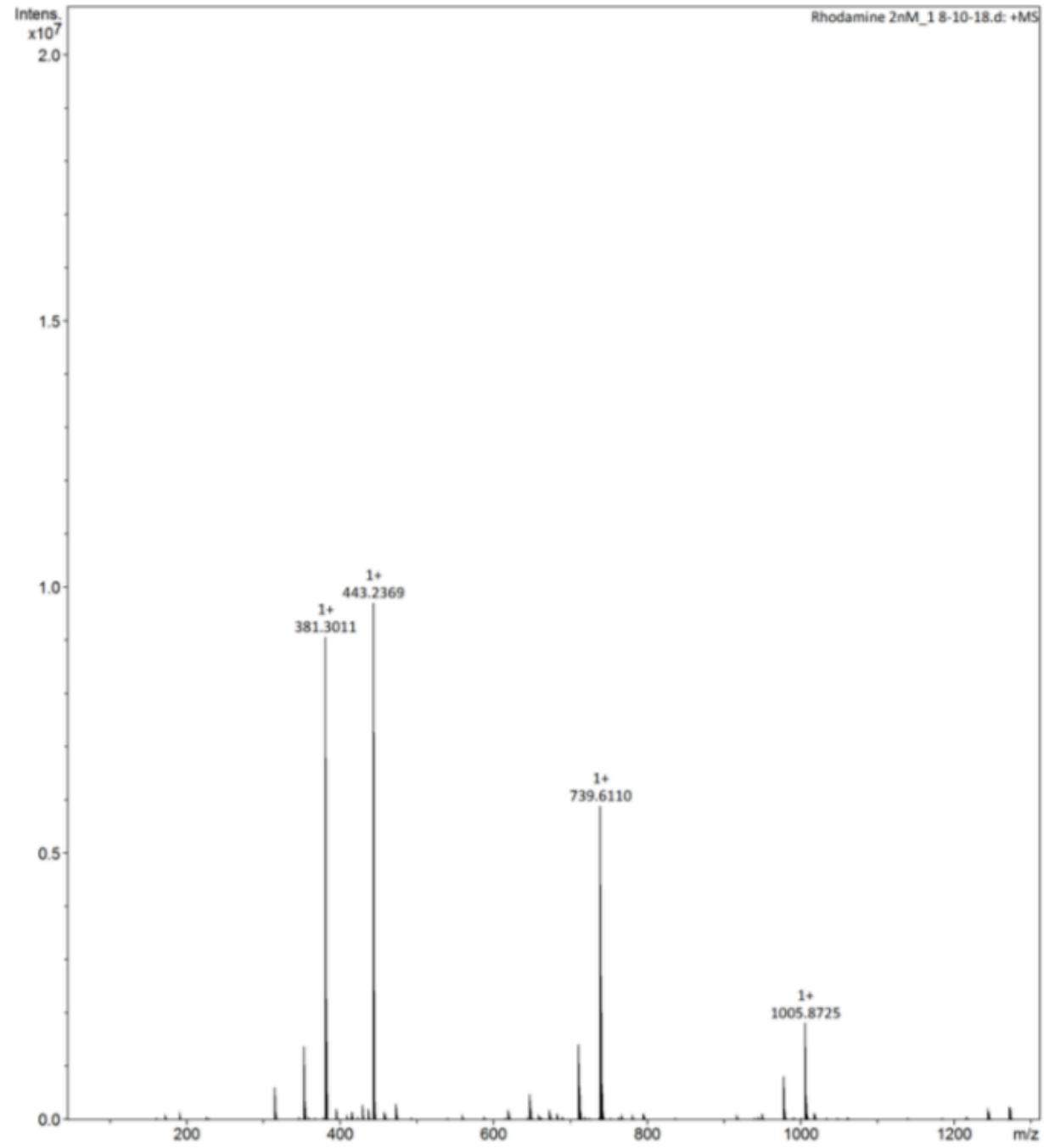

Rhodamine 1.5nM MS result

Generic Display Report

Analysis Info

Analysis Name	D:\Data\Qamar\Rhodamine 1.5nM_2 8-10-18.d	Acquisition Date	8/10/2018 2:12:31 PM
Method	Small Molecules - DI - MS.m	Operator	Chapman
Sample Name	QAMAR	Instrument	impact II
Comment			

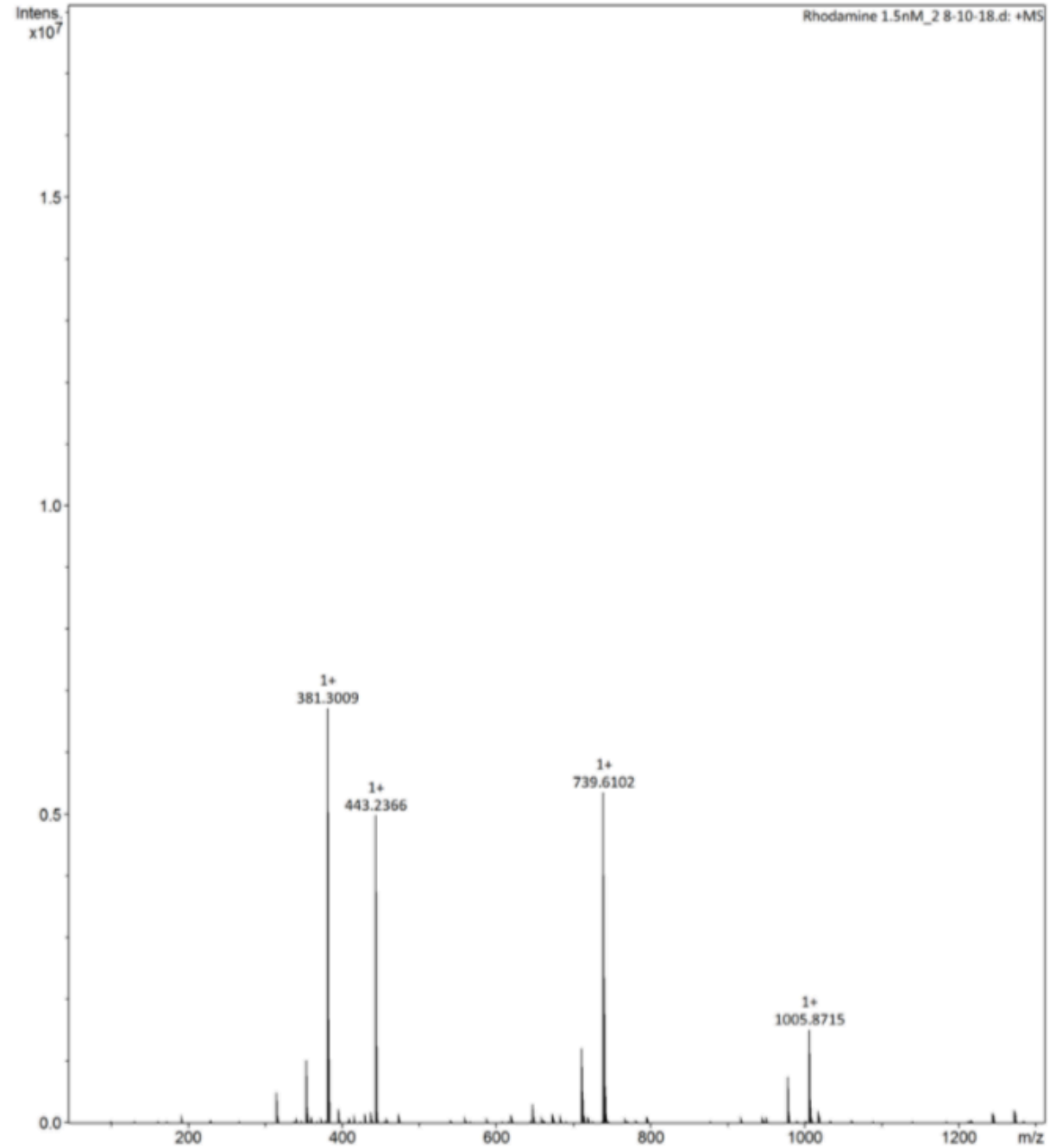

Rhodamine 1nM MS result

Generic Display Report

Analysis Info

Analysis Name	D:\Data\Qamar\Rhodamine 1nM_2 8-10-18.d	Acquisition Date	8/10/2018 2:00:21 PM
Method	Small Molecules - DI - MS.m	Operator	Chapman
Sample Name	QAMAR	Instrument	impact II
Comment			

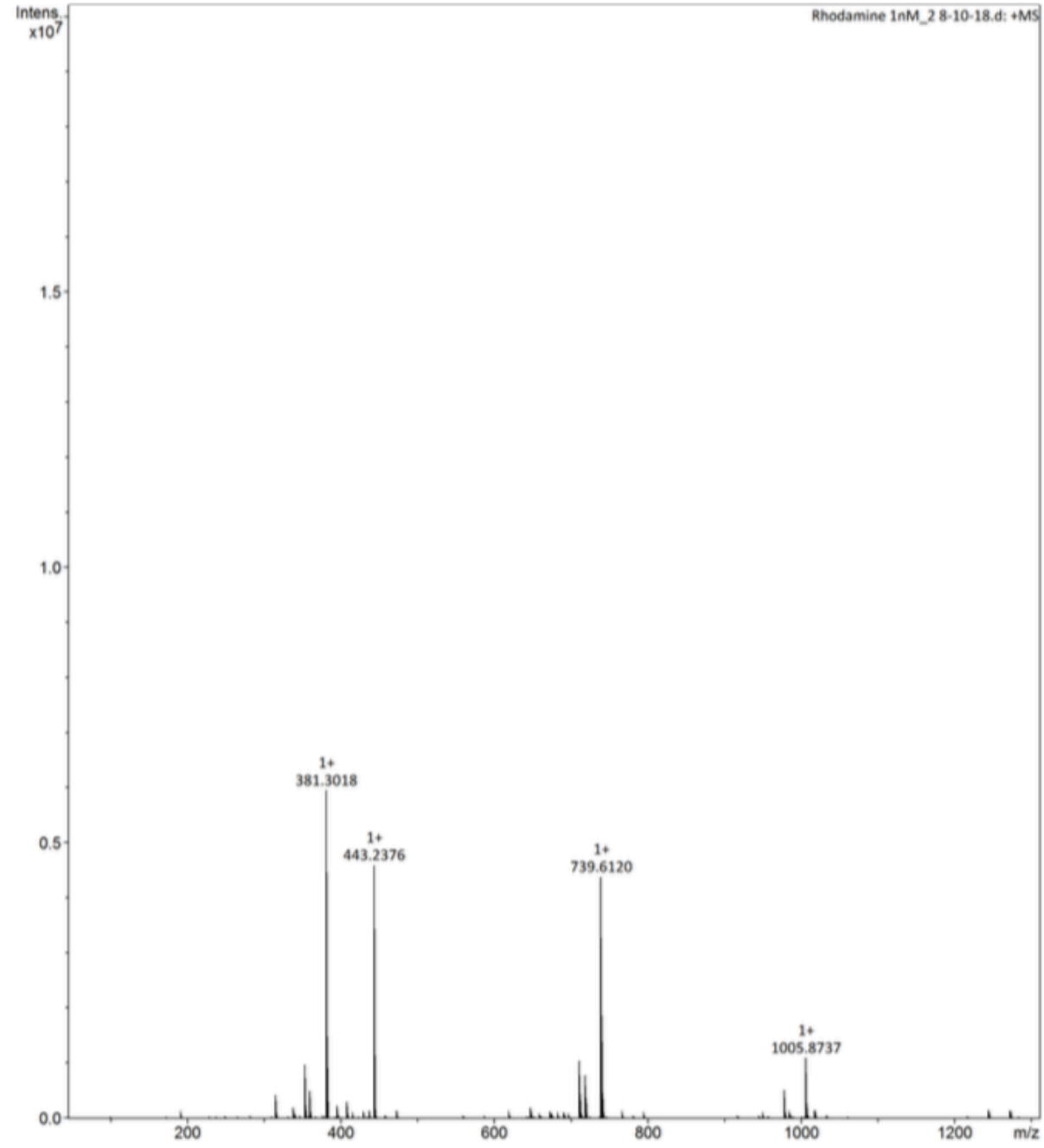

Rhodamine 0.5nM MS result

Generic Display Report

Analysis Info

Analysis Name	D:\Data\Qamar\Rhodamine 0.5nM.d	Acquisition Date	8/6/2018 11:48:07 AM
Method	Small Molecules - DI - MS.m	Operator	bsyed
Sample Name	qamar	Instrument	impact II
Comment			

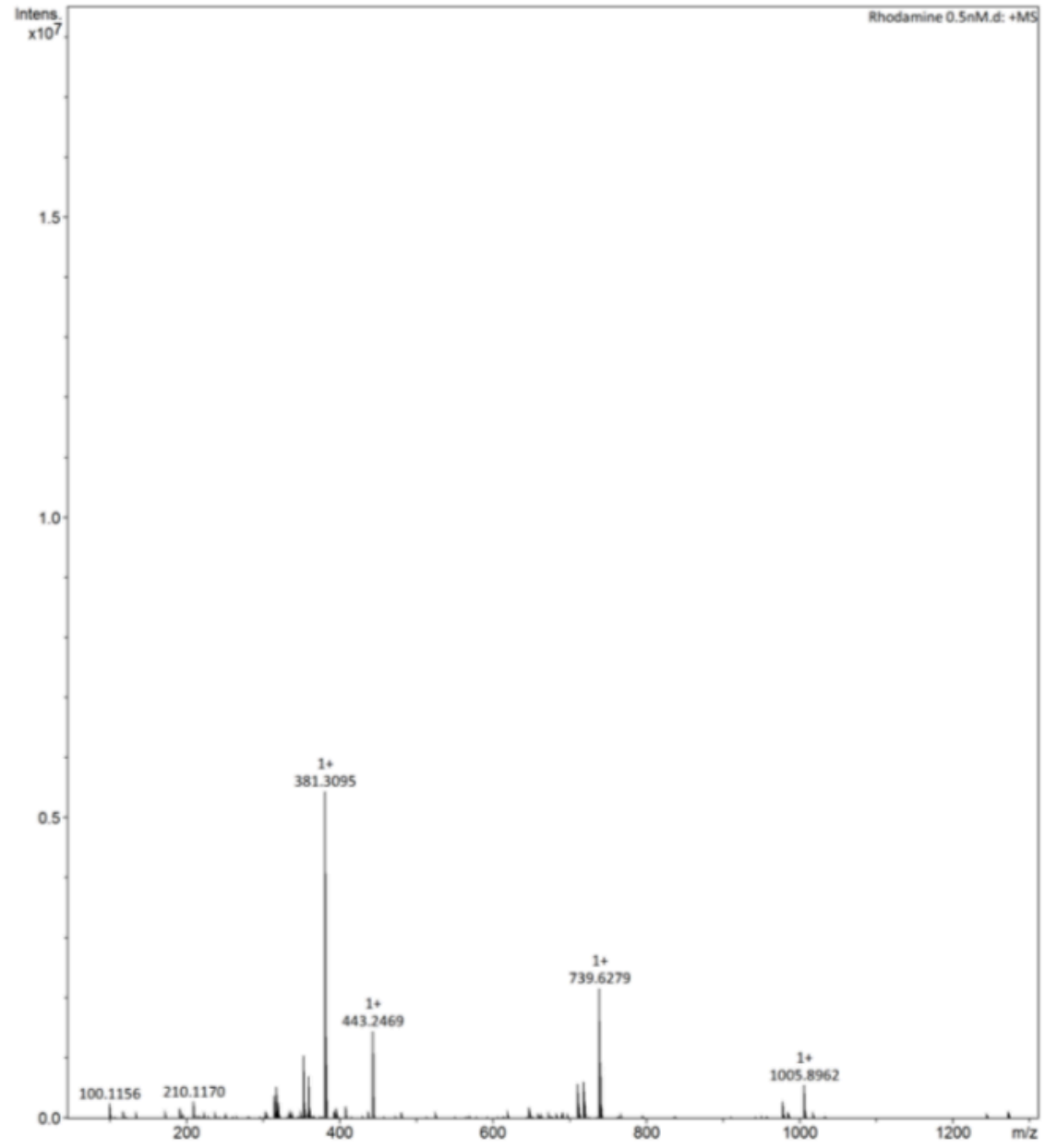

Rhodamine 0.3nM MS result

Generic Display Report

Analysis Info

Analysis Name	D:\Data\Qamar\Rhodamine 0.3nM_3 8-10-18.d	Acquisition Date	8/10/2018 12:59:31 PM
Method	Small Molecules - DI - MS.m	Operator	Chapman
Sample Name	QAMAR	Instrument	impact II
Comment			

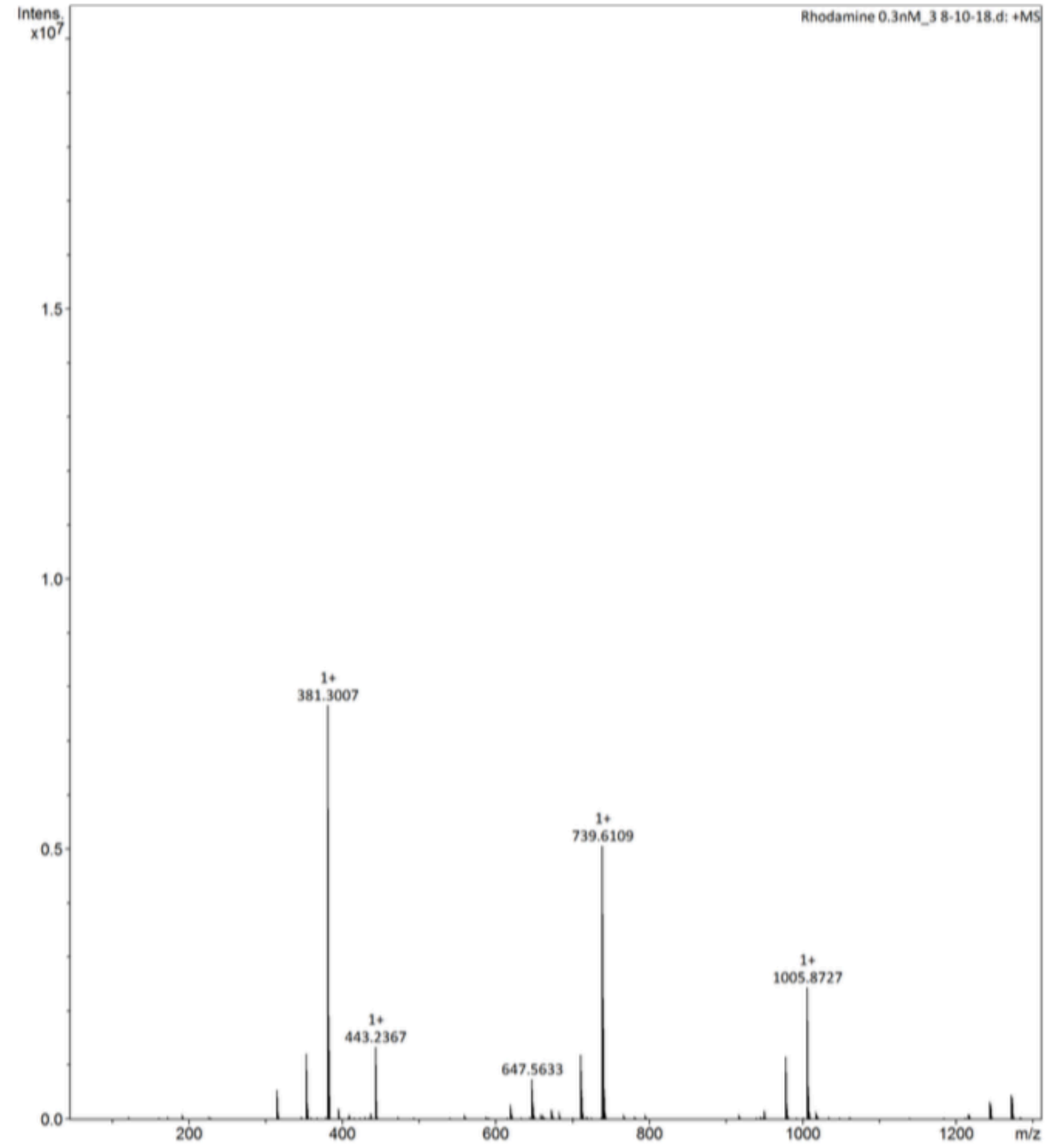

Rhodamine 0.1nM MS result

Generic Display Report

Analysis Info

Analysis Name	D:\Data\Qamar\Rhodamine 0.1nM1 8-16-18.d	Acquisition Date	8/16/2018 2:39:27 PM
Method	Small Molecules - DI - MS.m	Operator	bsyed
Sample Name	qamar	Instrument	impact II
Comment			

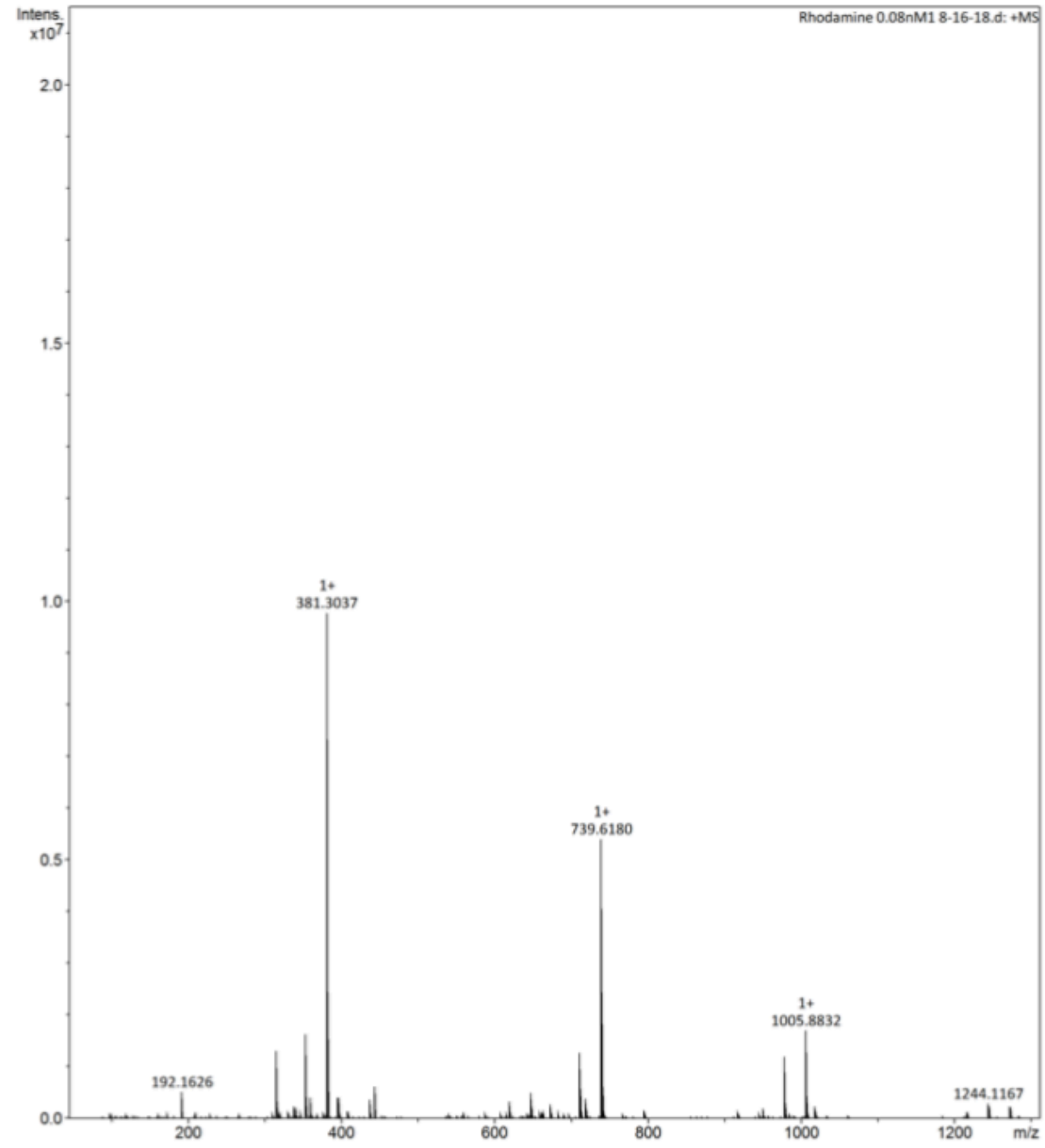

Rhodamine 3nM LC/MS result

Display Report

Analysis Info

Analysis Name	D:\Data\3nM_RB1_01_135.d	Acquisition Date	4/3/2019 3:25:04 AM
Method	Gen_SM_AutoMsMs.m	Operator	Demo User
Sample Name	3nM	Instrument	impact II 1825265.10094
Comment			

Acquisition Parameter

Source Type	ESI	Ion Polarity	Positive	Set Nebulizer	1.8 Bar
Focus	Not active	Set Capillary	4500 V	Set Dry Heater	220 °C
Scan Begin	50 m/z	Set End Plate Offset	-500 V	Set Dry Gas	8.0 l/min
Scan End	1300 m/z	Set Charging Voltage	2000 V	Set Divert Valve	Waste
		Set Corona	0 nA	Set APCI Heater	0 °C

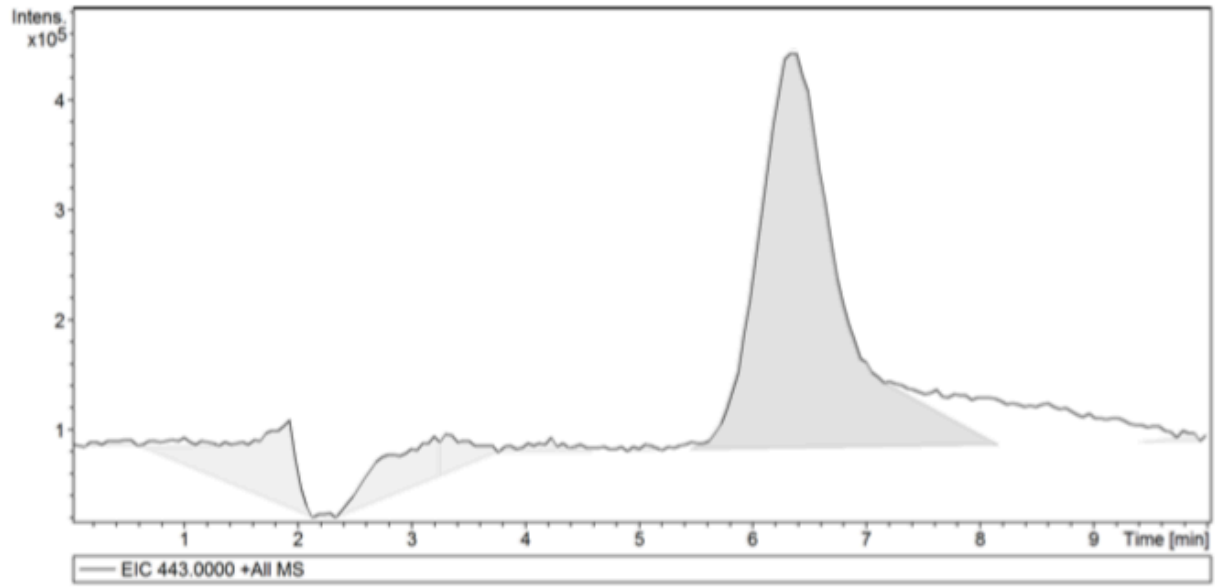

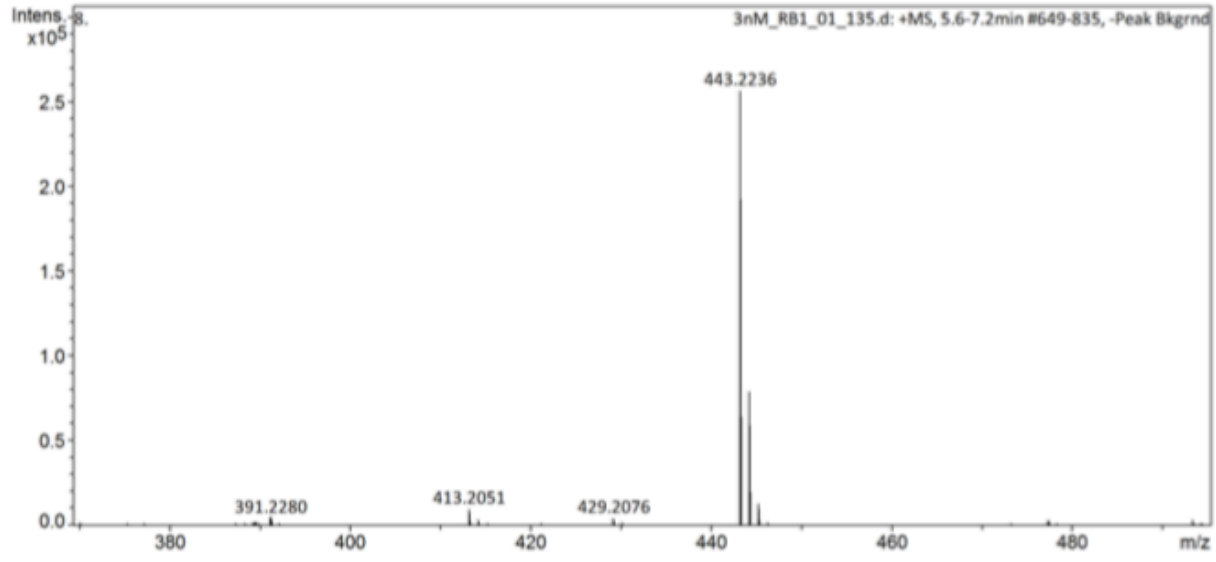

Rhodamine 2.5nM LC/MS result

Display Report

Analysis Info

Analysis Name	D:\Data\2.5nM_RA8_01_134.d	Acquisition Date	4/3/2019 3:13:46 AM
Method	Gen_SM_AutoMsMs.m	Operator	Demo User
Sample Name	2.5nM	Instrument	impact II 1825265.10094
Comment			

Acquisition Parameter

Source Type	ESI	Ion Polarity	Positive	Set Nebulizer	1.8 Bar
Focus	Not active	Set Capillary	4500 V	Set Dry Heater	220 °C
Scan Begin	50 m/z	Set End Plate Offset	-500 V	Set Dry Gas	8.0 l/min
Scan End	1300 m/z	Set Charging Voltage	2000 V	Set Divert Valve	Waste
		Set Corona	0 nA	Set APCI Heater	0 °C

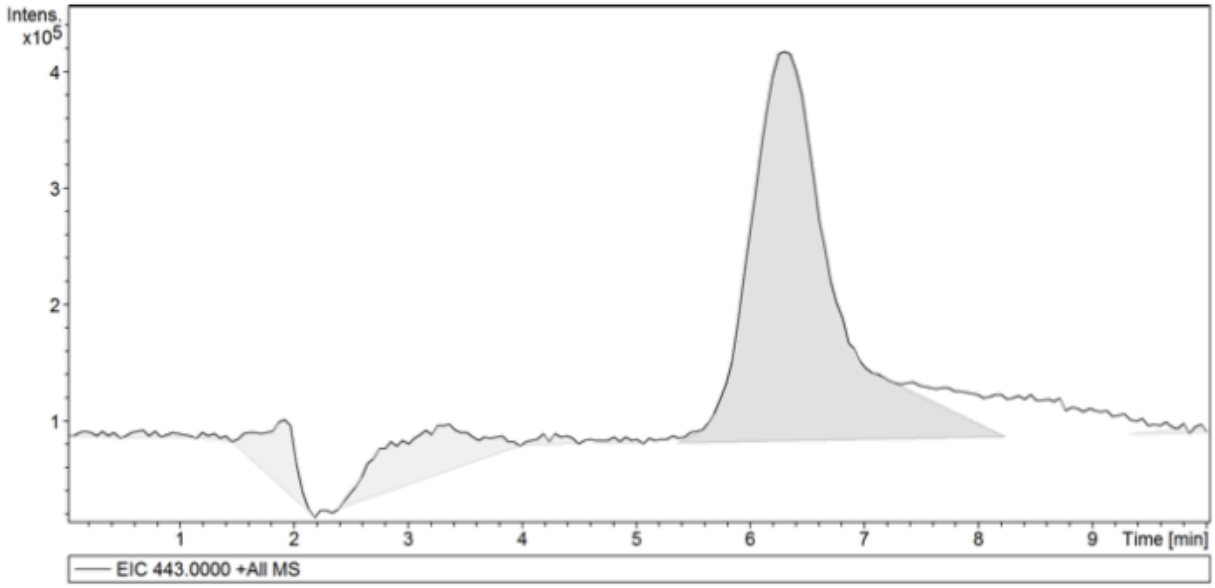

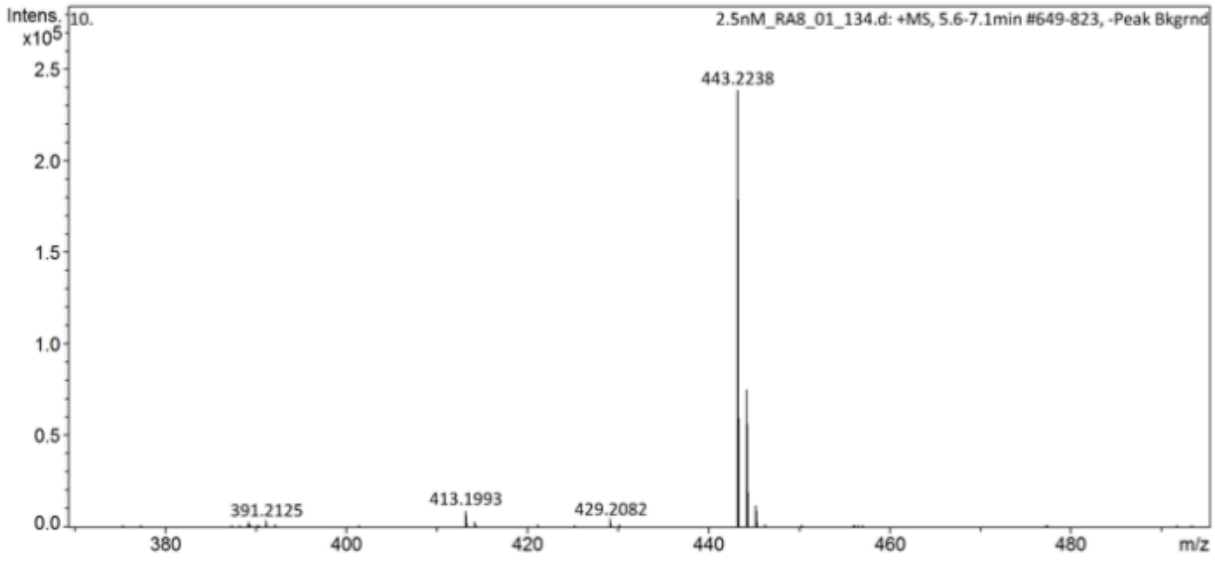

Rhodamine 2nM LC/MS result

Display Report

Analysis Info

Analysis Name	D:\Data\2nM_RA7_01_133.d	Acquisition Date	4/3/2019 3:02:26 AM
Method	Gen_SM_AutoMsMs.m	Operator	Demo User
Sample Name	2nM	Instrument	impact II 1825265.10094
Comment			

Acquisition Parameter

Source Type	ESI	Ion Polarity	Positive	Set Nebulizer	1.8 Bar
Focus	Not active	Set Capillary	4500 V	Set Dry Heater	220 °C
Scan Begin	50 m/z	Set End Plate Offset	-500 V	Set Dry Gas	8.0 l/min
Scan End	1300 m/z	Set Charging Voltage	2000 V	Set Divert Valve	Waste
		Set Corona	0 nA	Set APCI Heater	0 °C

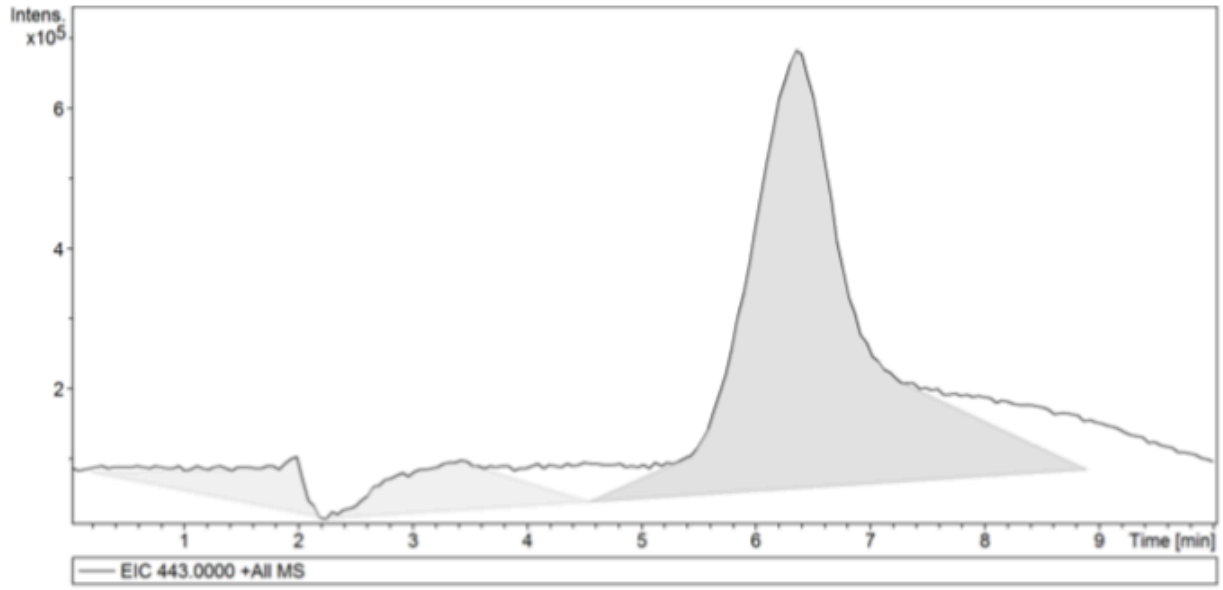

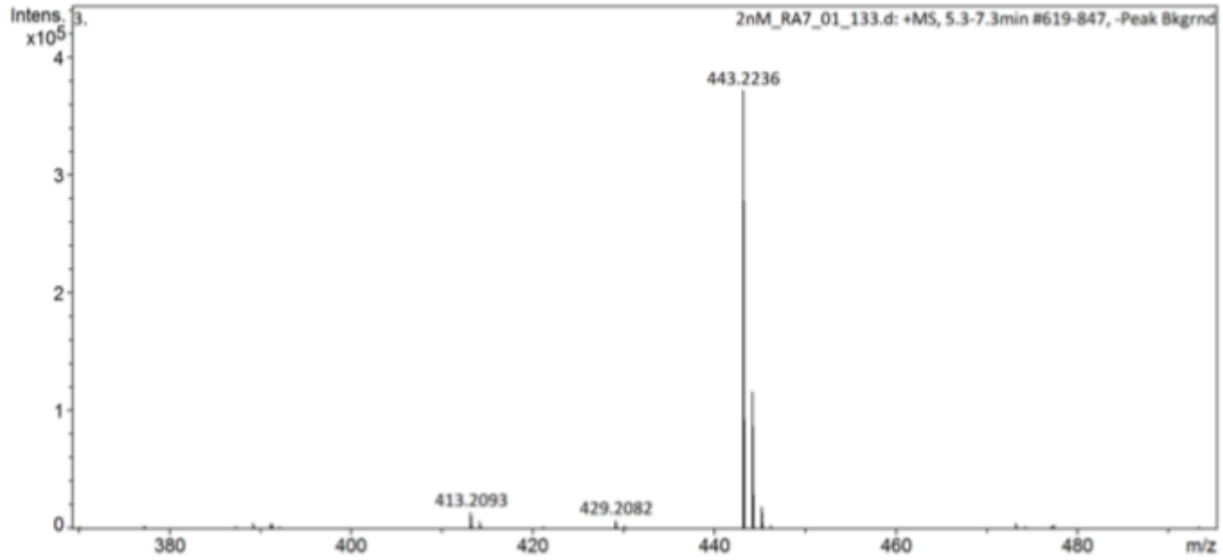

Rhodamine 1.5nM LC/MS result

Display Report

Analysis Info

Analysis Name	D:\Data\1.5nM_RA6_01_132.d	Acquisition Date	4/3/2019 2:51:06 AM
Method	Gen_SM_AutoMsMs.m	Operator	Demo User
Sample Name	1.5nM	Instrument	impact II 1825265.10094
Comment			

Acquisition Parameter

Source Type	ESI	Ion Polarity	Positive	Set Nebulizer	1.8 Bar
Focus	Not active	Set Capillary	4500 V	Set Dry Heater	220 °C
Scan Begin	50 m/z	Set End Plate Offset	-500 V	Set Dry Gas	8.0 l/min
Scan End	1300 m/z	Set Charging Voltage	2000 V	Set Divert Valve	Waste
		Set Corona	0 nA	Set APCI Heater	0 °C

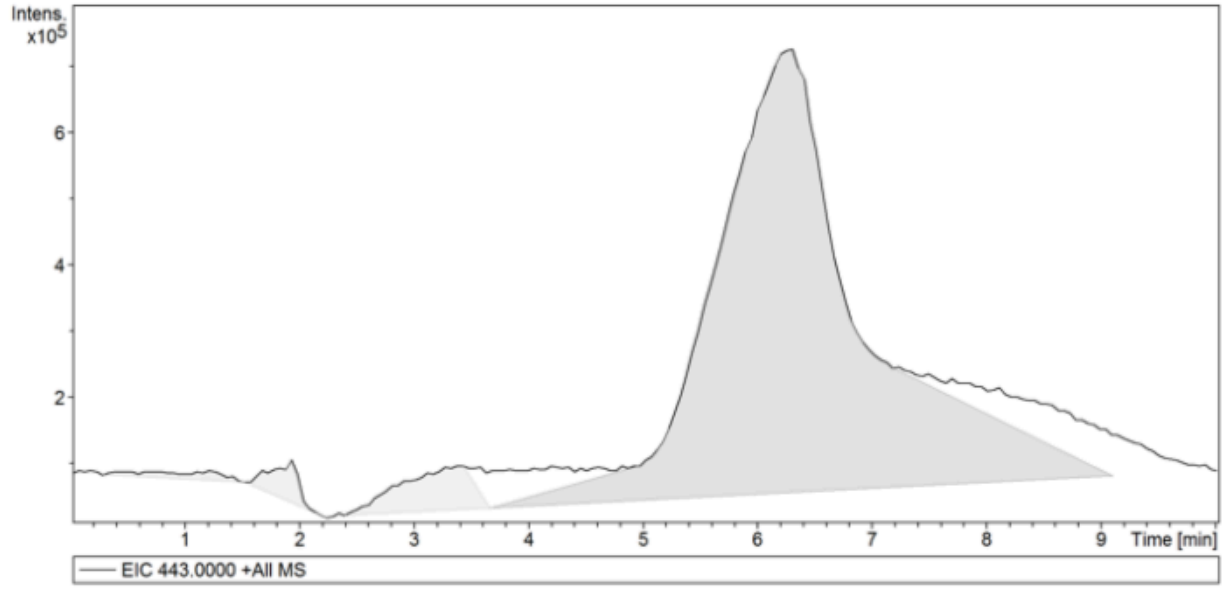

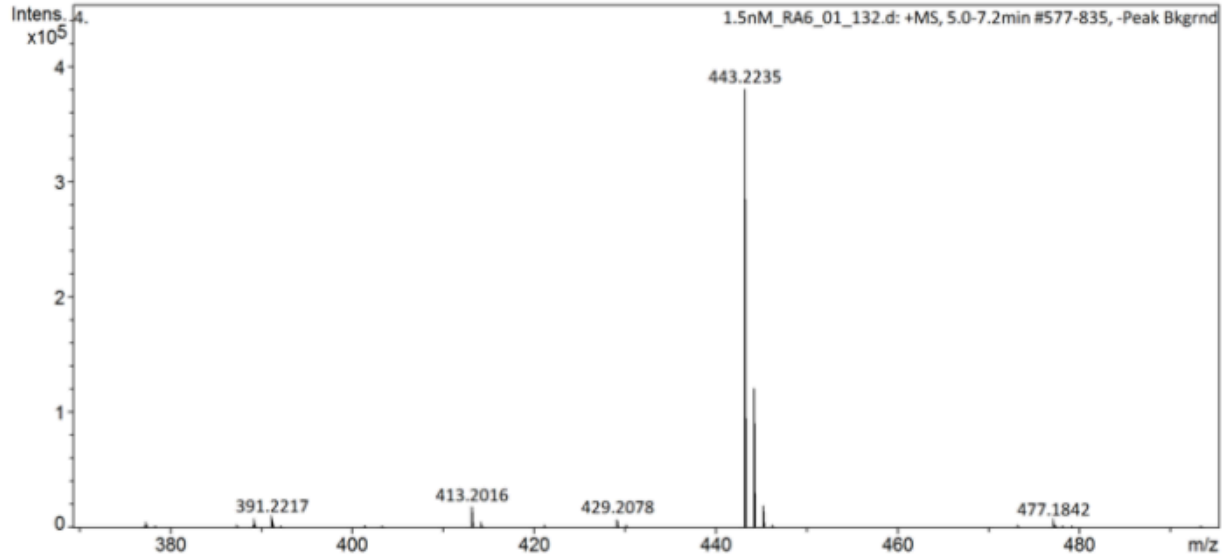

Rhodamine 1nM LC/MS result

Display Report

Analysis Info

Analysis Name	D:\Data\1nM_RA5_01_131.d	Acquisition Date	4/3/2019 2:39:45 AM
Method	Gen_SM_AutoMsMs.m	Operator	Demo User
Sample Name	1nM	Instrument	impact II 1825265.10094
Comment			

Acquisition Parameter

Source Type	ESI	Ion Polarity	Positive	Set Nebulizer	1.8 Bar
Focus	Not active	Set Capillary	4500 V	Set Dry Heater	220 °C
Scan Begin	50 m/z	Set End Plate Offset	-500 V	Set Dry Gas	8.0 l/min
Scan End	1300 m/z	Set Charging Voltage	2000 V	Set Divert Valve	Waste
		Set Corona	0 nA	Set APCI Heater	0 °C

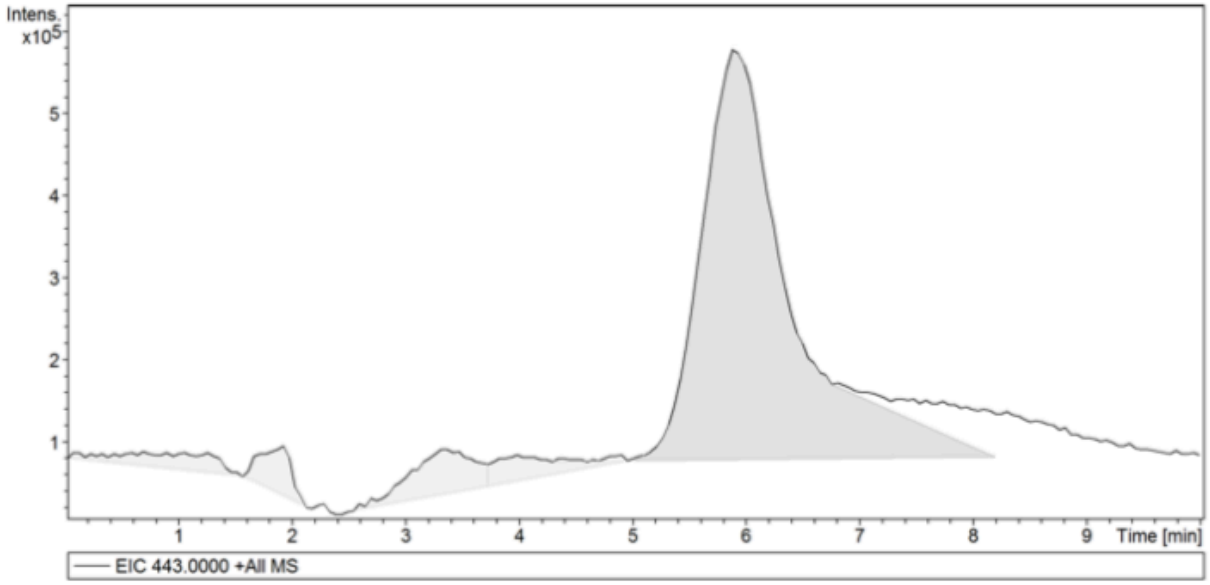

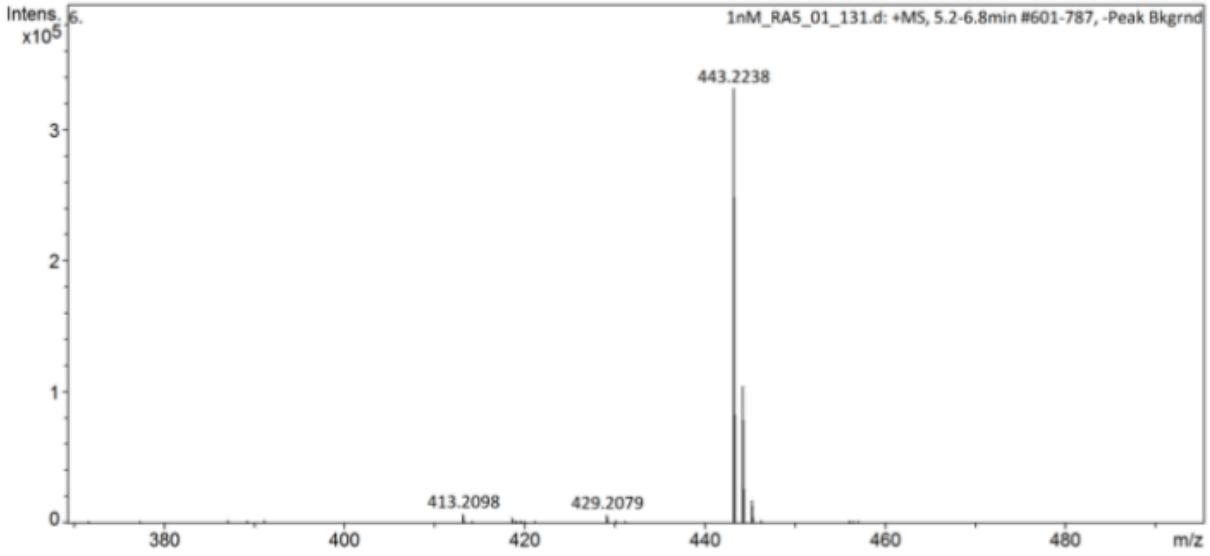

Rhodamine 0.5nM LC/MS result

Generic Display Report

Analysis Info

Analysis Name	D:\Data\0.5nM_RA4_01_130.d	Acquisition Date	4/3/2019 2:28:27 AM
Method	Gen_SM_AutoMsMs.m	Operator	Demo User
Sample Name	0.5nM	Instrument	impact II
Comment			

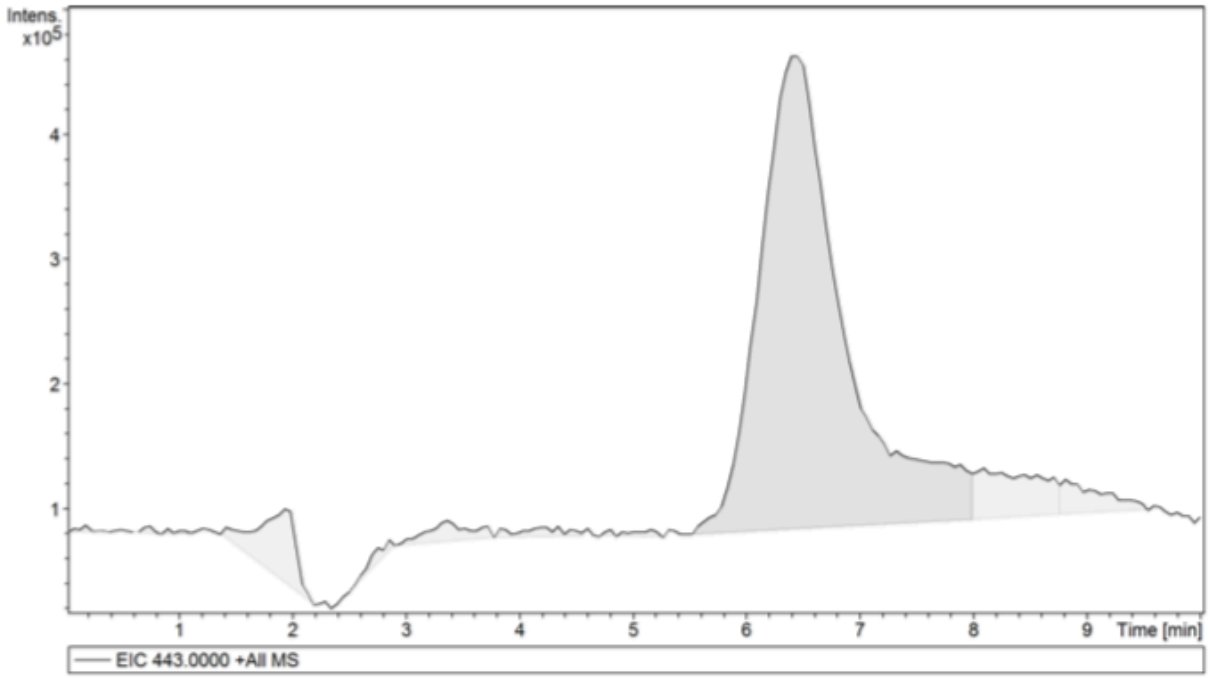

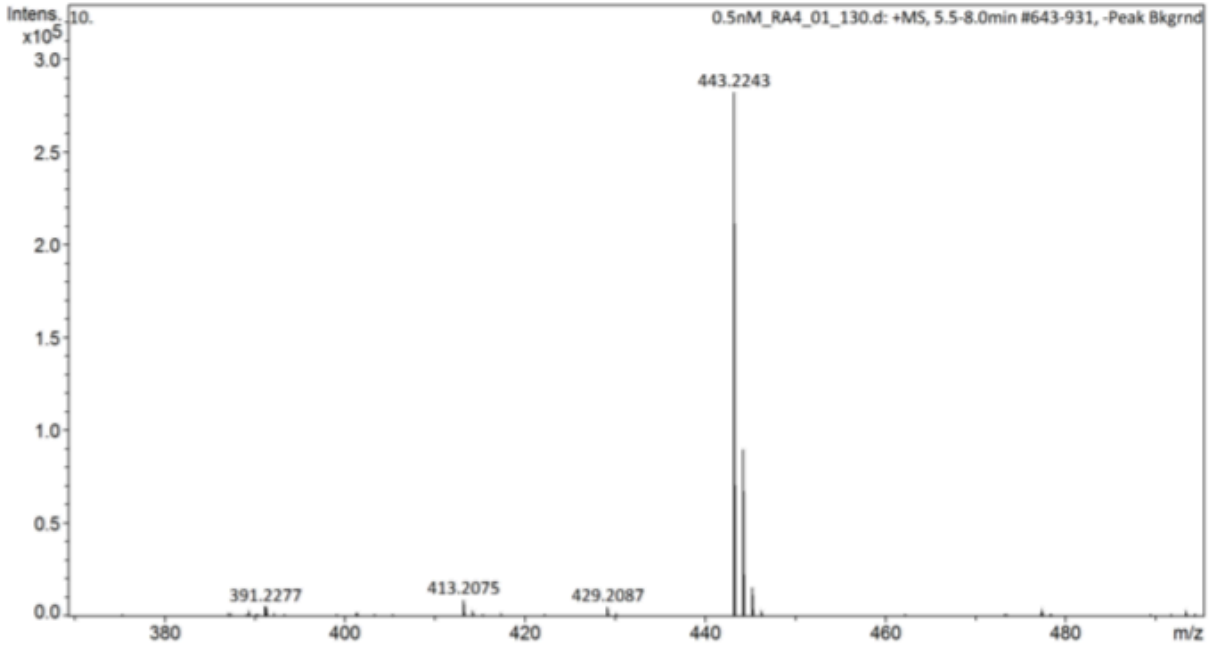

Rhodamine 0.3nM LC/MS result

Display Report

Analysis Info

Analysis Name	D:\Data\0.3nM_RA3_01_129.d	Acquisition Date	4/3/2019 2:17:06 AM
Method	Gen_SM_AutoMsMs.m	Operator	Demo User
Sample Name	0.3nM	Instrument	impact II 1825265.10094
Comment			

Acquisition Parameter

Source Type	ESI	Ion Polarity	Positive	Set Nebulizer	1.8 Bar
Focus	Not active	Set Capillary	4500 V	Set Dry Heater	220 °C
Scan Begin	50 m/z	Set End Plate Offset	-500 V	Set Dry Gas	8.0 l/min
Scan End	1300 m/z	Set Charging Voltage	2000 V	Set Divert Valve	Waste
		Set Corona	0 nA	Set APCI Heater	0 °C

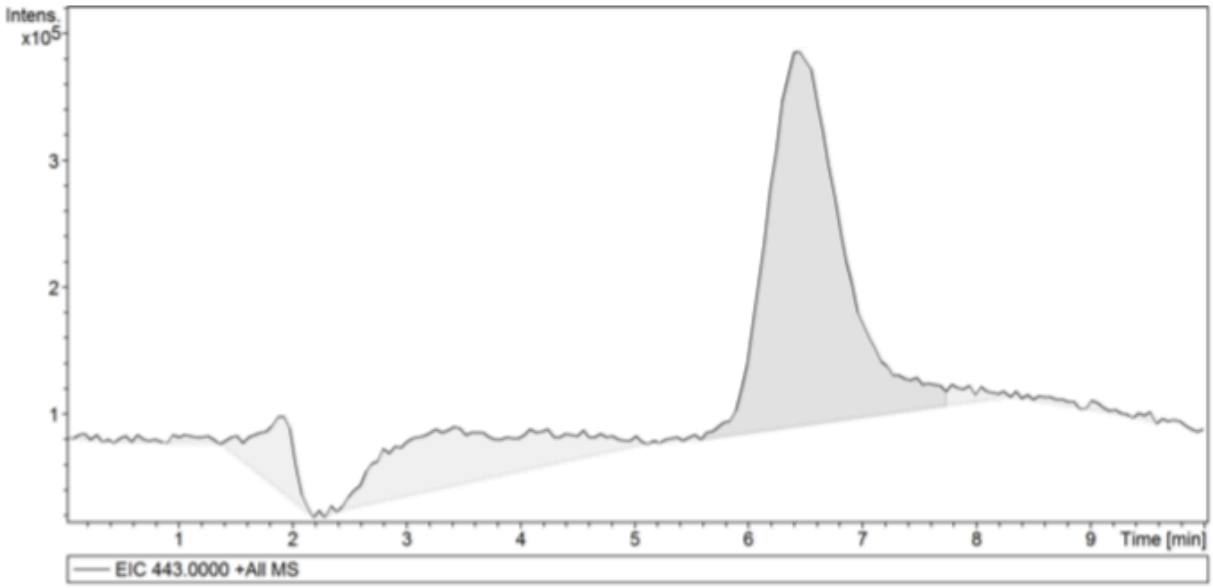

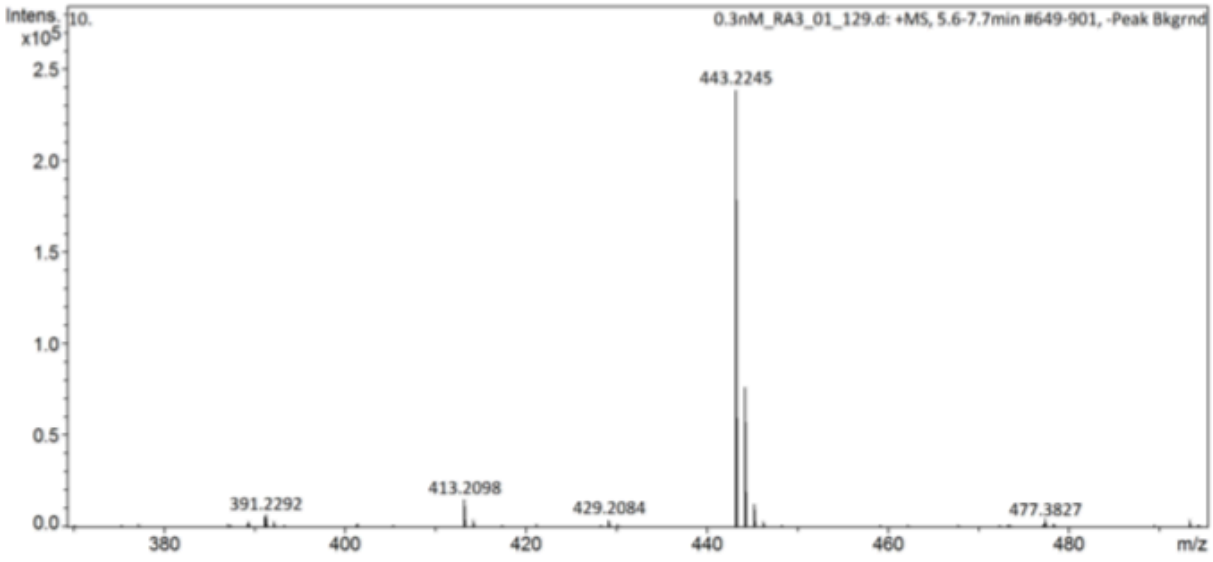

Rhodamine 3nM UV result

Area % Report

Data File: C:\Users\UPLC system 2\Desktop\rhodamine 030419\3nM2019-04-04 13-51-30 (GMT -07-00).dat
Method: C:\Enterprise\Projects\Hitachi\Method\Rhodamine1.met
Acquired: 4/4/2019 1:52:46 PM (GMT -07:00)
Printed: 4/8/2019 11:12:08 AM (GMT -07:00)

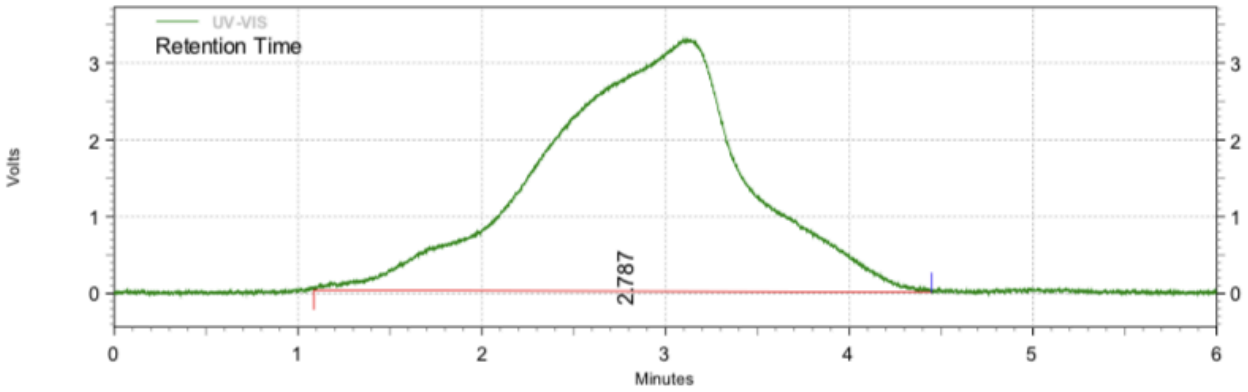

UV-VIS Results

Retention Time	Area	Area %	Height	Height %
2.787	825824	100.00	11121	100.00
Totals	825824	100.00	11121	100.00

Rhodamine 2.5nM UV result

Area % Report

Data File: C:\Users\UPLC system 2\Desktop\rhodamine 030419\2.5nM2019-04-04 13-59-01 -07-00).dat (GMT
Method:
Acquired: C:\Enterprise\Projects\Hitachi\Method\Rhodamine1.met
Printed: 4/4/2019 2:00:15 PM (GMT -07:00)

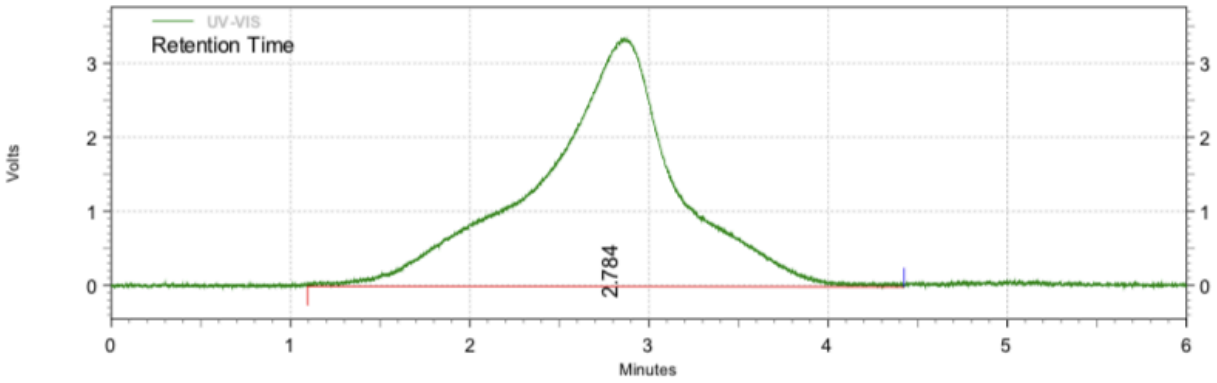

UV-VIS Results

Retention Time	Area	Area %	Height	Height %
2.784	793298	100.00	12470	100.00

Totals	793298	100.00	12470	100.00

Rhodamine 2nM UV result

Area % Report

Data File: C:\Users\UPLC system 2\Desktop\rhodamine 030419\2nM2019-04-04 13-44-03 -07-00).dat (GMT
Method:
Acquired: C:\Enterprise\Projects\Hitachi\Method\Rhodamine1.met
Printed: 4/4/2019 1:45:15 PM (GMT -07:00)

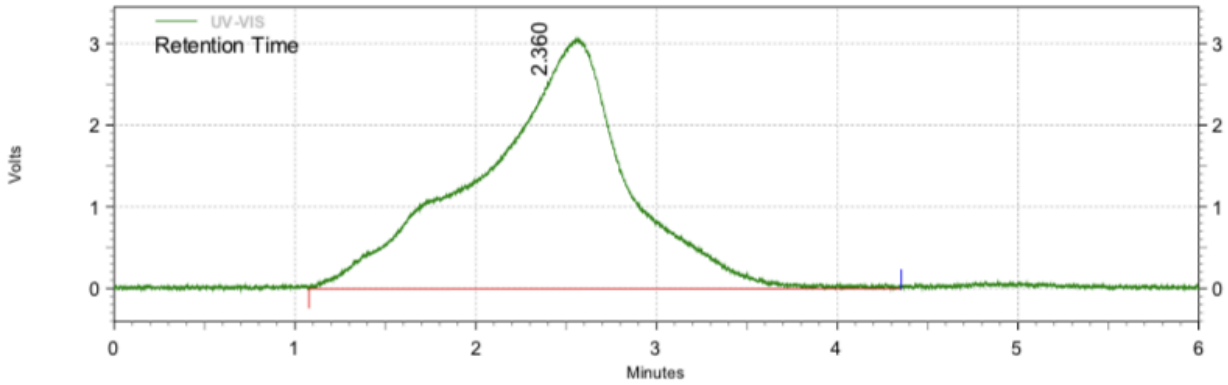

UV-VIS Results

Retention Time	Area	Area %	Height	Height %
2.360	704323	100.00	9369	100.00

Totals	704323	100.00	9369	100.00

Rhodamine 1.5nM UV result

Area % Report

Data File: C:\Users\UPLC system 2\Desktop\rhodamine 030419\1.5nM2019-04-04 14-06-28 -07-00).dat (GMT
Method:
Acquired: C:\Enterprise\Projects\Hitachi\Method\Rhodamine1.met
Printed: 4/4/2019 2:07:45 PM (GMT -07:00)

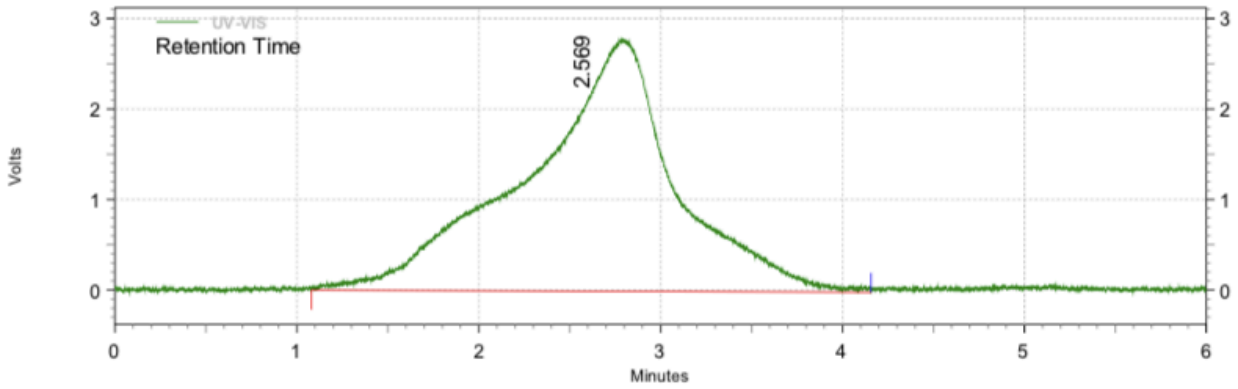

UV-VIS Results

Retention Time	Area	Area %	Height	Height %
2.569	680484	100.00	8000	100.00
Totals	680484	100.00	8000	100.00

Rhodamine 1nM UV result

Area % Report

Data File: C:\Users\UPLC system 2\Desktop\rhodamine 030419\1nM2019-04-04 13-36-33 (GMT -07-00).dat
Method: C:\Enterprise\Projects\Hitachi\Method\Rhodamine1.met
Acquired: 4/4/2019 1:37:51 PM (GMT -07:00)
Printed: 4/8/2019 11:11:25 AM (GMT -07:00)

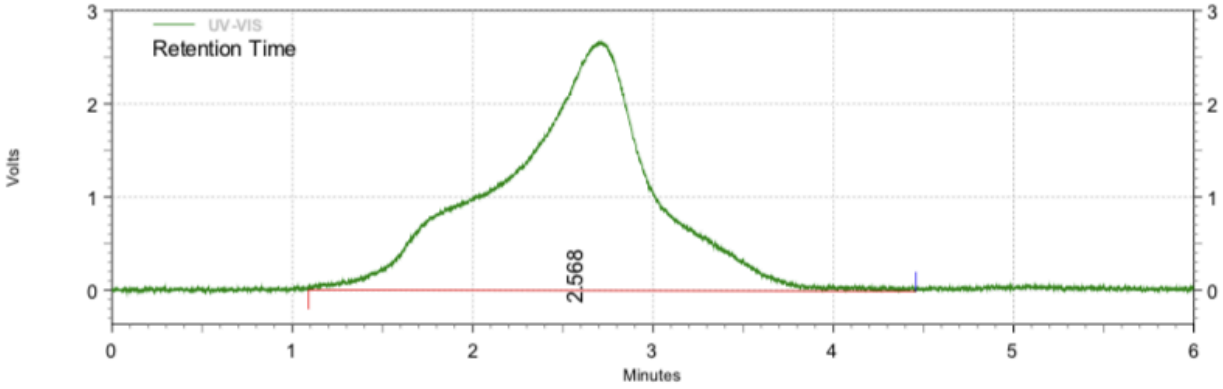

UV-VIS Results

Retention Time	Area	Area %	Height	Height %
2.568	620265	100.00	9027	100.00
Totals	620265	100.00	9027	100.00

Rhodamine 0.5nM UV result

Area % Report

Data File: C:\Users\UPLC system 2\Desktop\rhodamine 030419\0.5nM2019-04-04 13-14-07 -07-00).dat (GMT
Method:
Acquired: C:\Enterprise\Projects\Hitachi\Method\Rhodamine1.met
Printed: 4/4/2019 1:15:23 PM (GMT -07:00)

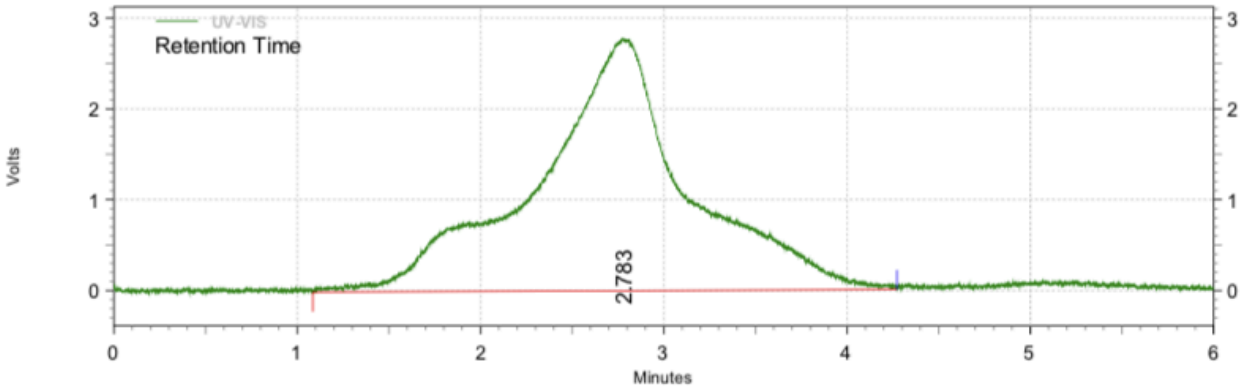

UV-VIS Results

Retention Time	Area	Area %	Height	Height %
2.783	593762	100.00	11100	100.00

Totals	593762	100.00	11100	100.00

Rhodamine 0.3nM UV result

Area % Report

Data File: C:\Users\UPLC system 2\Desktop\rhodamine 030419\0.3nM2019-04-04 13-29-04 -07-00).dat (GMT
Method:
Acquired: C:\Enterprise\Projects\Hitachi\Method\Rhodamine1.met
Printed: 4/4/2019 1:30:20 PM (GMT -07:00)

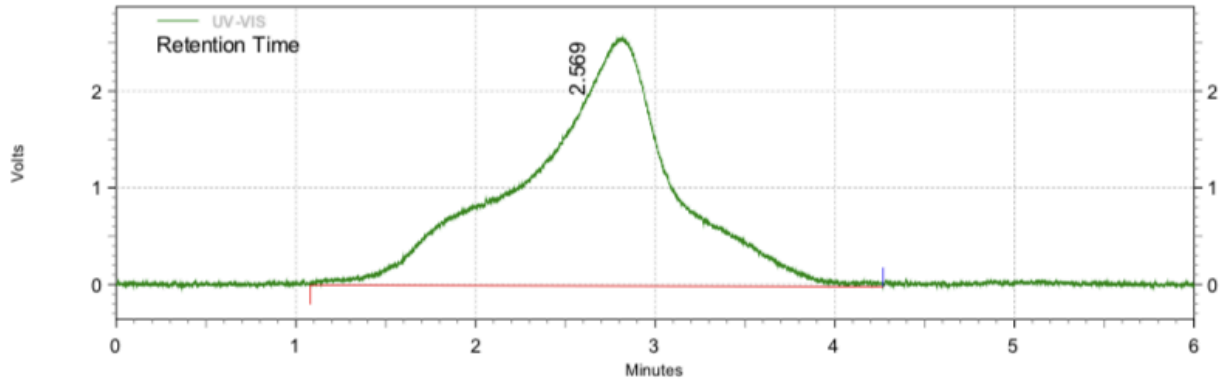

UV-VIS Results

Retention Time	Area	Area %	Height	Height %
2.569	570155	100.00	6987	100.00
Totals	570155	100.00	6987	100.00

Doxorubicin 3μM MS result

Generic Display Report

Analysis Info

Analysis Name	D:\Data\Qamar\DOXO 3 mM 3 18 JUL.d	Acquisition Date	7/18/2018 1:09:39 PM
Method	Small Molecules - DI - MS.m	Operator	Chapman
Sample Name	20 MIN- JULY 17	Instrument	impact II
Comment			

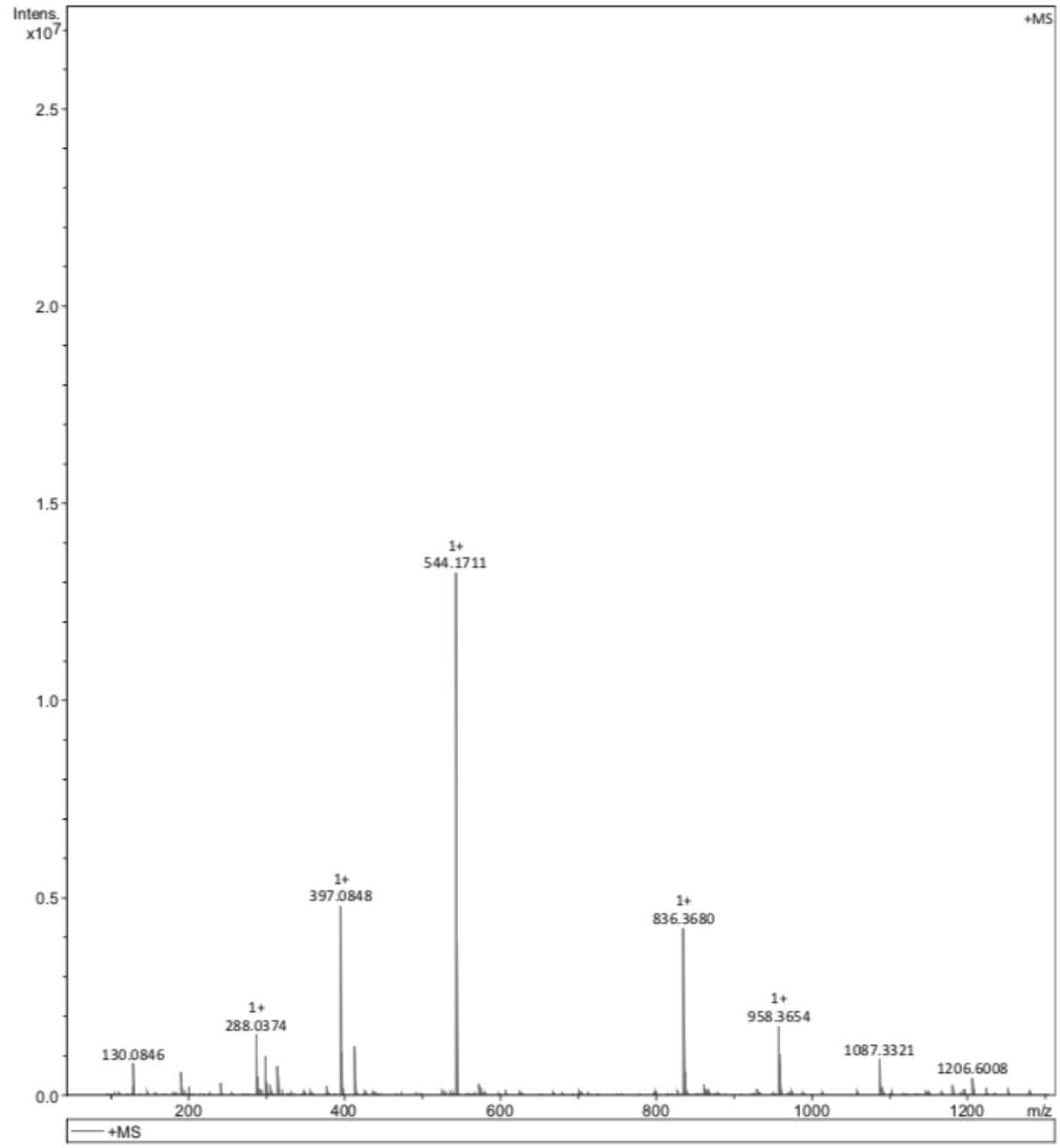

Doxorubicin 1.5µM MS result

Generic Display Report

Analysis Info

Analysis Name	D:\Data\Qamar\DOXO 1.5 mM 3 18 JUL.d	Acquisition Date	7/18/2018 1:20:37 PM
Method	Small Molecules - DI - MS.m	Operator	Chapman
Sample Name	20 MIN- JULY 17	Instrument	impact II
Comment			

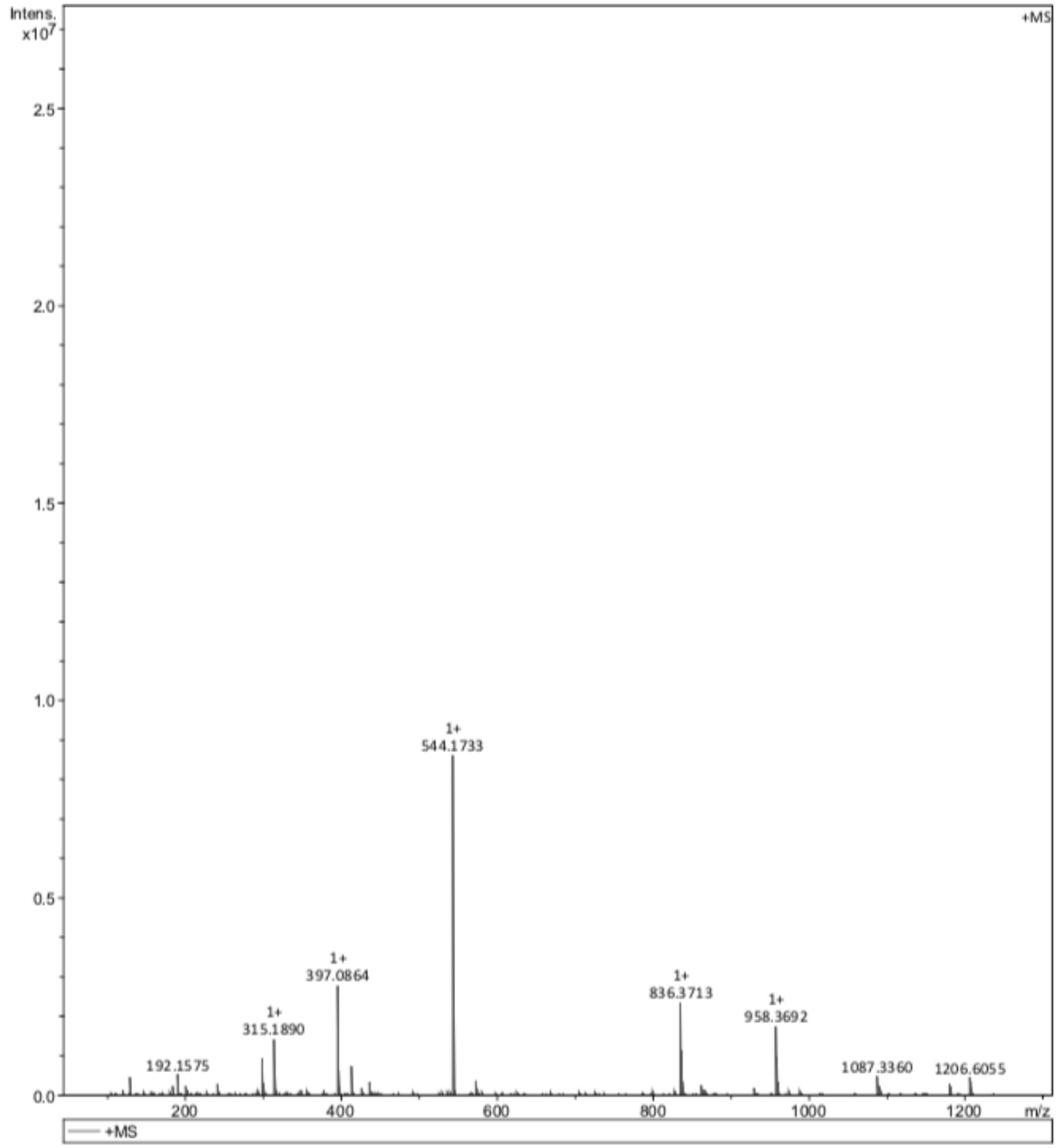

Doxorubicin 1μM MS result

Generic Display Report

Analysis Info

Analysis Name	D:\Data\Qamar\DOXO 1 mM 2 18 JUL.d	Acquisition Date	7/18/2018 1:29:07 PM
Method	Small Molecules - DI - MS.m	Operator	Chapman
Sample Name	20 MIN- JULY 17	Instrument	impact II
Comment			

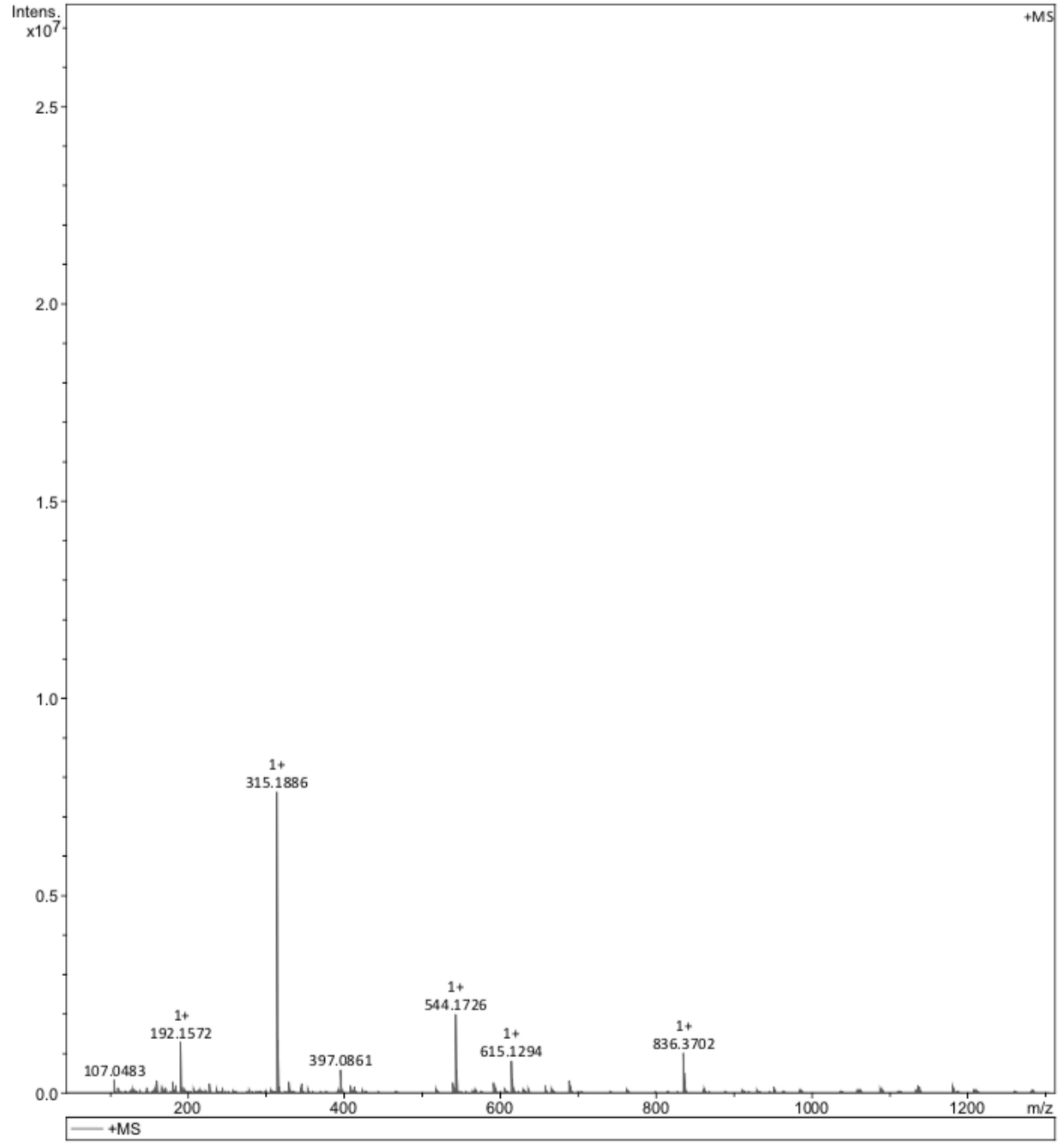

Doxorubicin 500nM MS result

Generic Display Report

Analysis Info

Analysis Name	D:\Data\Qamar\DOXO 500nM 19 JUL .d	Acquisition Date	7/19/2018 3:44:25 PM
Method	New Method.m	Operator	Chapman
Sample Name	Blanlk1	Instrument	impact II
Comment			

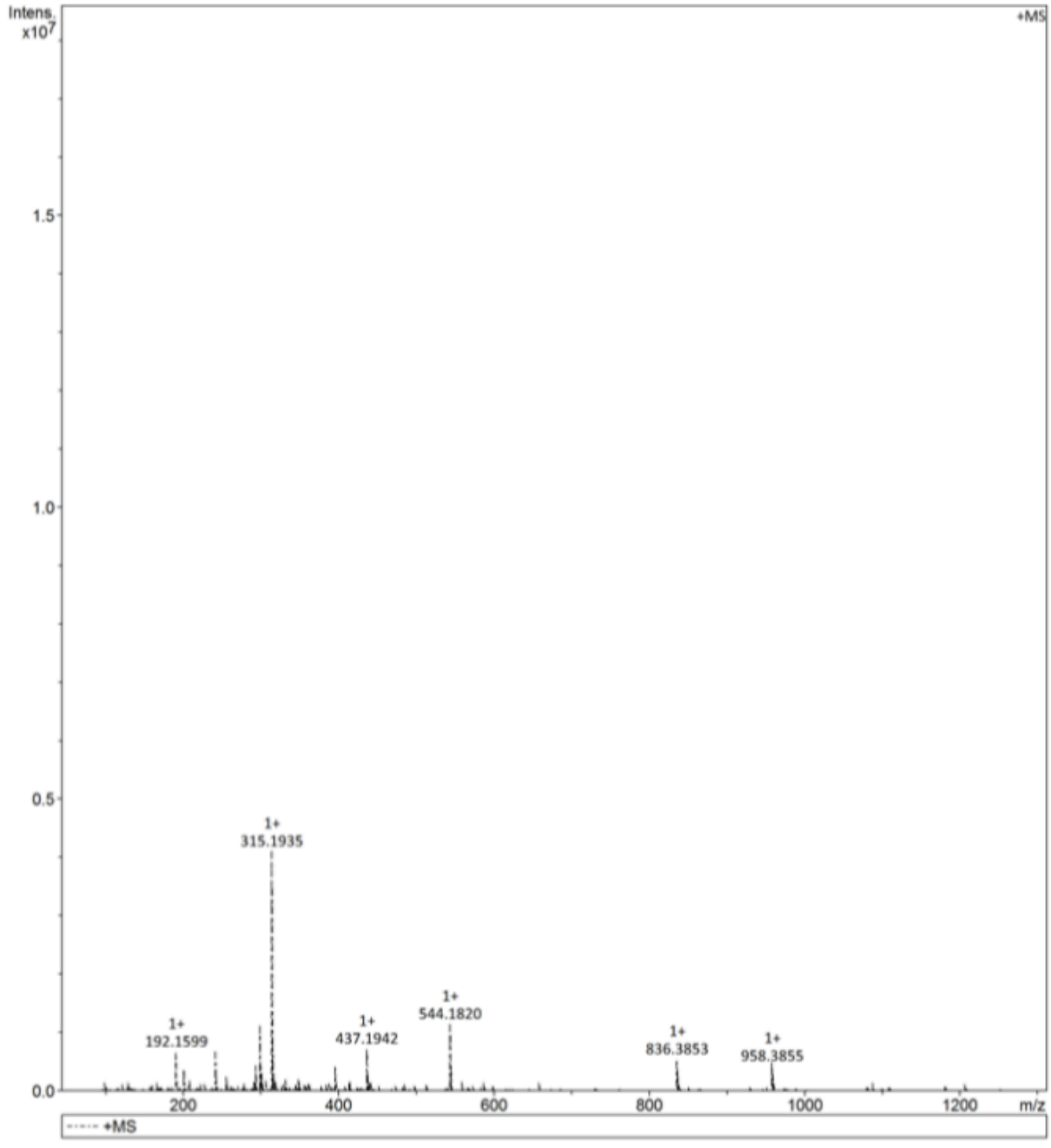

Doxorubicin 450nM MS result

Generic Display Report

Analysis Info

Analysis Name	D:\Data\Qamar\DOXO 450nM 17 JUL.d	Acquisition Date	7/17/2018 4:38:00 PM
Method	Small Molecules - DI - MS.m	Operator	Chapman
Sample Name	20 MIN- JULY 17	Instrument	impact II
Comment			

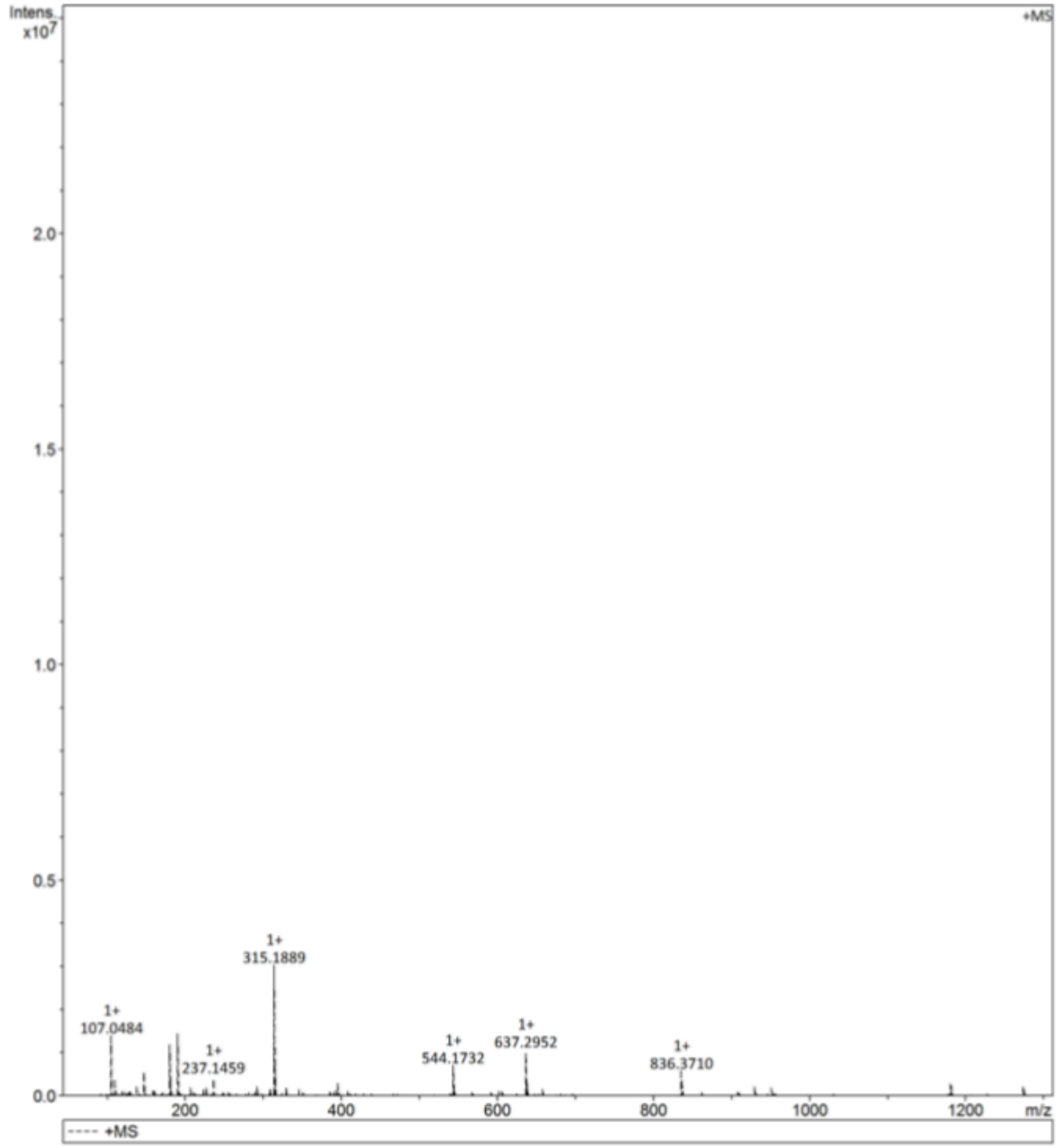

Doxorubicin 300nM MS result

Generic Display Report

Analysis Info

Analysis Name	D:\Data\Qamar\DOXO 300 nM 19 JUL .d	Acquisition Date	7/19/2018 4:02:45 PM
Method	Small Molecules - DI - MS.m	Operator	Chapman
Sample Name	Blanlk1	Instrument	impact II
Comment			

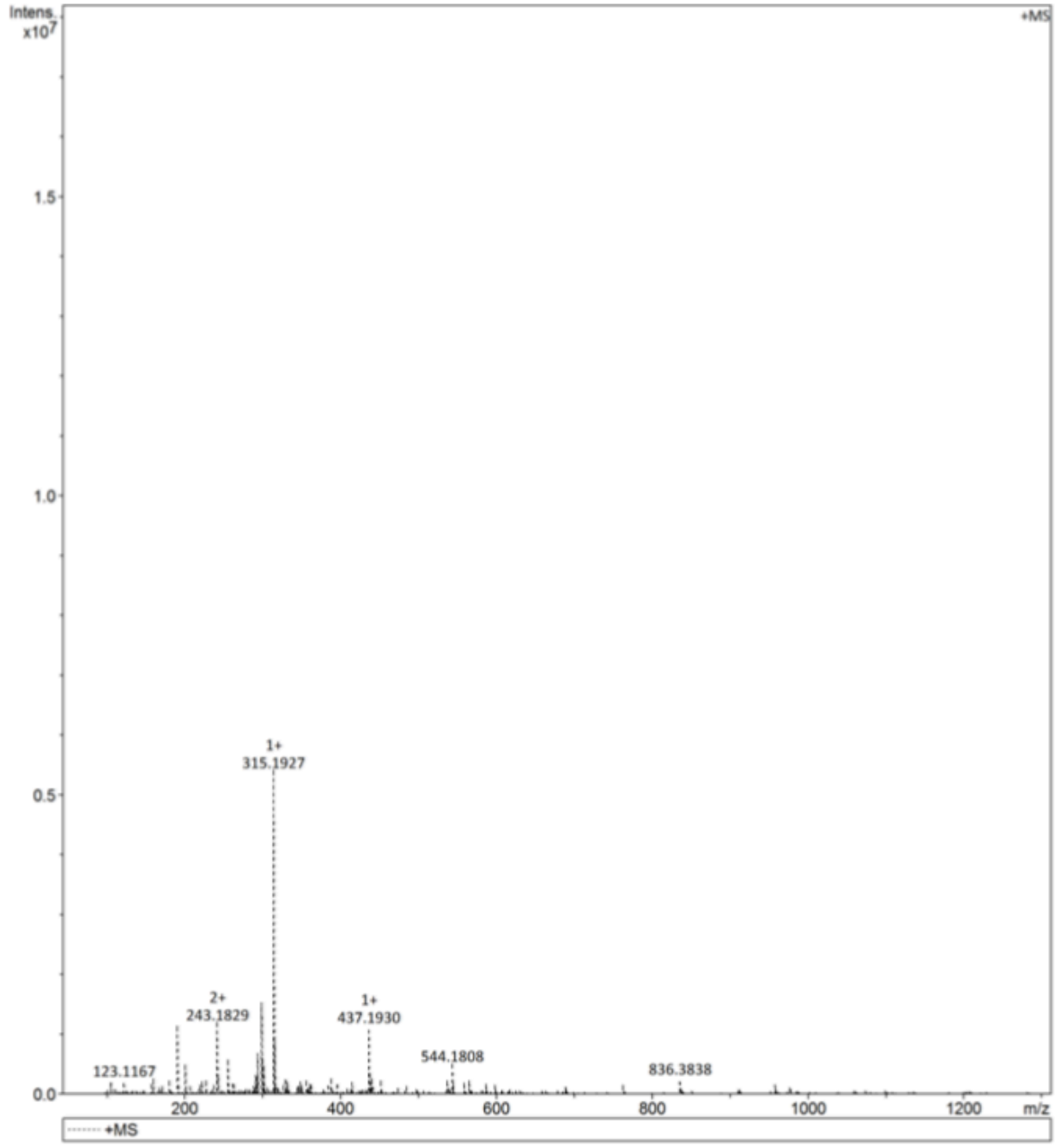

Doxorubicin 100nM MS result

Generic Display Report

Analysis Info

Analysis Name	D:\Data\Qamar\DOXO 100nM 17 JUL.d	Acquisition Date	7/17/2018 4:44:45 PM
Method	Small Molecules - DI - MS.m	Operator	Chapman
Sample Name	20 MIN- JULY 17	Instrument	impact II
Comment			

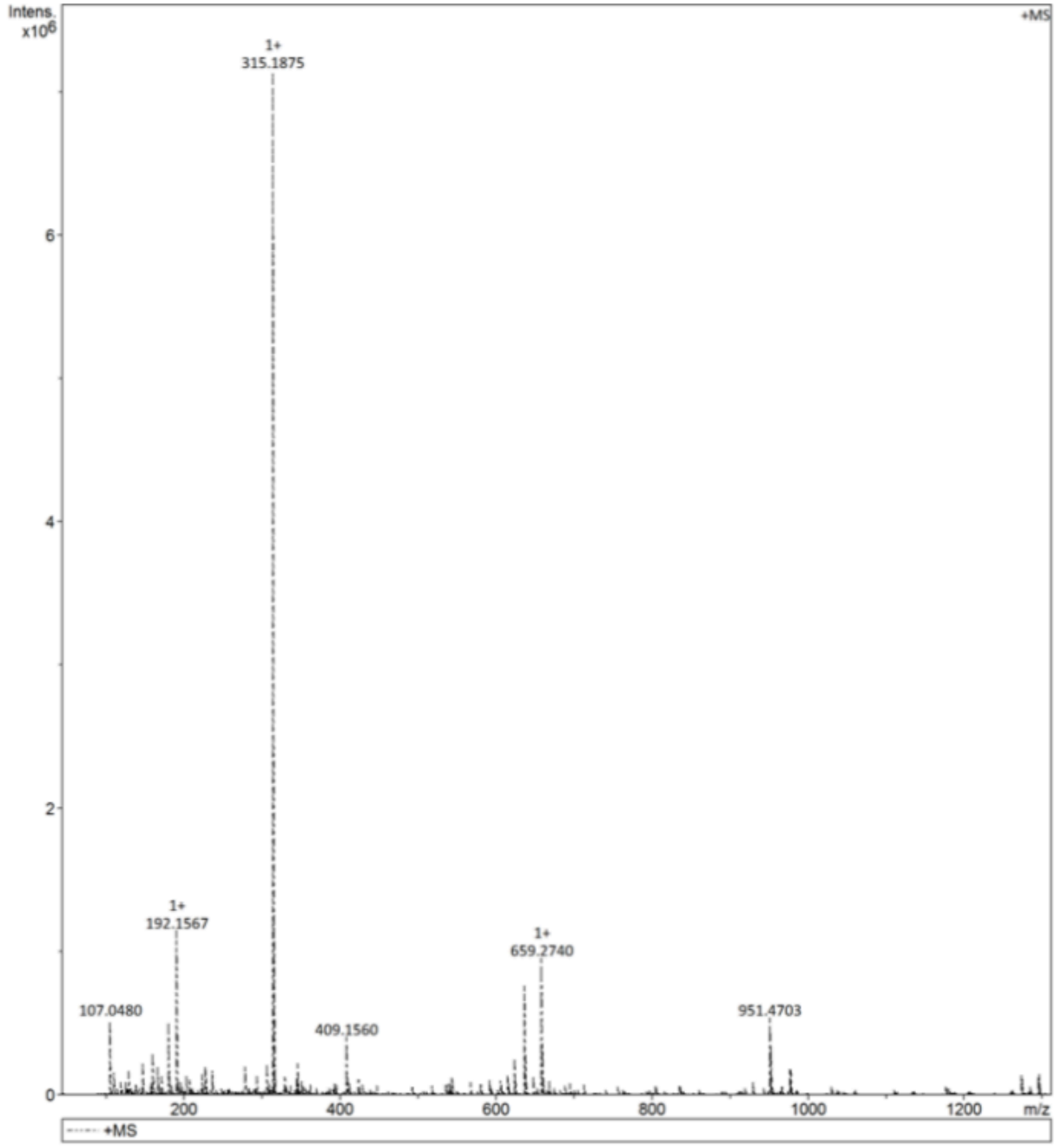

Doxorubicin 3μM LC/MS result

Display Report

Analysis Info

Analysis Name	D:\Data\Qamar\Data\3000 nM_RA6_01_57.d	Acquisition Date	3/20/2019 8:35:03 PM
Method	LCMS M6_2 C18 3um 50_4.6mm.m	Operator	Demo User
Sample Name	3000 nM	Instrument	impact II 1825265.10094
Comment			

Acquisition Parameter

Source Type	ESI	Ion Polarity	Positive	Set Nebulizer	3.0 Bar
Focus	Active	Set Capillary	4500 V	Set Dry Heater	200 °C
Scan Begin	50 m/z	Set End Plate Offset	-500 V	Set Dry Gas	12.0 l/min
Scan End	1300 m/z	Set Charging Voltage	2000 V	Set Divert Valve	Waste
		Set Corona	0 nA	Set APCI Heater	0 °C

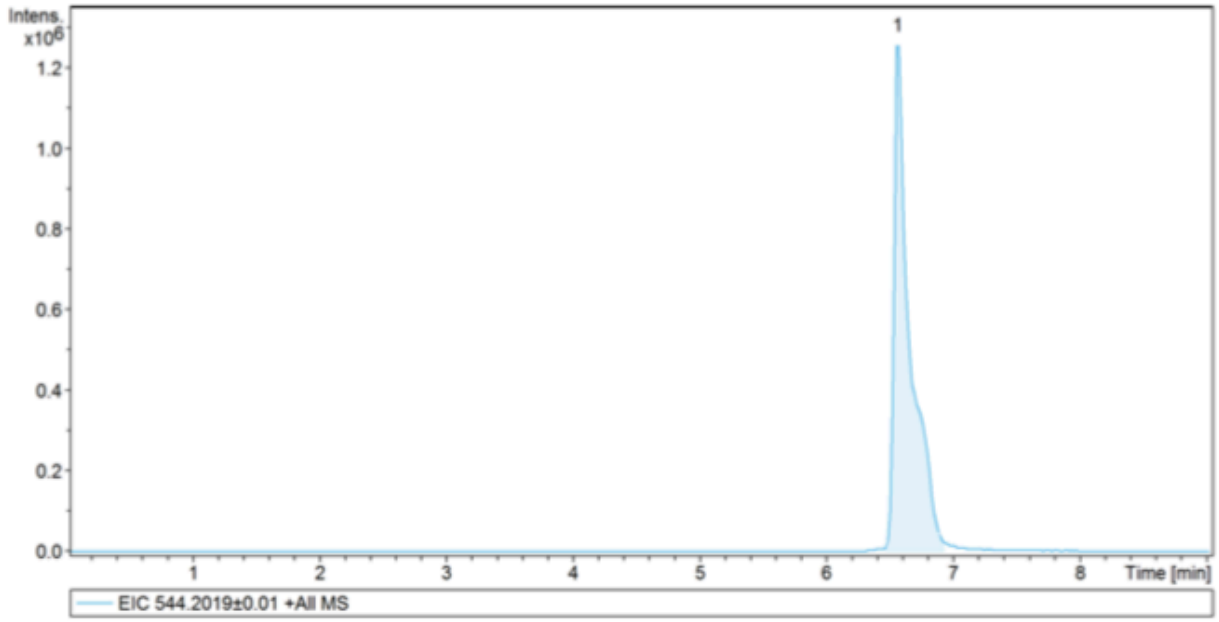

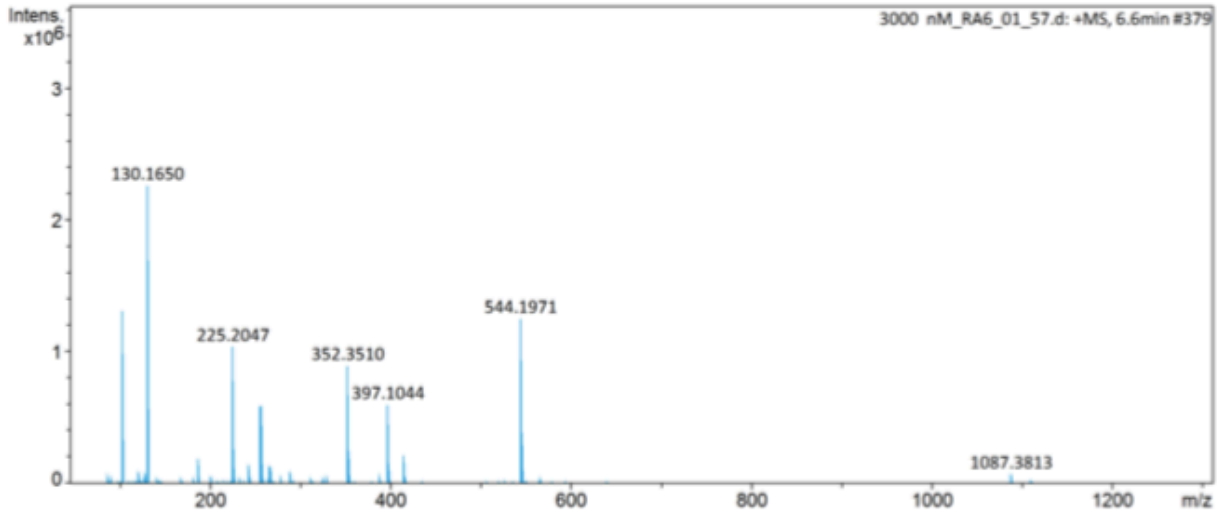

Doxorubicin 1μM LC/MS result

Display Report

Analysis Info

Analysis Name	D:\Data\Qamar\Data\1000 nM_RA5_01_56.d	Acquisition Date	3/20/2019 8:24:51 PM
Method	LCMS M6_2 C18 3um 50_4.6mm.m	Operator	Demo User
Sample Name	1000 nM	Instrument	impact II 1825265.10094
Comment			

Acquisition Parameter

Source Type	ESI	Ion Polarity	Positive	Set Nebulizer	3.0 Bar
Focus	Active	Set Capillary	4500 V	Set Dry Heater	200 °C
Scan Begin	50 m/z	Set End Plate Offset	-500 V	Set Dry Gas	12.0 l/min
Scan End	1300 m/z	Set Charging Voltage	2000 V	Set Divert Valve	Waste
		Set Corona	0 nA	Set APCI Heater	0 °C

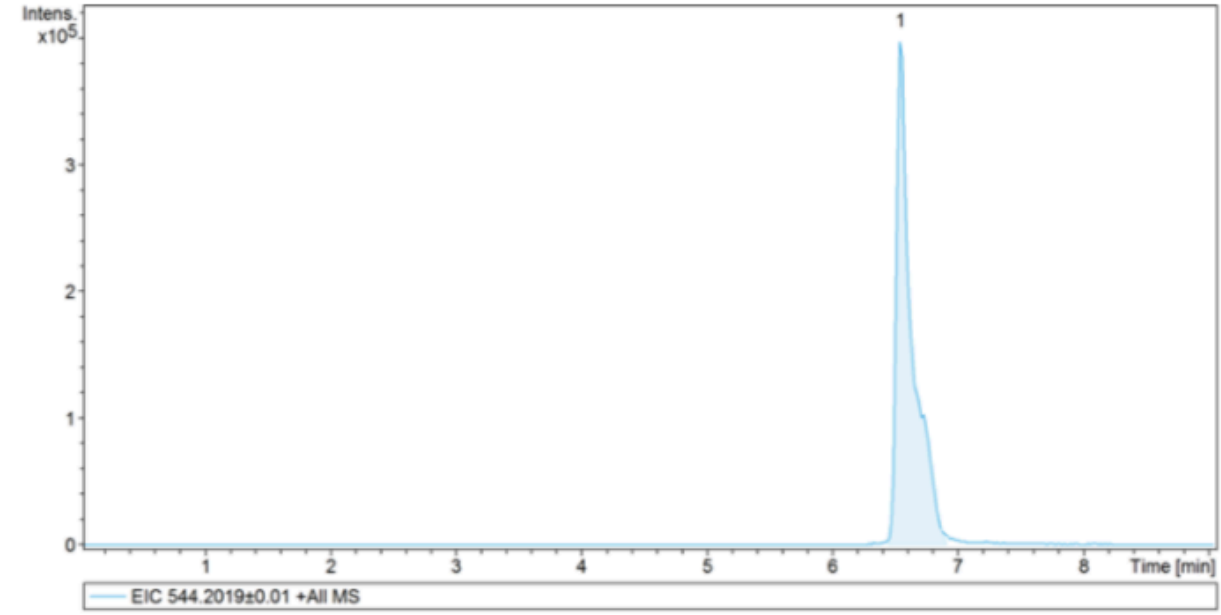

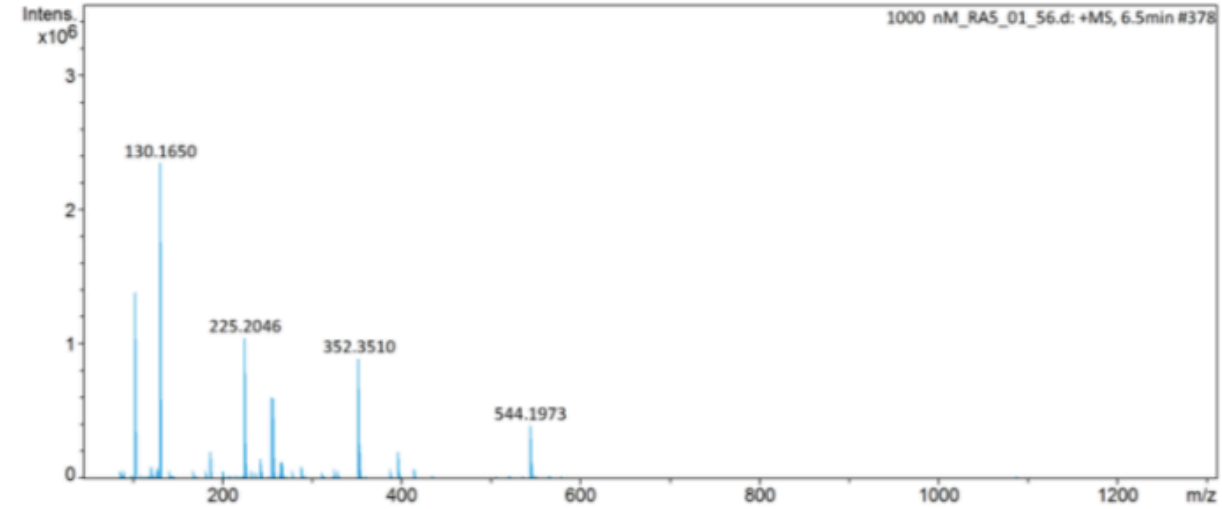

Doxorubicin 500nM LC/MS result

Display Report

Analysis Info

Analysis Name	D:\Data\Qamar\Data\500 nM_RA4_01_55.d	Acquisition Date	3/20/2019 8:14:40 PM
Method	LCMS M6_2 C18 3um 50_4.6mm.m	Operator	Demo User
Sample Name	500 nM	Instrument	impact II 1825265.10094
Comment			

Acquisition Parameter

Source Type	ESI	Ion Polarity	Positive	Set Nebulizer	3.0 Bar
Focus	Active	Set Capillary	4500 V	Set Dry Heater	200 °C
Scan Begin	50 m/z	Set End Plate Offset	-500 V	Set Dry Gas	12.0 l/min
Scan End	1300 m/z	Set Charging Voltage	2000 V	Set Divert Valve	Waste
		Set Corona	0 nA	Set APCI Heater	0 °C

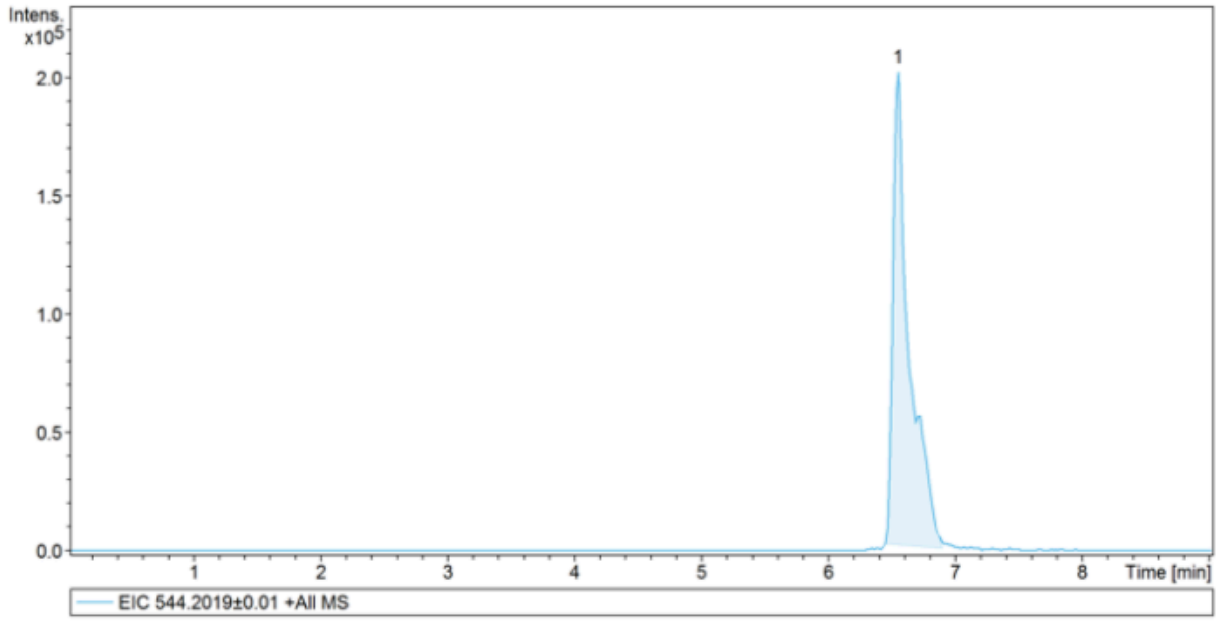

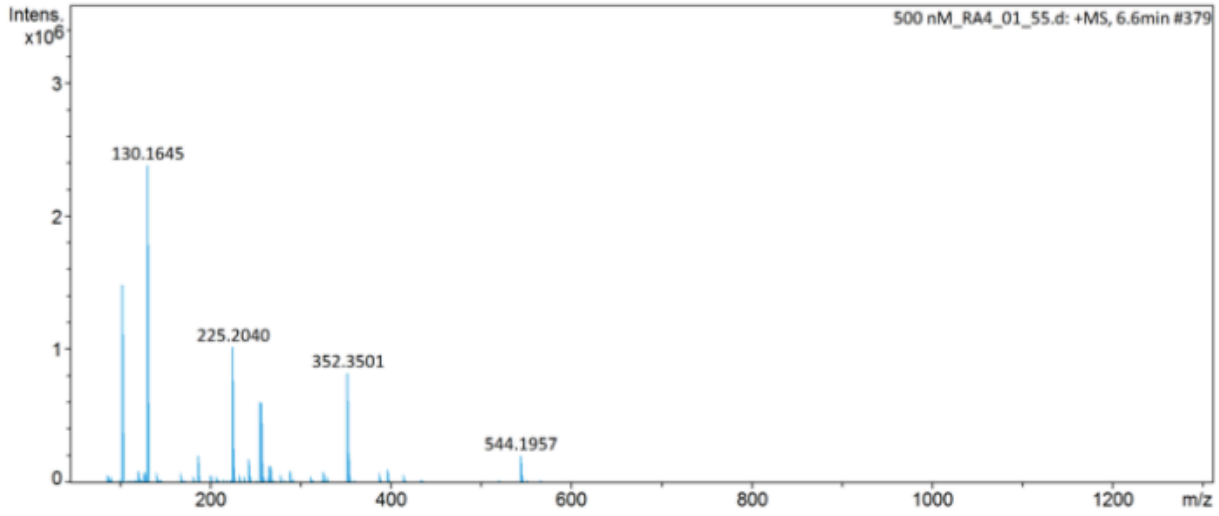

Doxorubicin 300nM LC/MS result

Display Report

Analysis Info

Analysis Name	D:\Data\Qamar\Data\300 nM_RA3_01_54.d	Acquisition Date	3/20/2019 8:04:29 PM
Method	LCMS M6_2 C18 3um 50_4.6mm.m	Operator	Demo User
Sample Name	300 nM	Instrument	impact II 1825265.10094
Comment			

Acquisition Parameter

Source Type	ESI	Ion Polarity	Positive	Set Nebulizer	3.0 Bar
Focus	Active	Set Capillary	4500 V	Set Dry Heater	200 °C
Scan Begin	50 m/z	Set End Plate Offset	-500 V	Set Dry Gas	12.0 l/min
Scan End	1300 m/z	Set Charging Voltage	2000 V	Set Divert Valve	Waste
		Set Corona	0 nA	Set APCI Heater	0 °C

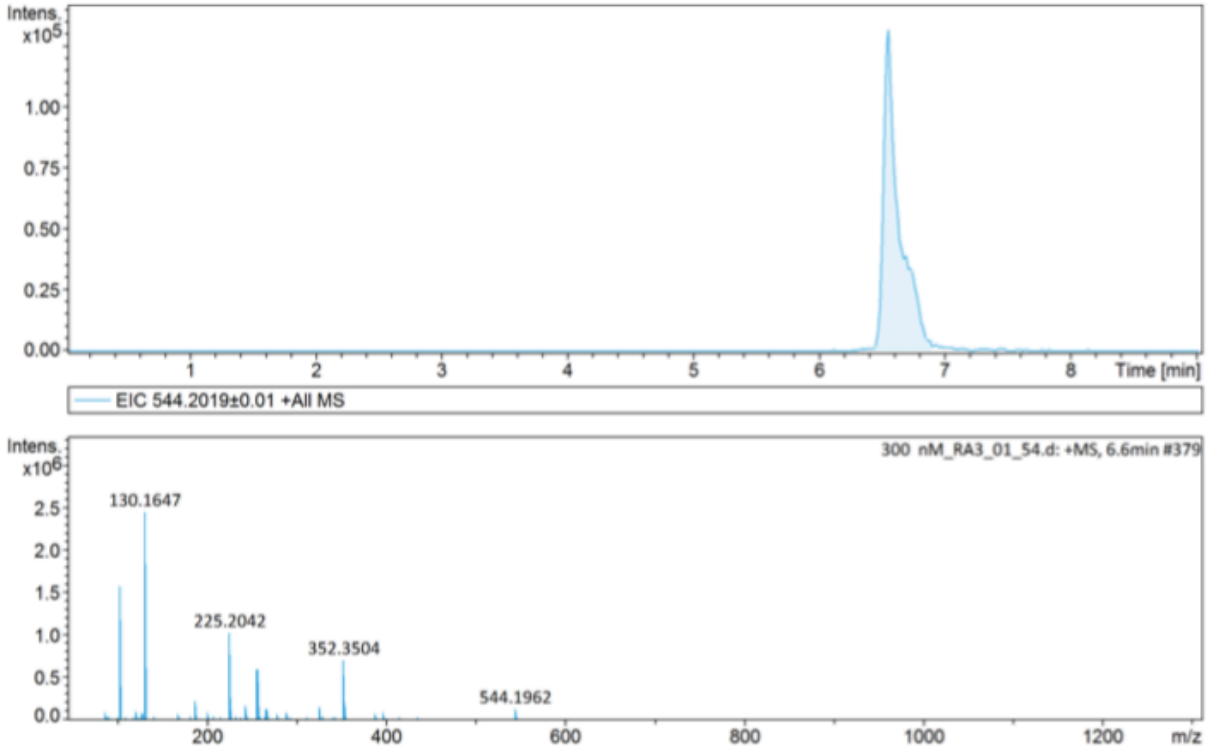

Doxorubicin 3µM UV result

Area % Report

Data File: C:\Users\UPLC system 2\Desktop\Qamar\3000nM2019-03-19 12-33-55 (GMT -07-00).dat
Method: C:\Enterprise\Projects\Hitachi\Method\Doxo_1.met
Acquired: 3/19/2019 12:35:09 PM (GMT -07:00)
Printed: 3/19/2019 3:08:43 PM (GMT -07:00)

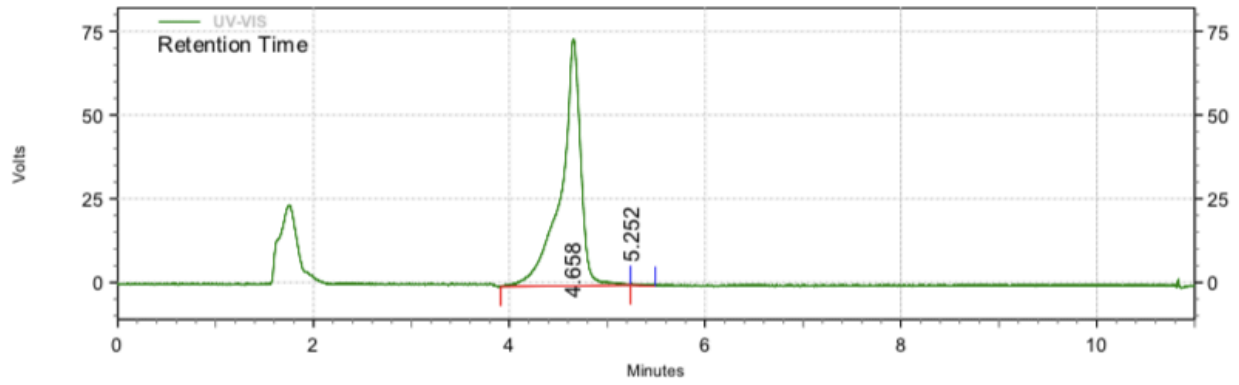

UV-VIS Results

Retention Time	Area	Area %	Height	Height %
4.658	4112004	99.63	295228	99.32
5.252	15157	0.37	2008	0.68
Totals	4127161	100.00	297236	100.00

Doxorubicin 1µM UV result

Area % Report

Data File: C:\Users\UPLC system 2\Desktop\Qamar\1000nM2019-03-19 12-08-45 (GMT -07-00).dat
Method: C:\Enterprise\Projects\Hitachi\Method\Doxo_1.met
Acquired: 3/19/2019 12:10:01 PM (GMT -07:00)
Printed: 3/19/2019 3:08:10 PM (GMT -07:00)

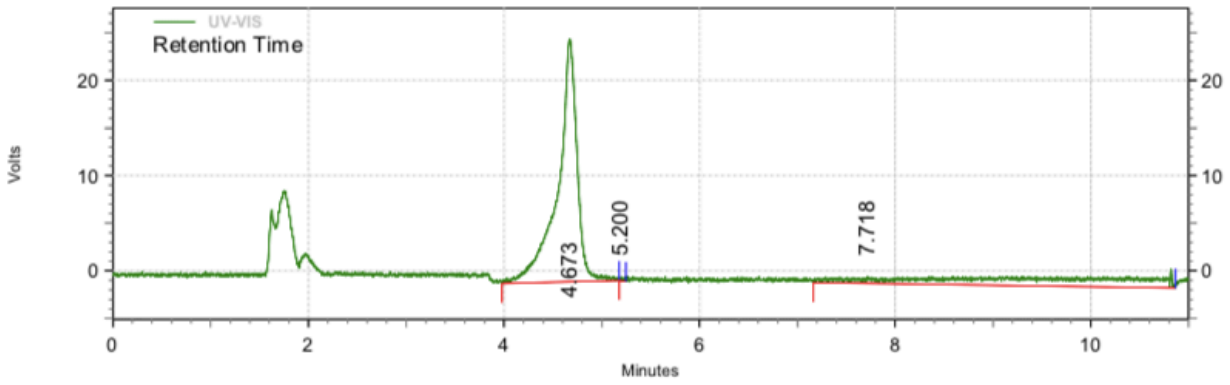

UV-VIS Results

Retention Time	Area	Area %	Height	Height %
4.673	1390421	70.94	101824	95.83
5.200	3515	0.18	1507	1.42
7.718	566105	28.88	2928	2.76
Totals	1960041	100.00	106259	100.00

Doxorubicin 500nM UV result

Area % Report

Data File: C:\Users\UPLC system 2\Desktop\Qamar\500nM2019-03-19 11-43-36 (GMT -07-00).dat
Method: C:\Enterprise\Projects\Hitachi\Method\Doxo_1.met
Acquired: 3/19/2019 11:44:56 AM (GMT -07:00)
Printed: 3/19/2019 3:07:12 PM (GMT -07:00)

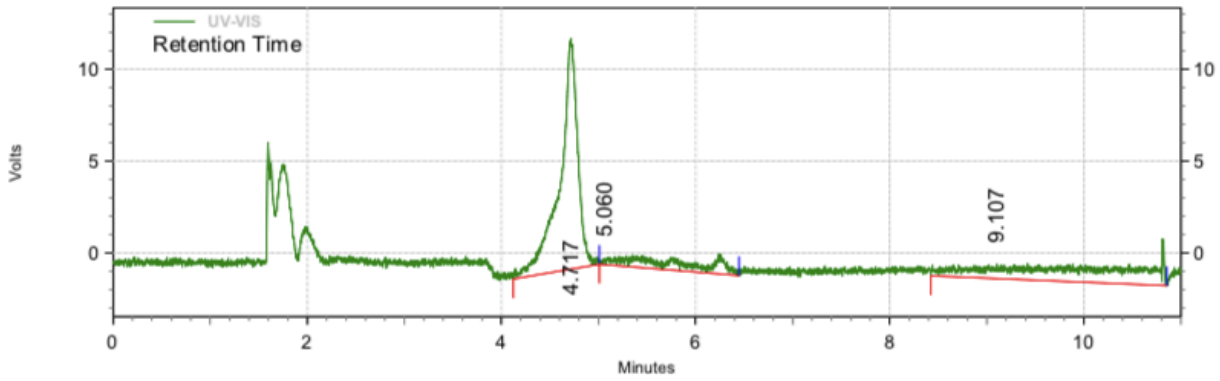

UV-VIS Results

Retention Time	Area	Area %	Height	Height %
4.717	641976	57.02	50165	91.75
5.060	126443	11.23	1369	2.50
9.107	357434	31.75	3139	5.74
Totals	1125853	100.00	54673	100.00

Doxorubicin 300nM UV result

Area % Report

Data File: C:\Users\UPLC system 2\Desktop\Qamar\300nM2019-03-19 11-18-34 (GMT -07-00).dat
Method: C:\Enterprise\Projects\Hitachi\Method\Doxo_1.met
Acquired: 3/19/2019 11:19:51 AM (GMT -07:00)
Printed: 3/19/2019 2:56:01 PM (GMT -07:00)

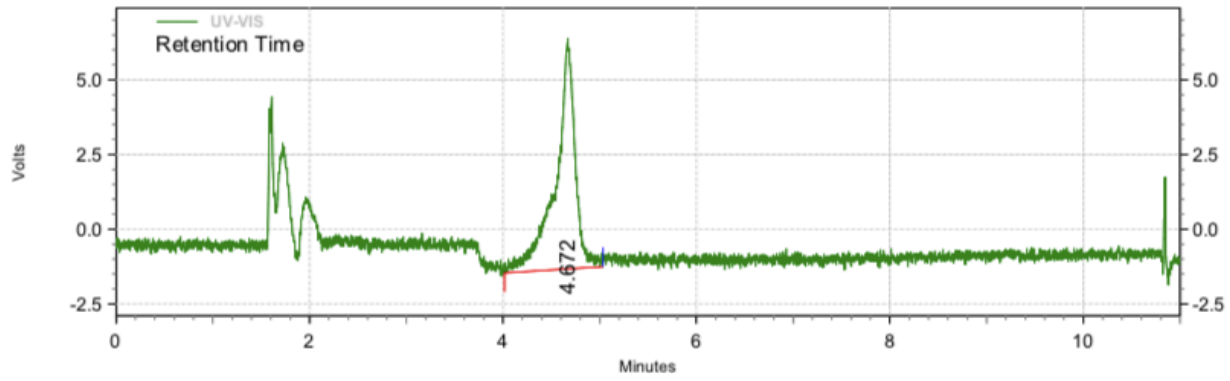

UV-VIS Results

Retention Time	Area	Area %	Height	Height %
4.672	427897	100.00	30821	100.00
Totals	427897	100.00	30821	100.00